

IN-20

**NASA CR-189229
RI/RD92-139**

(NASA-CR-189229) ORBIT TRANSFER
ROCKET ENGINE TECHNOLOGY PROGRAM
Final Report, Jun. 1983 - May 1992
(Rockwell International Corp.)
127 p

N94-26542

Unclas

G3/20 0208999

FINAL REPORT

ORBIT TRANSFER ROCKET ENGINE TECHNOLOGY PROGRAM

By

N. B. GUSTAFSON AND T. J. HARMON

Rocketdyne Division
Rockwell International Corporation

Prepared For

NATIONAL AERONAUTICS AND SPACE ADMINISTRATION

October, 1993

NASA-Lewis Research Center
Cleveland, Ohio 44135

Contract No. NAS3-23773

FOREWORD

The work reported herein was conducted by the Advanced Programs and Engineering personnel of Rocketdyne, a Division of Rockwell International Corporation, under Contract NAS3-23773 from June 1983 to May 1992. P. Richter, Lewis Research Center, was the NASA Project Manager. R. Pauckert was the Rocketdyne Project Manager, and T. Harmon the Project Engineer. N. Gustafson was responsible for the compilation of data from the contract technical efforts and the preparation of this summary report.

TABLE OF CONTENTS

FORWARD.....	i
TABLE OF CONTENTS	ii
LIST OF FIGURES.....	iii
LIST OF TABLES.....	v
INTRODUCTION.....	1
SUMMARY.....	1
TECHNICAL OVERVIEW	3
TASK D - ADVANCED ENGINE STUDY.....	5
Phase I (D.1, D.2 and D.3).....	5
Phase II (D.4).....	14
Point Design (D.5).....	17
Trade Studies (D.6).....	22
TASK B - TURBOMACHINERY TECHNOLOGIES	34
Two-Stage Partial Admission Turbines (B.1 and B.4).....	34
High Velocity Ratio Diffusing Crossovers (B.2)	41
Soft Wear Ring Seals (B.3 and B.5)	48
Advanced Bearing Concepts (B.6)	60
Fuel Turbopump Analysis (B.7).....	64
TASK C - COMBUSTION CHAMBER TECHNOLOGIES	67
Ribbed Wall Flow Tests (C.1)	67
Combustor Coolant Channel Selection (C.2).....	77
Combustor Calorimeter Experiments (C.3, C.4 and C.5)	81
TASK E - ICHM and Preflight Methods.....	87
Fiberoptic Shaft Monitoring (E.5)	91
Combustor Wall Condition Monitoring (E.5)	93
ICHM Elements (E.6).....	98
Automated Preflight Checkout (E.7)	105
TASK F - ENGINE TEST FIRINGS.....	108
BIBLIOGRAPHY	120

LIST OF FIGURES

1. Orbit Transfer Rocket Engine Test Program Schedule	4
2. Phase I Study Logic Diagram.....	6
3. OTV 7.5Klbf Engine Flow Schematic with Turbine Shutoff Valve	11
4. Failure Mode Effects and Reliability Analysis Review and Applicability	12
5. Modular Engine, Top View.....	13
6. Phase II Study Logic Diagram.....	15
7. Maintenance Plan Evolution	18
8. Advanced Engine Study Logic Diagram.....	19
9. OTVE Design Point Engine Balance.....	21
10. Advanced Engine Parametrics, Chamber Pressure Versus Thrust	24
11. Advanced Engine Parametrics, Vacuum Isp Versus Thrust.....	24
12. Advanced Engine Parametrics, Engine Length Versus Thrust.....	25
13. Advanced Engine Parametrics, Engine Diameter Versus Thrust	25
14. Advanced Engine Parametrics, Isp Versus Mixture Ratio.....	27
15. Advanced Engine Parametrics, Chamber Pressure Versus Mixture Ratio.....	27
16. Advanced Engine Study Task D.6 Engine Variation Studies - 6:1 & 12:1 Mixture Ratio.....	31
17. Advanced Engine Study Task D.6 Engine Variation Studies - 20:1 Throttling.....	32
18. Revised OTVE Turbine Bypass Reroute Schematic	33
19. Two-Stage Partial Admission Turbine Tester.....	36
20. Turbine Tester Instrumentation Parameter Locations	37
21. Two-Stage Partial Admission Turbine Efficiency vs Velocity Ratio (0 Degrees Nozzle Variation)	39
22. Two Stage Partial Admission Turbine Equivalent Flowrate vs Equivalent Pressure Ratio (0 Degrees Nozzle Variation)	40
23. MK49-F High Pressure Liquid Hydrogen Turbopump Crossover Section.....	42
24. High Velocity Ratio Diffusing Crossover Passages	43
25. High Velocity Ratio Diffusing Crossover Tester Instrumentation.....	45
26. Scaled MK49-F Stage Head in Water vs Flow Ratio.....	47
27. Scaled MK49-F Stage Efficiency in Water vs Flow Ratio	49
28. MK49-F Soft Seal Locations	51
29. MK49-O Soft Seal Locations.....	52
30. Promoted Ignition Tester	56
31. ABMA Oxygen Test Cell.....	57
32. High Pressure LOX Impact Housing.....	58
33. Friction and Wear Test Chamber.....	59

LIST OF FIGURES (CONTINUED)

34.	OTVE Hydrostatic Bearing Tester	62
35.	OTVE High Pressure Fuel Turbopump	66
36.	Hot Air Test Chamber Components	71
37.	Hot Air Test Setup Schematic	72
38.	Typical Measured Panel Temperature Rise.....	73
39.	Cold Flow Test Fixture - Hot Gas Rib Configuration.....	74
40.	Cold Flow Test Setup Schematic.....	75
41.	Nondimensionalized Scaled Velocities Along Midline Between Ribs	76
42.	Ribbed Combustor Heat Transfer Results	78
43.	Selected Rib Configurations	79
44.	Cold Flow Test Fixture - Coolant Channel Configuration	82
45.	Predicted Liner Temperature Change With Enhanced Channels.....	83
46.	Selected Channel Configurations.....	84
47.	Integrated Component Evaluator (I. C. E.) Thrust Chamber Assembly - Enhanced Heat Transfer Combustor Configuration	85
48.	0.040 Inch Ribbed Circumferentially Cooled Calorimeter	86
49.	800 psia Pc Heat Flux vs Mixture Ratio.....	88
50.	0.040 Inch Ribbed Calorimeter 800 and 1000 psia Pc Test Results	88
51.	Smooth Wall Calorimeter 800 and 1000 psia Pc Test Results.....	89
52.	Heat Transfer Enhancement Comparison - 15 klbf Engine	89
53.	Heat Transfer Enhancement vs Pc for 16 Inch Cylinder and 20 Inch Full Combustor.....	90
54.	Rotating Hardware Demonstrator Configuration.....	92
55.	Probe View of Pattern	92
56.	Ultrasonic Test Apparatus.....	94
57.	Ultrasonic Test Results.....	95
58.	Experimental Trace of an Automatic Pitch/Catch Eddy Current Scan of a Copper Test Piece with 20-Mil Land/Channel Widths.....	96
59.	Differential Eddy Current Scan Showing Strong Signals From Three Thin Wall Channels.....	97
60.	Cutaway View of an Electromagnetic Acoustic Transducer (EMAT).....	99
61.	Thin Wall Channel Detection in Test Specimen Using EMAT Technology	100
62.	ICHM Requirements and Corresponding Functions.....	101
63.	OTVE ICHM Element Architecture	102
64.	OTV Engine with Sensor Locations	104
65.	I.C.E. Combustion System Components	113
66.	Installed I.C.E. Engine.....	114

LIST OF TABLES

1. Engine Design Driver Missions	7
2. 1990's OTV Engine Characteristics - Phase I	8
3. Results of Engine Optimization Runs For 7500 lb Thrust Advanced Technology Engines	10
4. 1990's OTV Engine Characteristics - Phase II	16
5. Orbit Transfer Propulsion Requirements and Goals	20
6. Advanced OTV Engine Weights (lbm)	23
7. Thrust Parametrics Off-Design Mixture Ratio Scans	28
8. Expansion Area Ratio Parametrics	29
9. Two-Stage Partial Admission Turbine Test Matrix	38
10. High Velocity Ratio Diffusing Crossover Test Matrix.....	46
11. MK49-F Seal Clearance Influence on Performance.....	50
12. Soft Wear Ring Seal Operational Characteristics.....	53
13. Major Seal Material Properties Needed.....	54
14. OTVE Turbopump Bearing Comparison Summary.....	61
15. Hydrostatic Bearing Material Candidates.....	65
16. Hot Gas Side Rib Selection Matrix	68
17. Coolant Side Channel Geometry Selection Matrix	80
18. Sensor Technology Selections.....	103
19. OTV ICHM Cost Estimate Summary	106
20. OTV Preflight Requirements.....	107
21. Method Readiness Assessment.....	108
22. Technology Readiness Level Definitions.....	109
23. Element Development Costs	110
24. Development Program Costs (M\$, 91).....	111
25. Integrated Component Evaluator Test Log.....	115
26. I.C.E. Engine System Test Log.....	118

INTRODUCTION

The objective of the Orbital Transfer Rocket Engine Technology Program, contract NAS3-23773 for NASA-LeRC, was to define an advanced near term (1990's) space-based Orbit Transfer Vehicle Engine (OTVE) system and develop the technologies applicable to its construction, maintenance, and operations. This final report summarizes the work accomplished during the period from June 1983 to May 1992. It comprised analytical, design and experimental efforts designated Tasks A through F. This report is not intended as a comprehensive explanation of this body of work, but as an overview. It summarizes the previously reported results and findings of each task and subtask. For a complete listing of final reports containing more detailed information on the various subtasks, the reader is referred to the bibliography section of this document.

SUMMARY

The OTVE technology contract was conceived in order to develop space based upper stage engine technologies. Prior mission and vehicle studies had provided general requirements for such an engine, and previous engine studies provided a departure point for future engine development. This program was designed to define and scope the technologies relevant to an OTVE through the mid 1990's and evaluate them through analysis and component experimentation. The technologies developed and tested were then to be incorporated into ongoing revisions of an OTVE system design. Following this method, the OTVE would progress through a series of configurations to include all advanced concepts evaluated under this contract.

Due to funding limitations, not all technologies identified were fully assessed experimentally and some studies were halted before all their planned objectives were completed. All design tasks were completed which allowed the delivery of complete engine conceptual designs of 15,000 lb and 7500 lb thrust engines with a body of supporting design and technology requirements data to NASA-LeRC.

The OTVE technology contract was divided into several technology tasks according to components, and one reporting task. Task A included all monthly, interim, and final reporting efforts. Task B comprised the turbomachinery studies. Task C consisted of thrust chamber improvement efforts. In Task D the engine system was revised according

to component advancements, leading ultimately to an engine point design. Various derivatives of the point design were also generated in parametric studies. Task E dealt with engine controls, health monitoring and engine maintenance. Under Task F, components were tested in an engine systems test bed environment.

The advanced turbomachinery studies of Task B included the analysis and testing of several technological innovations for OTV size pumps and turbines. A two stage partial admission turbine was tested in several configurations to verify analytical performance predictions and to reveal possible design enhancements for the MK49-F turbopump. High velocity ratio diffusing crossovers were fabricated and tested to determine performance and correct any design deficiencies. The use of soft wear ring seals was studied, with candidate materials evaluated against heating, wear, and ignition requirements. Advanced bearing concepts were also analyzed to determine the optimal configuration for the advanced OTVE. Lastly, a fuel pump rotordynamic analysis taking into account these technologies was also performed.

In Task C, a ribbed combustor design was developed. A range of promising configurations of rib and channel geometries were determined analytically. Selected rib candidates were tested in hot air flows to determine heat enhancement compared to a smooth walled chamber. Boundary layer analyses were also conducted using laser velocimeter data from cold flow testing. The results of these tests led to the choice of a recommended rib geometry. A channel geometry was chosen on the basis of cold flow laser velocimeter data from tests similar to those conducted for the rib candidates. To verify the predicted heat enhancement effects, a ribbed calorimeter spool was tested under hot fire conditions.

Under Task D, the optimum engine thrust, performance and envelope were established for the NASA specified expander power cycle and for the set of OTV missions as defined by NASA-MSFC. Optimal nozzle contours were generated and quick disconnects to support component modularity for the point design engine were designed. Results of a Failure Modes and Effects Analysis (FMEA), and maintenance and reliability studies were also incorporated into the engine system under this task. In addition, results from component studies were included in the engine optimization process in which the engine underwent three complete design iterations; Phase I, Phase II and the final point design.

The point design itself was also the basis of further studies. It was used as the baseline for a series of parametric trades on engine thrust, mixture ratio and area ratio in subtask D.6. The baseline engine was again used to define the control system and the health monitoring and maintenance operations necessary for a space-based engine in Task E. In addition, selected components for engine monitoring were developed under Task E, including combustor wall thickness measuring devices and a fiberoptic shaft monitor. These monitoring devices were incorporated into preflight engine readiness checkout procedures developed and evaluated under this task.

In Task F, in conjunction with complementary Rocketdyne efforts, the Integrated Component Evaluator (ICE) was assembled to demonstrate the performance and operational characteristics of an advanced expander cycle rocket engine and component technology concepts in its systems environment. The MK49 turbopumps had previously been installed on the ICE for component tests to determine start sequence transients and head versus flow excursions at various power levels. Under Task F, the pumps were connected to the thrust chamber assembly and an engine sub-system checkout was employed to gradually transition into full engine test operations. A system blowdown was then performed to determine actual oxygen and hydrogen system resistances and valve characteristics. This was followed by short transitions into main combustor ignition and mainstage operation. Extended testing was prevented by a fuel pump anomaly.

A contract schedule showing the progress and completion of each OTV task and subtask is presented in Figure 1. Some subtask final reports were dated a significant amount of time after efforts were halted. This was a result of either (1) planned or optional efforts which were suspended or left unfunded until the time of closure, or (2) a delay in the report review process.

TECHNICAL OVERVIEW

Under the OTV contract, component study tasks were accomplished concurrently while working toward current engine system goals and requirements. Because tasks were conducted in parallel, efforts under given task and subtask numbers did not necessarily follow each other in order. In the interests of clarity, the task descriptions in this report also deviate from the letter and number orders designated. The engine studies in Task D

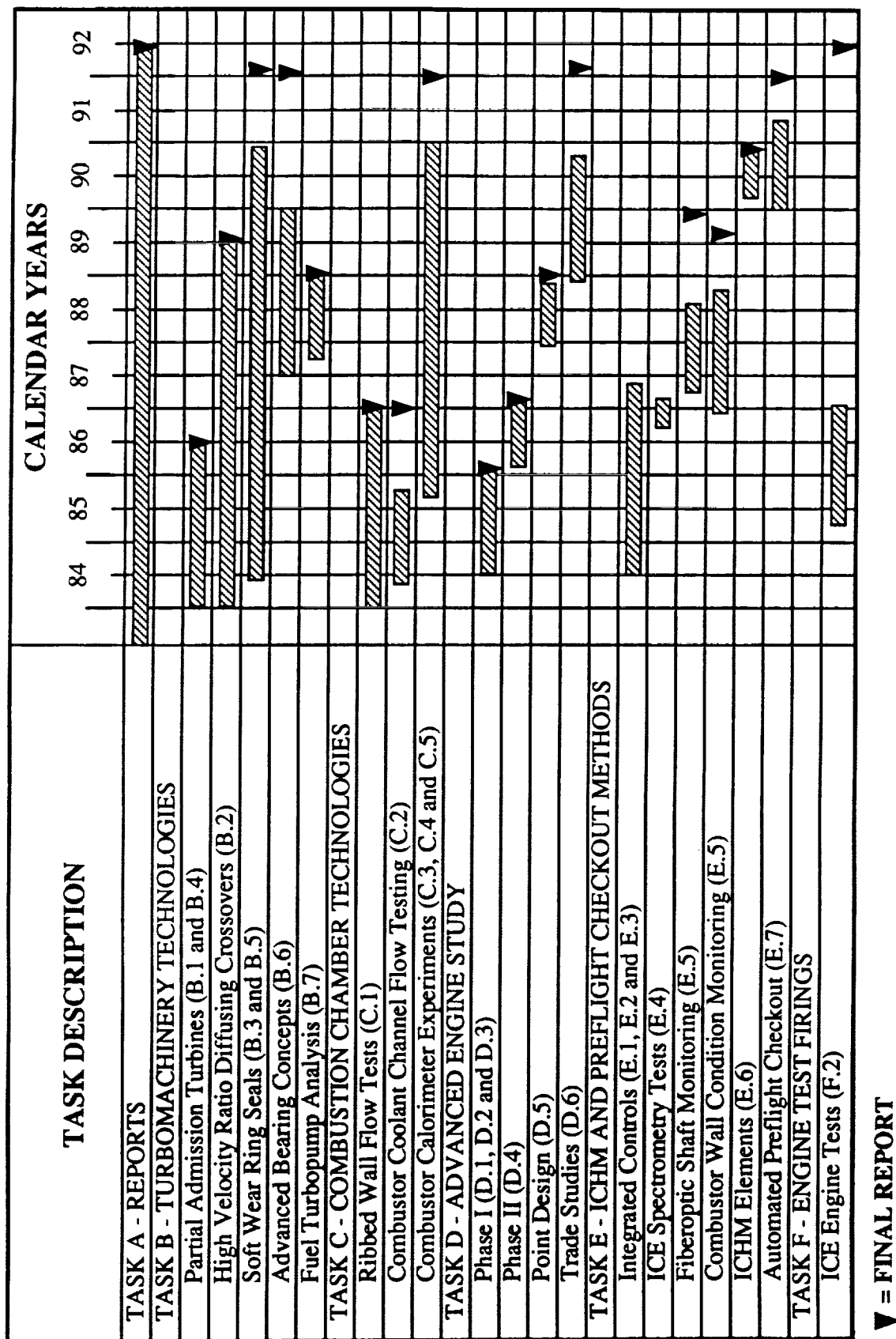


Figure 1: Orbit Transfer Rocket Engine Test Program Schedule

are first described, after which the turbomachinery improvements of Task B and the advanced combustor work of Task C follow. Lastly, the Integrated Control and Health Monitoring (ICHM) efforts in Task E and the engine testing in Task F are presented. Task A was an administrative task under which contract reports for all subtasks were written, and therefore need not be described.

TASK D - ADVANCED ENGINE STUDY

The Advanced Engine Study, Task D, was originally outlined as a four year effort in which the OTVE design would be iterated to allow resolution of vehicle/engine integration issues as well as advanced engine performance, operations and maintenance issues. In Phase I, comprising subtasks D.1, D.2 and D.3, an engine design was developed which was driven by vehicle/mission factors, space maintenance requirements and an FMEA. In Phase II, subtask D.4, the propulsion system requirements for the OTVE were updated and results of component technology tasks completed to date were used to upgrade the engine design. Another systems update in subtask D.5 resulted in the engine point design. The point design was evaluated at off-design conditions and in subtask D.6, trade studies based on the point design were performed.

Phase I

A logic diagram for the Phase I development of the baseline engine is given in Figure 2, graphically showing the process used in the first OTVE design iteration. After an in-depth review of vehicle trade studies and derived requirements provided by four vehicle contractors, a 7500 lbf thrust baseline engine was selected as the optimum for OTVE applications. The missions which drove this selection are listed in Table 1.

Nine prioritized requirements were derived from these missions. The utmost priority was that the engine be suitable for space basing. Second, it must be suitable for ground basing. The third requirement was to be man-ratable. Next, the engine had to have high specific impulse both at high and low thrust. Tank head idle start capability and having no constraints on cool-down time between burns were also required. Light weight and a size compatible with servicing came next. The final requirement was compatibility with aeroassist OTV operation. Characteristics of the engine chosen to fulfill these requirements are summarized in Table 2 along with the initial engine characteristics determined

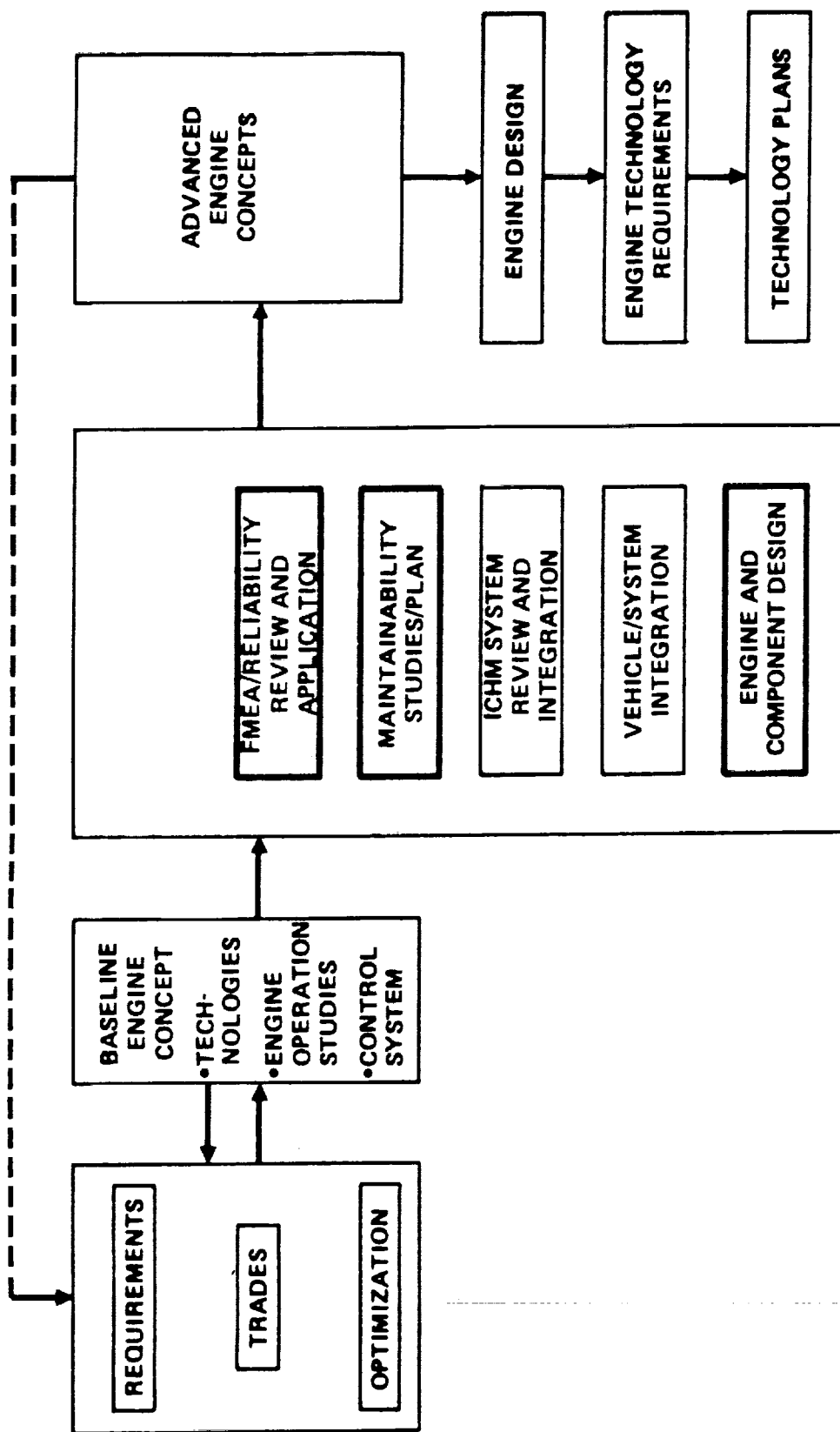


Figure 2: Phase I Study Logic Diagram

Table 1: Engine Design Driver Missions

MISSION TYPE	FIRST FLIGHT DATE	RATIONALE
MULTIPLE PAYLOAD DELIVERY 12876 UP 2166 DOWN	1993	PERFORMANCE DRIVER FOR GROUND-BASED QTV
MOLNIYA AND GPS MISSIONS	1993	MISSION OPERATION DIFFICULTY FOR SPACE-BASED OPERATION
UNMANNED SERVICE 7K UP 4.51K DOWN	1995	FIRST RENDEZVOUS AND DOCKING AUTONOMOUS RENDEZVOUS AND DOCKING DRIVES FLIGHT OPERATIONS AND EQUIPMENT COMPLEXITY
GEO DELIVERY 20K UP 0 DOWN	1996	EARLIEST REQUIRED MISSION MOST FREQUENT MISSION
GEO MANNED SERVICE 14K UP 14K DOWN	1997	ENERGY/PROPELLANT WEIGHT DRIVER PAYLOAD LENGTH IMPACT ON AEROASSIST MISSION DURATION (20 DAYS) MAN-RATING REQUIREMENTS
LUNAR DELIVERY AND RETURN 80K UP 15K DOWN	2006	PERFORMANCE DRIVER HIGHEST RETURN VELOCITY (12-21 DAYS)
PLANETARY 11.9071K C ₃ -60	2006	MISSION OPERATIONS: RETURN FROM BEYOND ESCAPE VELOCITY POSSIBLE PERFORMANCE DRIVER

Table 2: 1990's OTV Engine Characteristics - Phase I

	<u>INITIAL</u>	<u>PHASE I UPDATES</u>
PROPELLANTS	LO ₂ /LH ₂	✓
THRUST, lb		
NOMINAL	10,000 – 25,000	7500
LOW THRUST	2,000	✓
THROTTLING (CONTINUOUS)	NONE	✓
THRUST BUILDUP TIME, sec	1 – 2	✓
BOOST PUMPS		
VEHICLE	NONE	✓
ENGINE	LOW NPSH	✓
APPLICATION COMPATIBILITY	AFT CARGO CARRIER, AEROASSIST	✓
STOWED SIZE, in.		
ENGINE LENGTH	55	60
ENGINE DIAMETER	71	✓
THRUST VECTOR CONTROL, deg.	±4	+6
INERT GAS REQUIREMENT		
VALVE ACTUATION	HELIUM	✓
PURGES	NONE	✓

previously in the Orbit Transfer Rocket Engine Technology Program completed in November 1983, shown for comparison.

After the general engine configuration had been decided, component technologies were identified which would increase engine performance, reliability or operability. Engines incorporating various technologies were then analyzed and a baseline was chosen from these according to system needs, reliability and maintenance standards and development time limitations. Eleven of the engine variations considered, including the chosen baseline, are detailed in Table 3. An engine flow schematic of the baseline engine is represented in Figure 3.

Engine operation studies were conducted on the baseline engine to define and optimize design parameters. All components and the engine system were evaluated at on-design and off-design conditions. Both thrust and mixture ratio variations were investigated. This was followed by a review of the FMEA and reliability analyses which were conducted under the ICHM Task E.1. In this review, the impact of the FMEA on engine design was assessed and methods for FME mitigation and reliability improvements through component design evolution, engine and cycle design evolution, redundancy schemes, and ICHM evolution were generated. A flow chart outlining this process is shown in Figure 4.

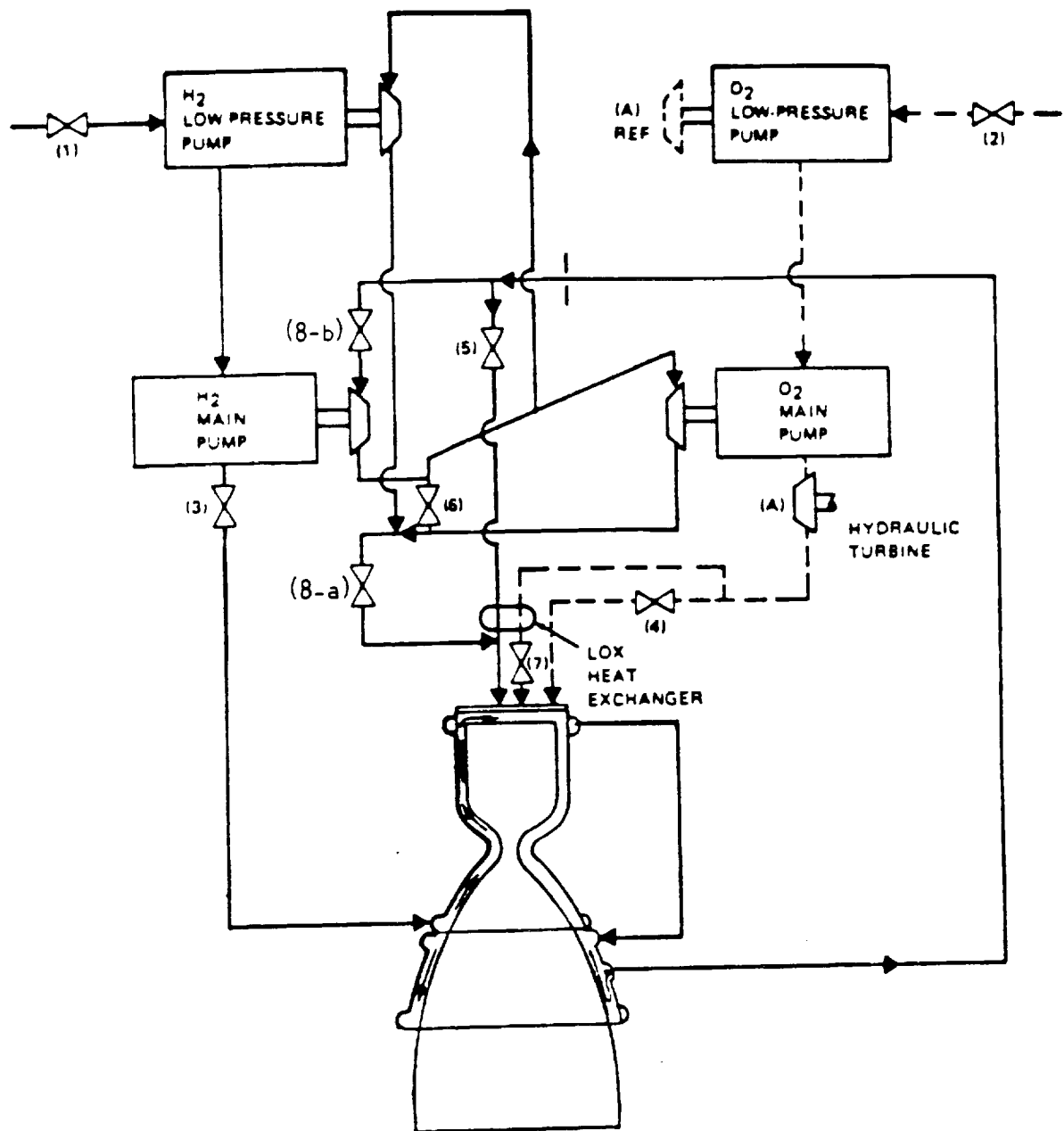
Concurrently, an initial space-based maintenance philosophy was established and requirements for its implementation were determined. This maintenance philosophy centered on the benefits of a modular engine concept and the use of advanced sensors for health monitoring. An annotated sketch of the OTVE in its modular configuration is shown in Figure 5. In the modular, ICHM approach, engine servicing would be done on an as-needed basis determined by the health monitoring systems as opposed to a more frequent scheduled routine. Space-based servicing such as this requires advanced fluid disconnects easily operable by an EVA astronaut or robotic manipulator. Several preliminary design concepts for space operable fluid disconnects were generated during this study. These concepts were evaluated and ranked based on coupling operation, performance, fabrication, development, and maintenance.

As part of the advanced engine system evolution, a comprehensive list of innovative ideas was identified and evaluated by the respective components specialists in order to ascertain their benefits to the engine design. Many of these concepts were offshoots of the FMEA review and maintainability studies and thus are integral parts of the space-based

Table 3: Results of Engine Optimization Runs For 7500 lb. Thrust
Advanced Technology Engines

ENGINE PARAMETERS	REFERENCE	CASE NUMBER							CHOSEN AS BASELINE			
		1	2	3	4-0	5	4-F	6		7	8	9
TURBOCHARGERY LIMITS												
COMBUSTION TYPE	ADV. (1)	S.O.A. (2)	S.O.A. (2)	ADV. RIBBED	ADV. RIBBED	ADV. RIBBED	ADV. RIBBED	ADV. RIBBED	ADV. RIBBED	ADV. RIBBED	ADV. RIBBED	ADV. RIBBED
NO. OF HPFT STAGES	2	2	2	2	2	2	2	2	2	2	2	2
HPFT ADMISSION	PARTIAL	PARTIAL	PARTIAL	PARTIAL	PARTIAL	PARTIAL	PARTIAL	PARTIAL	PARTIAL	PARTIAL	PARTIAL	PARTIAL
NO. OF HPOR STAGES	1	1	1	1	1	1	1	1	1	1	1	1
NO. OF HPFP STAGES	4	4	4	4	4	4	4	4	4	4	4	4
HPFP SPEED LIMIT, RPM	200000	200000	200000	200000	200000	300000	300000	200000	200000	200000	200000	200000
LPOT DRIVE TYPE	F-F (3)	F-F	F-F	F-F	F-F	F-F	F-F	GH2	F-F	F-F	F-F	F-F
SOFT WEARL SEALS	N/A	N/A	N/A	N/A	N/A	N/A	N/A	N/A	N/A	N/A	N/A	N/A
GOX DRIVE	N/A	N/A	N/A	N/A	N/A	N/A	N/A	N/A	N/A	N/A	N/A	N/A
CHAMBER PRESSURE, PSIA	1576	1387	1215	1214	1515	1626	1478	1534	1565	1831	YES	YES
SPECIFIC IMPULSE, SEC	488.86	487.7	484.94	486.53	488.34	489.16	488.32	488.64	488.82	490.4	YES	YES
NOZZLE AREA RATIO	970	1042	909	914	847	994	975	1107	1048	1081	976	976
HPFT BYPASS, PERCENT	10	10	10	10	10	10	10	10	10	10	10	10
HPFTP EFF. PRODUCT, %	31.39	30.71	34.84	27.9	31.57	32.06	32.86	31.35	30.24	34.49	32.07	32.07
COMB. HEAT LOAD, BTU/SEC	6440	6402	3965	6366	6425	6453	6432	6432	6430	6502	6356	6356
NOZZLE HEAT LOAD, BTU/SEC	1416	1561	1721	1687	1428	1392	1485	1461	1431	1293	2019	2019
REGEN. HEAT LOAD, BTU/SEC	N/A	N/A	N/A	N/A	N/A	N/A	N/A	N/A	43	N/A	N/A	N/A
HPFP SPEED, RPM	199661	118733	133255	200000	198894	247254	296159	195367	199345	199560	200000	200000
HPFP EFFICIENCY, PERCENT	48.98	48.44	53.76	55.46	49.25	50.18	52.24	49.07	47.77	56.38	62.63	62.63
HPFP DIS. PRESSURE, PSIA	6559	5078	4164	4058	6472	6895	5335	6540	6908	7733	5747	5747
HPFP DIAMETER, IN.	2.36	3.37	2.67	1.81	2.35	1.97	1.65	2.38	2.45	2.44	2.15	2.15
HPFP TIP SPEED, FT/SEC	2057	1749	1552	1580	2039	2128	2134	2032	2131	2125	1877	1877
HPFT PRESSURE RATIO	2.23	1.91	1.97	1.8	2.20	2.27	1.89	2.22	2.38	2.31	3.02	3.02
HPFT EFFICIENCY, PERCENT	61.4	63.4	64.8	50.3	64.1	63.9	62.9	63.9	63.3	61.9	51.2	51.2
HPFT DIAMETER, IN	1.99	2.95	2.33	2.21	2.16	1.81	1.30	2.05	2.05	2.14	2.08	2.08
HPFT VELOCITY RATIO	.262	.258	.268	.346	.288	.292	.287	.266	.26	.276	.271	.271
HPFT BLADE HEIGHT, IN.	.273	.29	.368	.087	.259	.198	.155	.259	.245	.243	.120	.120
HPFT ADMISSION, FRACTION	.225	.198	.181	1.0	.218	.321	.806	.228	.226	.395	.775	.775
HPFT AN**2, (IN-RPM)**2 E-10	9.72	5.04	6.46	2.56	9.92	9.98	7.35	9.12	9.29	6.51	3.12	3.12
HPFT DN (MM-RPM) E-6	2.92	1.87	1.90	2.54	2.9	3.45	3.68	2.87	2.97	2.92	2.67	2.67
HPFT INLET TEMP., DEG-R	1129	1121	795	1103	1125	1129	1112	1133	1143	1119	890	890
HPFT PITCH VELOCITY, FT/SEC	1731	1529	1357	1931	1881	1951	1679	1752	1788	1863	1814	1814

- (1) RELAXED TO A HIGHER VALUE
(2) PARAMETER CHANGE UNDERLINED
(3) FULL-FLOW HYDRAULIC DRIVE



- | | | |
|----------|---|--|
| (1) IFV | - | INLET FUEL VALVE |
| (2) IOV | - | INLET OXIDIZER VALVE |
| (3) MFV | - | MAIN FUEL VALVE |
| (4) MOV | - | MAIN OXIDIZER VALVE |
| (5) TBV | - | TURBINE BYPASS VALVE |
| (6) OTBV | - | OXIDIZER TURBINE BYPASS VALVE |
| (7) GOV | - | GASEOUS OXIDIZER VALVE |
| (8) TSV | - | TURBINE SHUTOFF VALVE |
| (A) | - | (LOCATED AT EITHER A OR B)
FULL FLOW HYDRAULIC TURBINE
FOR LOW PRESSURE LOX PUMP |

Figure 3: OTV 7.5Klbf Engine Flow Schematic with Turbine Shutoff Valve

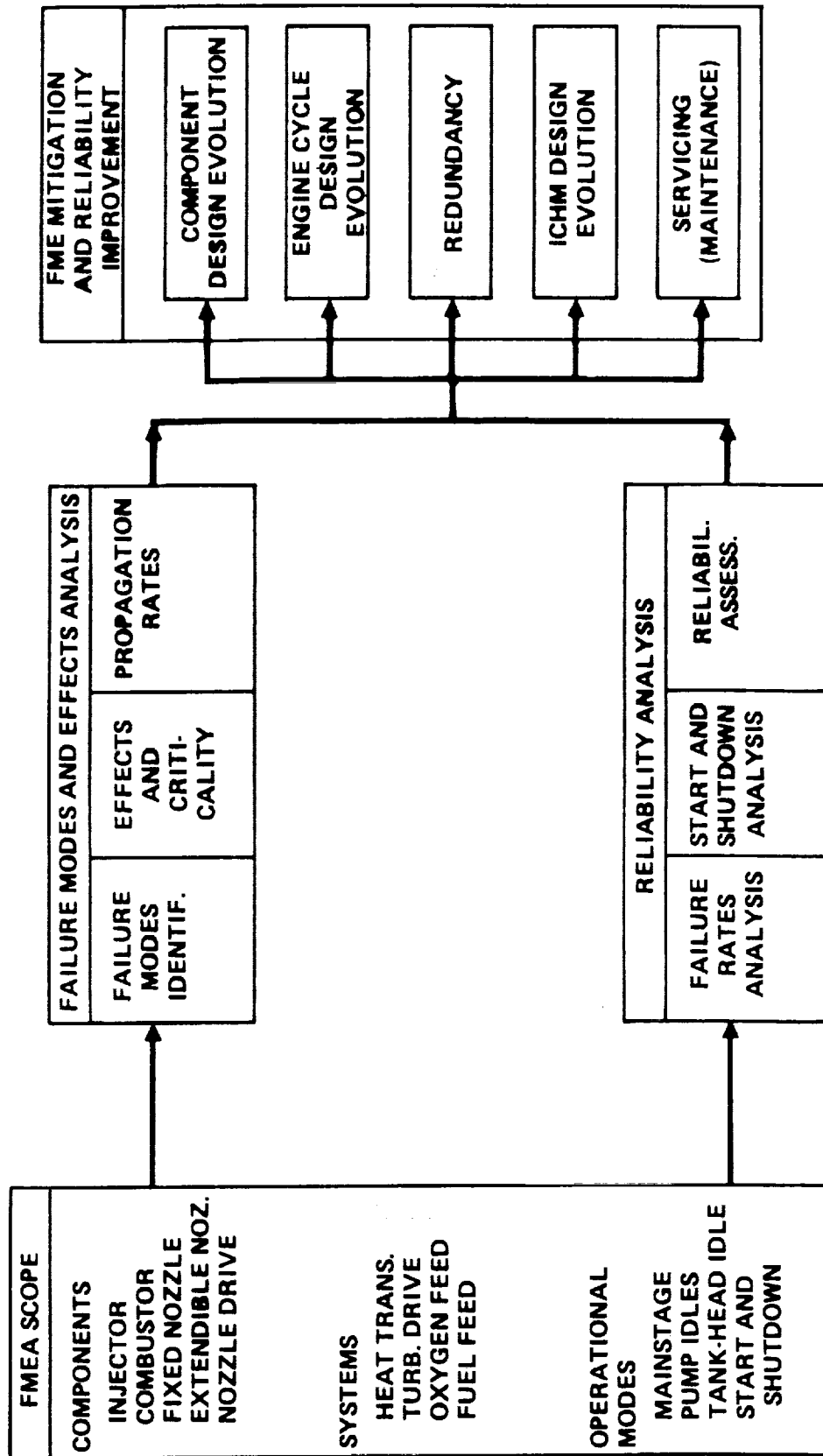


Figure 4: Failure Mode Effects and Reliability Analysis Review and Applicability

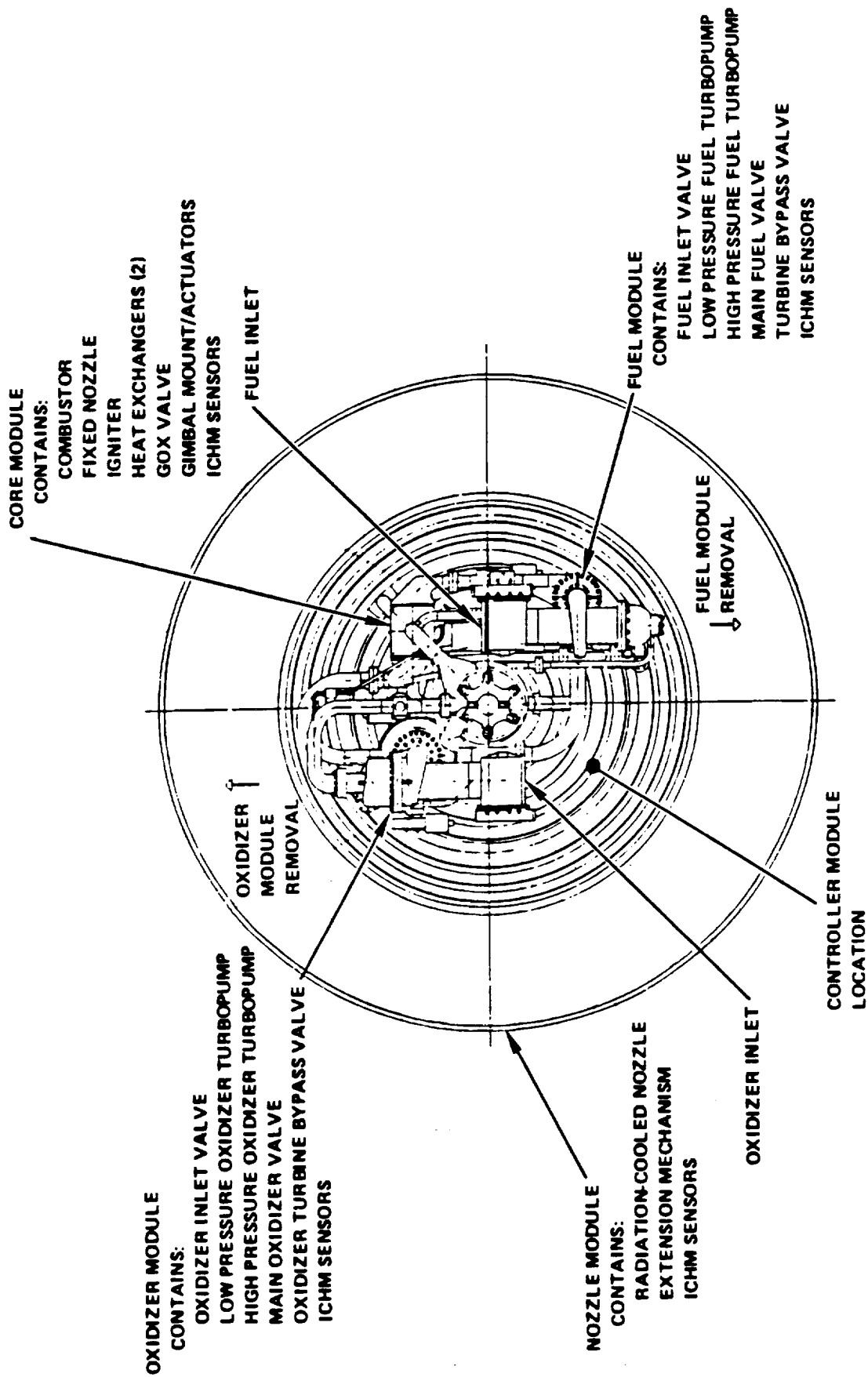


Figure 5: Modular Engine, Top View

maintenance philosophy. Some were developed under this contract in component technology tasks. Others included valve designs and improvements, an igniter design, retractable nozzle technologies and quick disconnect concepts. Technology plans were generated in later engine revisions for several of these concepts which were deemed worthy of further investigation with fruition expected within the time frames of interest.

Phase II

The study logic diagram for subtask D.4, Phase II of the OTV engine design, is shown in Figure 6. It depicts the process followed in updating the Phase I engine system to the next level of detail and design confidence. Major advances were made in the engine design, the maintenance plan and in the space operable disconnect designs.

A survey of current vehicle studies was conducted in order to identify any revisions in the propulsion system requirements since completion of the phase I study. No major changes had been established. Only minor revisions affecting gimbaling and throttling requirements were identified for the Phase II engine system. Changes in engine requirements/characteristics from Phase I to Phase II are listed in Table 4.

Updated heat transfer data generated in the Enhanced Heat Load Thrust Chamber Study (Task C.1) were reviewed and incorporated into the Steady State Design and Optimization Code used to generate the engine balance cases. The engine was then reoptimized with a new heat transfer correlation for the combustor cooling circuit. A slight reduction in the predicted performance was observed.

The minor changes identified in the Engine Design Update and Engine Concept Studies described above did not warrant an updated engine layout at the time. Instead, the effort originally budgeted for the layout was redirected toward component studies in preparation for the forthcoming point-design engine subtask, D.5. A nozzle contour analysis was chosen as the study that could be completed with the remaining funds. In this task, a Rao optimum contour was generated for the fixed nozzle envelope. Results of this more sophisticated analysis superseded the parabolic contour generated in the Phase I study.

In support of the maintenance plan, a compilation of component lives and life limiters for critical components including the combustor, nozzle, injector, turbomachinery, and valves/actuators was generated. Most of the components evaluated met the ultimate life

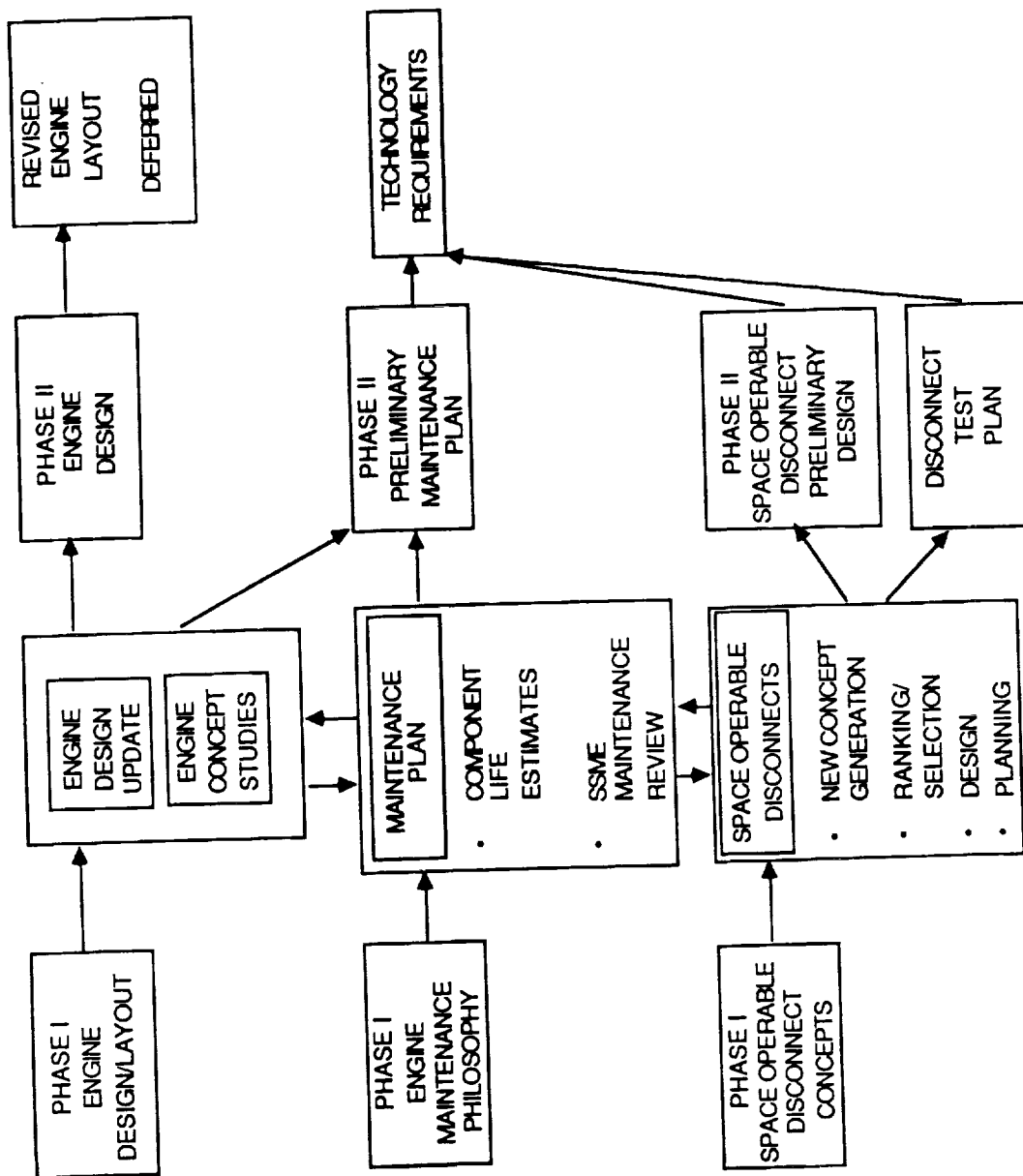


Figure 6: Phase II Study Logic Diagram

Table 4: 1990's OTV Engine Characteristics - Phase II

	<u>INITIAL</u>	<u>PHASE I UPDATES</u>	<u>PHASE II UPDATES</u>
PROPELLANTS	LO ₂ /LH ₂	✓*	✓
THRUST, LB			
NOMINAL	10,000-25,000	7500	5000-7500
LOW THRUST	2,000	✓	750 (IDLE)
THROTTLING (CONTINUOUS)	NONE	✓	NOT REQUIRED
THRUST BUILDUP TIME, SEC	1-2	✓	✓
BOOST PUMPS			
VEHICLE	NONE	✓	✓
ENGINE	LOW NPSH	✓	✓
APPLICATION COMPATIBILITY	AFT CARGO CARRIER, AEROASSIST	✓	✓
STOWED SIZE, IN			
ENGINE LENGTH	55	60	✓
ENGINE DIAMETER	71	✓	✓
THRUST VECTOR CONTROL, DEG	±4	±6	15 X 20
INERT GAS REQUIREMENT			
VALVE ACTUATION	HELIUM	✓	✓
PURGES	NONE	YES	YES

* ✓ = No Change

goal of 20 hours/ 500 cycles, with some thrust chamber elements requiring inspections and possible servicing prior to replacement.

In addition, a review of the Space Shuttle Main Engine (SSME) operations and maintenance manual was conducted with two purposes in mind: (1) to begin to outline the overall maintenance procedures for the OTVE, and (2) to identify technology requirements for streamlining space based OTV operations. Figure 7 shows the expected evolution of OTVE maintenance progressing from 1992 ground based plans to space based plans of the late 1990's.

With respect to the space operable disconnects for the OTVE, several concepts were identified. These were ranked in the categories of coupling assembly, coupling disassembly, misalignment accommodation, assembly verification, damage sensitivity, preload reliability, fabrication costs and development risk. From the rankings it was decided which disconnect candidates should be tested. A test plan was generated to indicate the types of tests necessary to demonstrate the pros and cons of each candidate. Conducting these tests, however, was not within the scope of this contract effort.

Point Design

Figure 8 shows how the engine point design was developed under subtask D.5 of the OTV contract. It followed directly from the Phase II design and technology requirements arrived at previously. In this process, the Phase II baseline system analysis was reviewed to ensure the requirements and goals given in Table 5 were met. Off-design studies were also conducted to assess the severity of the ranges of required component operation. Results of this effort indicated engine requirements and performance goals could be met.

The on-design engine balance for the 7500 lbf point design engine is shown in Figure 9. Given are pressures, temperatures and flowrates along with other important engine parameters. The closed expander cycle chosen is seen to drive its main turbines in series with a hot gas low pressure fuel turbine and an hydraulic low pressure LOX turbine. The heat exchanger shown is used for LOX gasification for autogenous tank pressurization and for tank head idle operation.

Component analyses included studies to optimize the engine system configuration. The injector/igniter configuration was chosen due to its strong historical precedence and

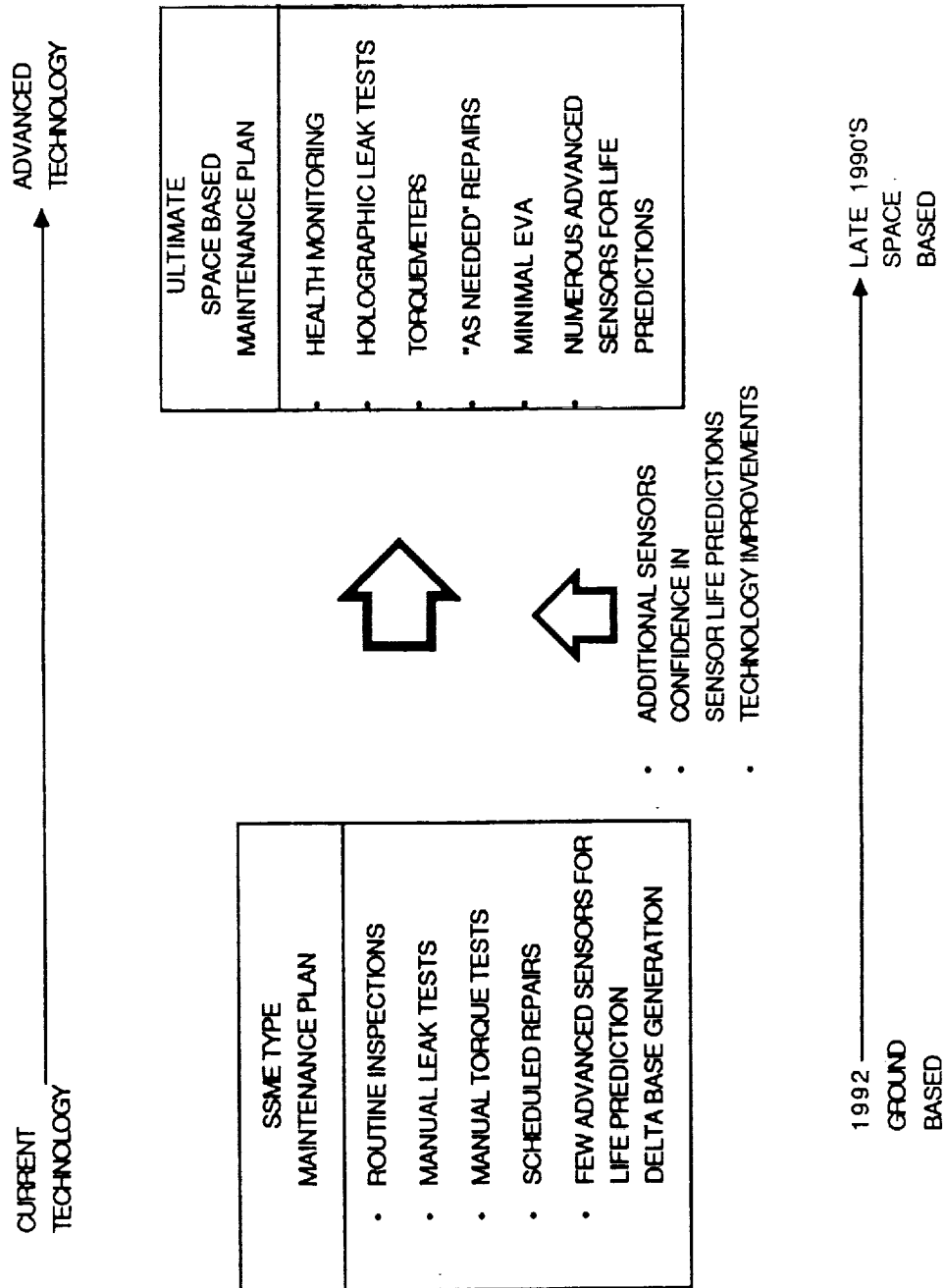


Figure 7: Maintenance Plan Evolution

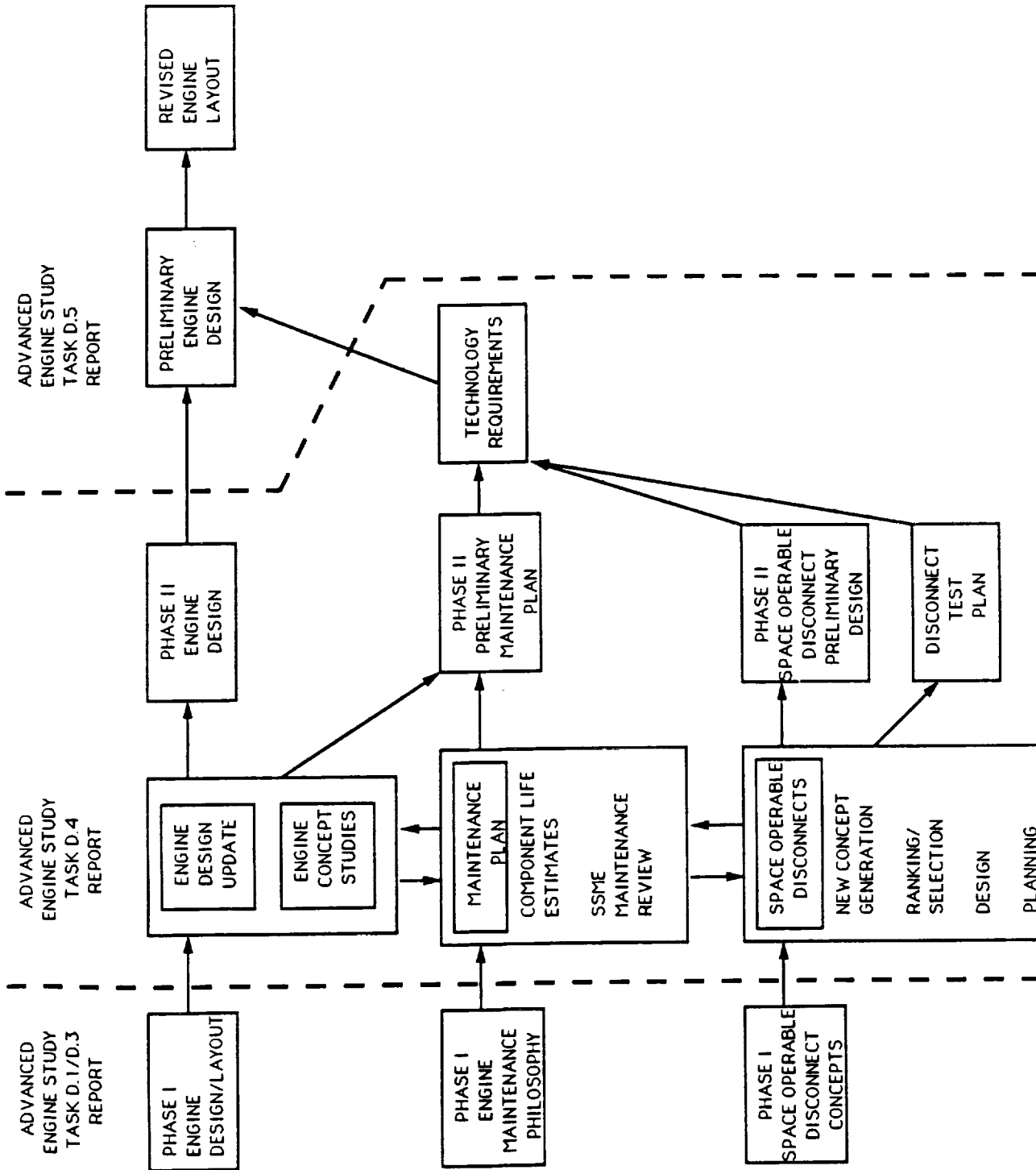


Figure 8: Advanced Engine Study Logic Diagram

Table 5: Orbit Transfer Propulsion Requirements and Goals

Requirements	
Propellants--fuel, oxidizer	Hydrogen, oxygen
Vacuum thrust	Design point engine thrust level is to be based on an orbit transfer vehicle total vacuum thrust level of 15,000 lbf with a minimum of two engines
Engine mixture ratio	Design point engine mixture ratio (O/F) will be 6.0 with capability for operation in the O/F range from 5.0 to 7.0
Propellant inlet conditions	Design point hydrogen and oxygen inlet temperatures will be 37.8°R and 162.7°R, respectively. Design point net positive suction head (NPSH) at full thrust will be 15 ft-lbf/lbm at the hydrogen pump inlet and 2 ft-lbf/lbm at the oxygen pump inlet
Design criteria	<p>The engine is to be man-rated</p> <p>The engine must be compatible with aero-assist return of the vehicle to low earth orbit</p> <p>The engine must be capable of being space based</p>
Gimbal	Engine gimbal requirements are +20 deg in the pitch and yaw planes
Start cycle	<p>Engine start to full thrust is to be accomplished using tank-head-idle and pumped-idle operating modes as shown below:</p> <ul style="list-style-type: none"> • Tank-head-idle: Propellants are supplied from the vehicle tanks at saturated conditions. This mode of operation is intended to settle propellants and thermally condition the engine. • Pumped-idle: Propellants are supplied initially at saturated conditions. Pumps operate at a power level sufficient to provide autogeneous pressurization of the vehicle propellant tanks to pump inlet design point NPSH levels. • Autogeneous pressurization continues during acceleration to and at full thrust.
Goals	
Vacuum-specific impulse	490 lbf/lbm/s (minimum)
Vacuum thrust throttling ratio	10:1
Weight	360 lbm (maximum total weight of main propulsion system engines)
Length (stowed)	TBD
Service life between overhauls	500 starts/20-h operation
Service free life	100 starts/4-h operation

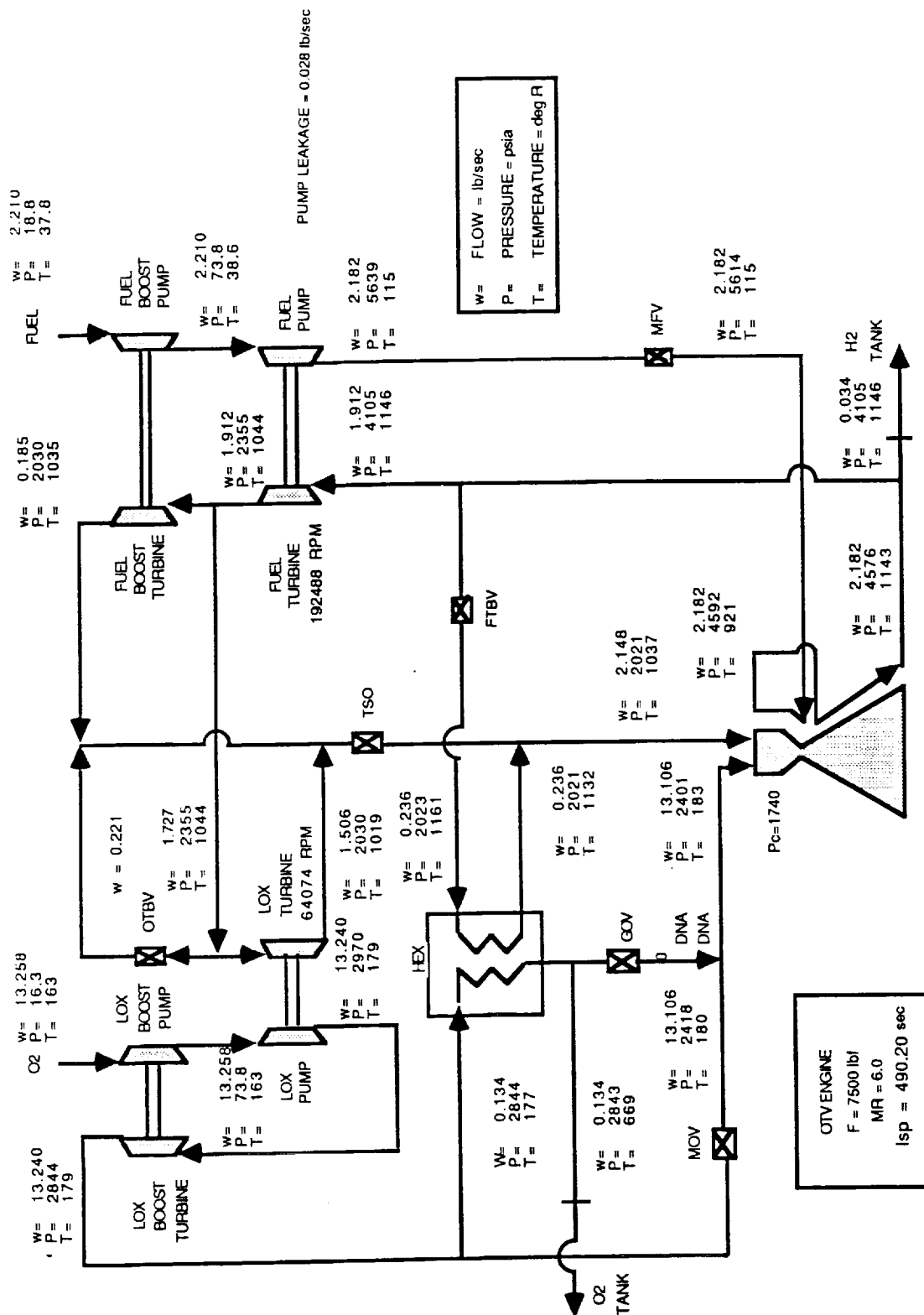


Figure 9: OTVE Design Point Engine Balance

demonstrated high performance. Design and analyses of the boost pumps were also conducted to the extent necessary to assure the validity of the interface with the high-pressure fuel and oxidizer turbopumps. Cross-sectional design layouts were completed showing the primary design features, basic dimensions, critical clearances and materials. Further results from ongoing component technology tasks B and C were incorporated into the engine point design. These included the effects of high-velocity diffusing crossovers, soft-wear ring seals, high speed bearings and a high pressure fuel pump design (Tasks B.2 through B.7), plus enhanced heat loads for the thrust chamber (Tasks C.1 through C.5). Valve, control and health monitoring advances from Task E were also reviewed and included. Design improvements for accommodating deep throttling were developed and documented.

Weights for all components of the point design engine were calculated, including those for the gimbal assembly, valves, controls, ducting and extendible nozzle mechanism. These weights are tabulated individually and by category in Table 6.

Trade Studies

In subtask D.6, the point design engine of subtask D.5 was used as the baseline for engine parametric studies in order to allow optimization of the engine to additional vehicle configurations and mission objectives. Thrust parametric data, including engine delivered specific impulse, mass and dimensional envelope, was generated for the advanced engine configuration over a thrust range from 7.5 klbf to 50 klbf. Engine mixture ratio was held constant at 6.0:1 for this scan with engine cycle balances being generated at intermediate thrust levels of 15, 25, and 35 klbf. Detailed heat transfer analysis was conducted at each thrust level for the combustor and nozzle. Photographic scaling with a constant length/diameter ratio for the combustor was employed for these parametrics.

Sample Results of the parametric thrust scan are given in Figures 10, 11, 12 and 13 for chamber pressure, specific impulse, engine length and diameter respectively. The chamber pressure was primarily influenced by three factors; heat extraction per pound of fuel, turbomachinery efficiency and coolant circuit pressure drop. Decreasing heat extraction and increasing turbopump efficiency and combustor pressure drops combined to give a relatively stable chamber pressure (P_c) after an initial sharp increase. Specific impulse followed the P_c trend since the nozzle expansion ratios are fairly constant. Photographic scaling resulted in steady increases in length and diameter with increasing thrust.

Table 6: Advanced OTV Engine Weights (lbm)

Thrust = 7500 lbf
 Chamber Pressure = 1576 psia
 Nozzle Area Ratio = 970:1

				<u>Subtotals</u>
Turbopumps	(L.P.)	(H.P.)		50.4
Fuel	3.2	25.1	28.3	
Oxidizer	5.0	17.1	22.1	
Gimbal Assembly				1.3
Thrust Chamber				159.0
				(130.2)*
Injector			3.5	
Combustion Chamber			30.1	
Fixed Nozzle			61.6	
Extendible Nozzle - Haynes 214			63.8	
(Extendible Nozzle - Carbon/Silicon Carbon)			(35.0)	
Valves and Controls				17.9
Propellant Valves			11.2	
Control Valves			1.8	
Controller Assembly			0.0	
Harnesses and Sensors			4.9	
Engine Systems				33.0
Propellant Ducting			3.6	
Extendible Nozzle Mechanism			14.9	
Interface Lines			0.8	
Pneumatic Control Lines			0.0	
Ignition System			3.1	
Heat Exchanger			10.6	
H2 Regenerator			0.0	
TOTAL				<u>261.6</u>
				(232.8)*

*232.8 Weight utilizes carbon/silicon carbide nozzle

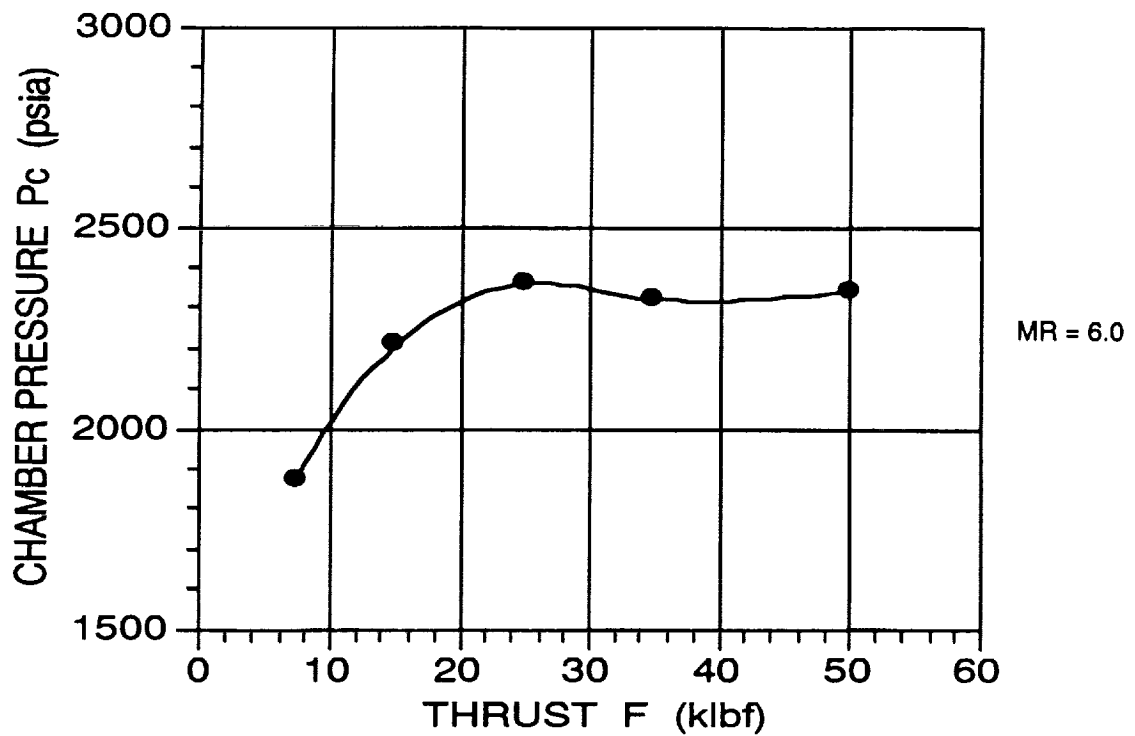


Figure 10: Advanced Engine Parametrics, Chamber Pressure Versus Thrust

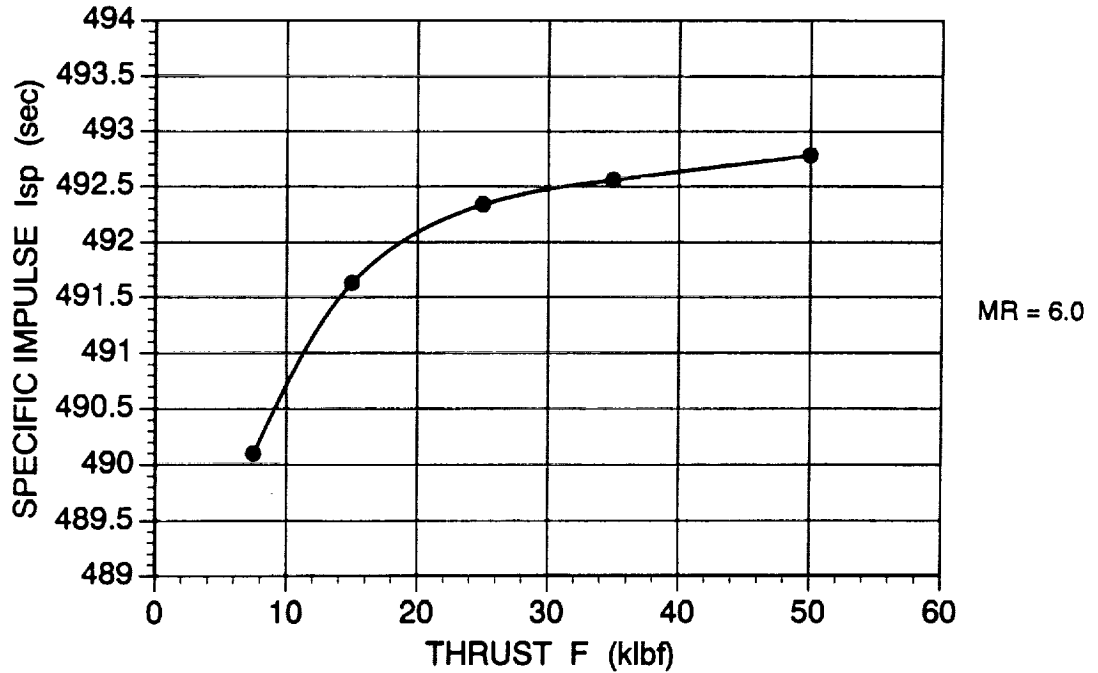


Figure 11: Advanced Engine Parametrics, Vacuum I_{sp} Versus Thrust

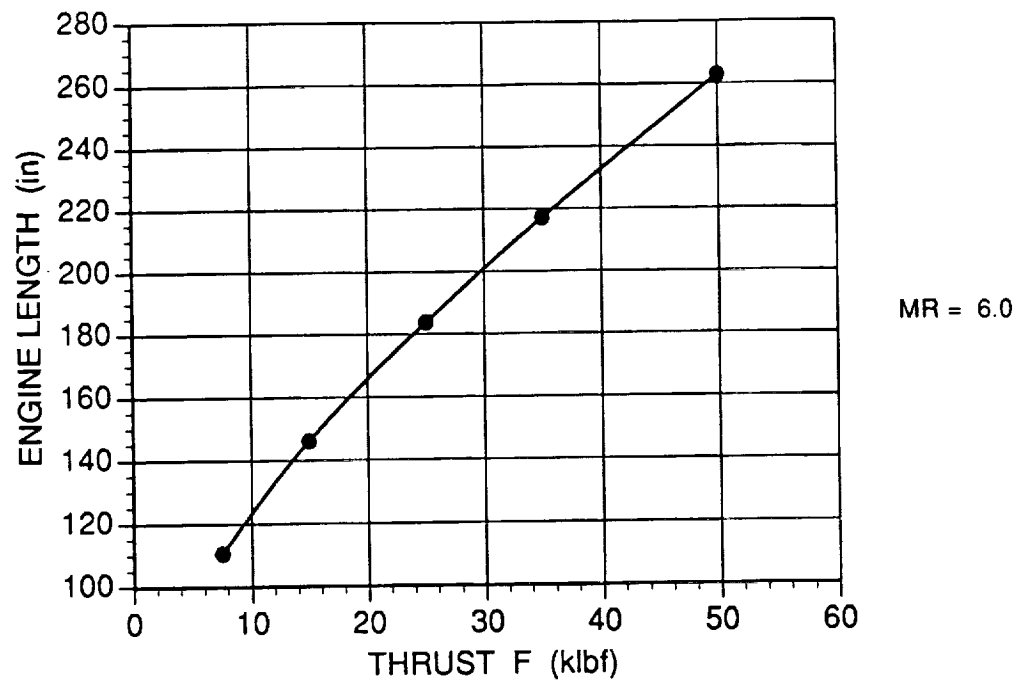


Figure 12: Advanced Engine Parametrics, Engine Length Versus Thrust

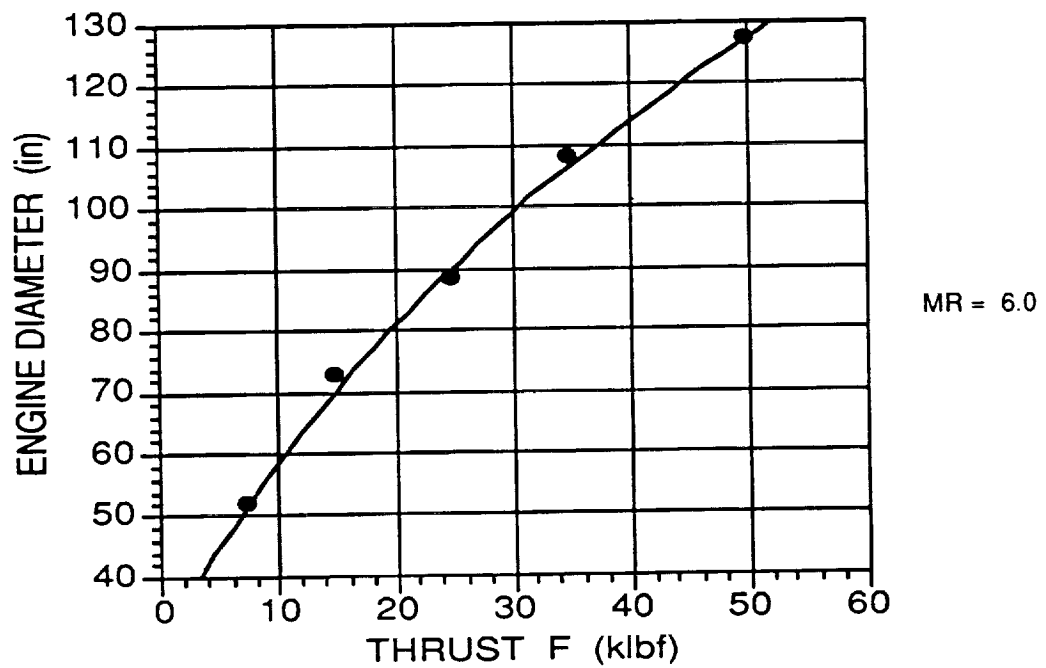


Figure 13: Advanced Engine Parametrics, Engine Diameter Versus Thrust

In addition to the thrust variations, a parametric scan of on-design mixture ratio (MR) was conducted. Mixture ratios of 5:1 and 7:1 were investigated to complement the 6:1 MR data at thrust levels of 7.5, 15 and 50 klbf. Specific Impulse and chamber pressure data from this study are represented in Figures 14 and 15. The trends seen were similar at all three thrust levels. Off-design engine cycle balances were also generated at MR's of 5.0:1 and 7.0:1 at the 7.5, 15, 25, 35 and 50 klbf thrust levels. A table of results from this parametric scan are in Table 7.

On-design parametric data were also generated over a range of nozzle area ratios from the end of the regeneratively cooled nozzle section to an area ratio of 1200. These parametrics were generated at each of the five thrust levels addressed above. Output data for these parametric scans included engine performance, envelope, and weight, and are listed in Table 8. All said parameters were seen to increase with area ratio as expected.

In the next phase of the program, a thrust level of 20 klbf was chosen under direction from NASA LeRC for engine requirement variation studies. These studies investigated the effects of increasing the throttling requirement from 10:1 to 20:1, and requiring the engine to operate at a maximum MR of 12:1. The methodologies used to gauge these effects and modify the engine if necessary to achieve these more stringent requirements are outlined in Figures 16 and 17 respectively.

Initial studies revealed that the baseline configuration which evolved out of the D.1 through D.5 advanced engine studies was incapable of operating at MR's above 9:1 due to insufficient power supplied to the oxidizer turbine. This situation was remedied by a flow circuit change and by incorporating additional LOX turbine bypass reserve at the on-design operating point. The flow circuit was altered by mixing the fuel turbine bypass flow with the fuel turbine exit flow after passing through the heat exchanger instead of mixing this flow with the remainder of the hydrogen just upstream of the injector. The new engine flow schematic is depicted in Figure 18. The schematic change, together with the increased on-design LOX turbine bypass, gave the LOX turbine enough power to operate at MR's up to the desired 12:1 ratio.

In addition to the off-design engine cycle balances generated at the extreme conditions, individual component analyses were conducted to identify potential problems encountered at the high MR and deep throttled operating points. Pump operating points were plotted on head-flow diagrams to verify stability. Propellant thermodynamic properties through the

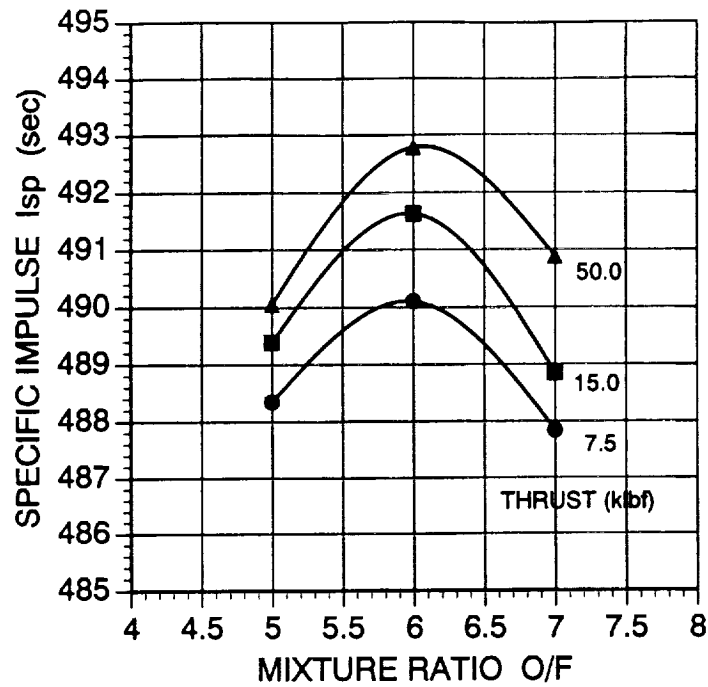


Figure 14: Advanced Engine Parametrics, I_{sp} Versus Mixture Ratio

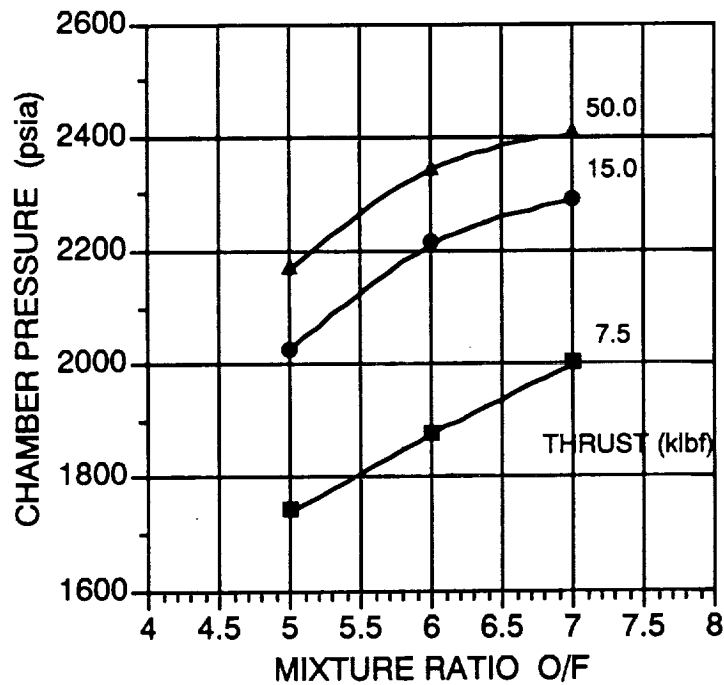


Figure 15: Advanced Engine Parametrics, Chamber Pressure Versus Mixture Ratio

Table 7: Thrust Parametrics Off-Design Mixture Ratio Scans

F (klbf)	MR (None)	Pc (psia)	Is (sec)	Lext (in)	Lret (in)	Diam. (in)
7.5	5	1941	489.82	110.6	56.8	51.5
7.5	6	1876	490.10			
7.5	7	1828	485.30			
15	5	2286	490.64			
15	6	2009	491.63	146.2	74.6	72.8
15	7	2147	487.83			
25	5	2442	491.21			
25	6	2360	492.34	183.8	93.4	88.2
25	7	2292	488.93			
35	5	2403	491.25			
35	6	2322	492.56	217.2	110.1	108.3
35	7	2253	489.36			
50	5	2425	491.39			
50	6	2343	492.78	262.8	132.9	127.5
50	7	2273	489.81			

Table 8: Expansion Area Ratio Parametrics

Thrust, Klb. (vac)	∈ Overall/ break	P _C , psia	Is, vac (sec)	L _{ext} , in	L _{ret} , in	D _{ext} , in	Weight lb.
7.5	1200/600	1876	490.79	114.1	66.3	54.8	291
7.5	900/600	1876	488.90	101.6	73.0	47.5	278
7.5	600/600	1876	488.49	86.7	86.7	38.8	248
15	1200/600	2209	492.04	146.7	84.4	71.4	414
15	900/600	2209	490.14	130.5	93.1	61.9	389
15	600/600	2209	489.65	111.0	111.0	50.6	334
25	1200/600	2360	492.38	181.4	103.7	89.1	588
25	900/600	2360	490.51	161.1	114.5	77.3	548
25	600/600	2360	489.80	136.8	136.8	63.2	469

Table 8: Expansion Area Ratio Parametrics (contd.)

Thrust, Klb. (vac)	€ Overall/ break	P _c , psia	I _s , vac (sec)	L _{ext} , in	L _{ret} , in	D _{ext} , in	Weight lb.
35	1200/600	2322	492.37	214.4	121.7	106.3	812
35	900/600	2322	490.50	190.2	134.7	92.2	736
35	600/600	2322	489.72	161.3	161.3	75.4	636
50	1200/600	2343	492.29	254.3	144.1	126.4	1168
50	900/600	2343	490.44	225.6	159.5	109.7	1040
50	600/600	2343	489.61	191.2	191.2	89.6	906

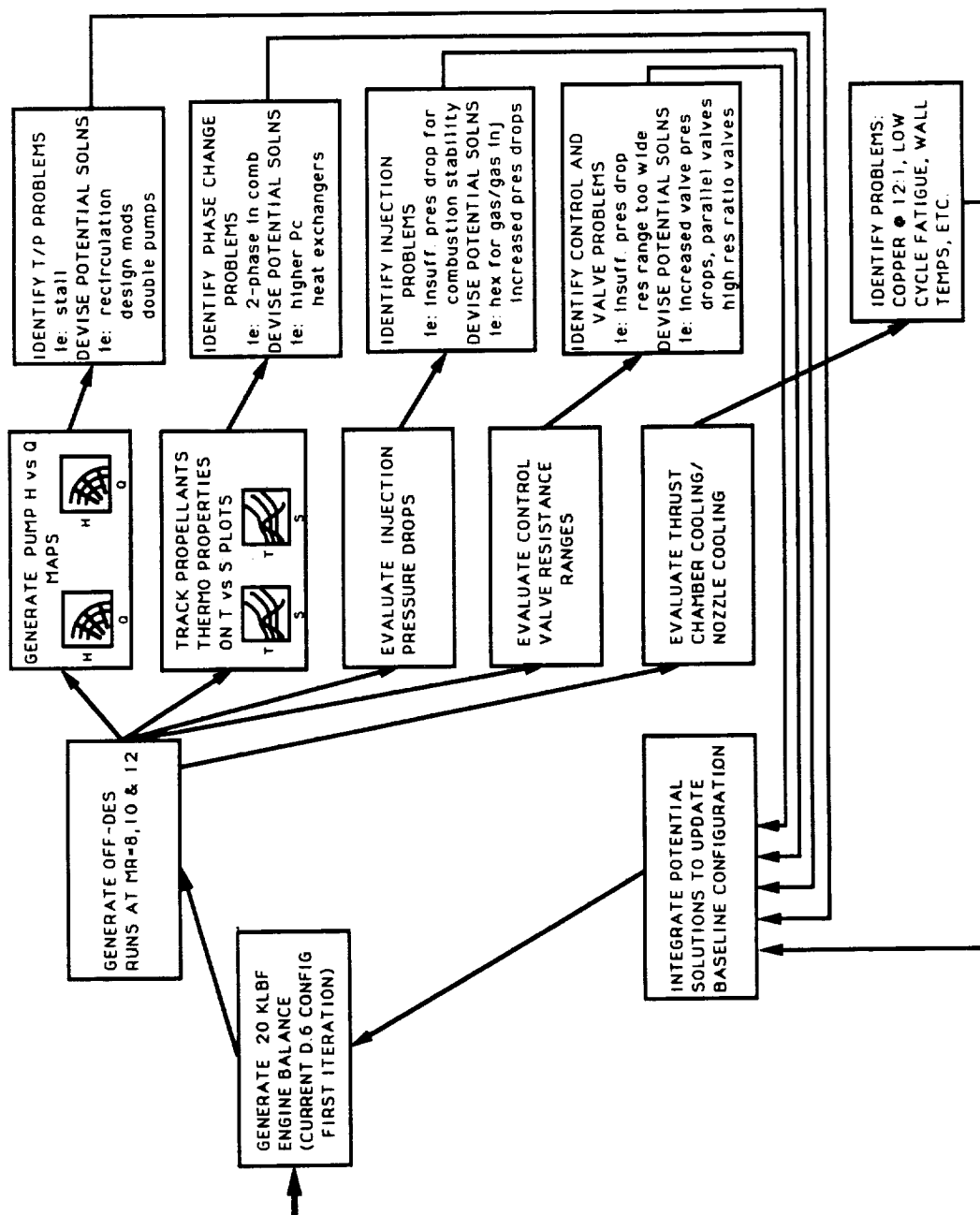


FIGURE 16: Advanced Engine Study Task D.6 Engine Variation Studies - 6:1 & 12:1 Mixture Ratio

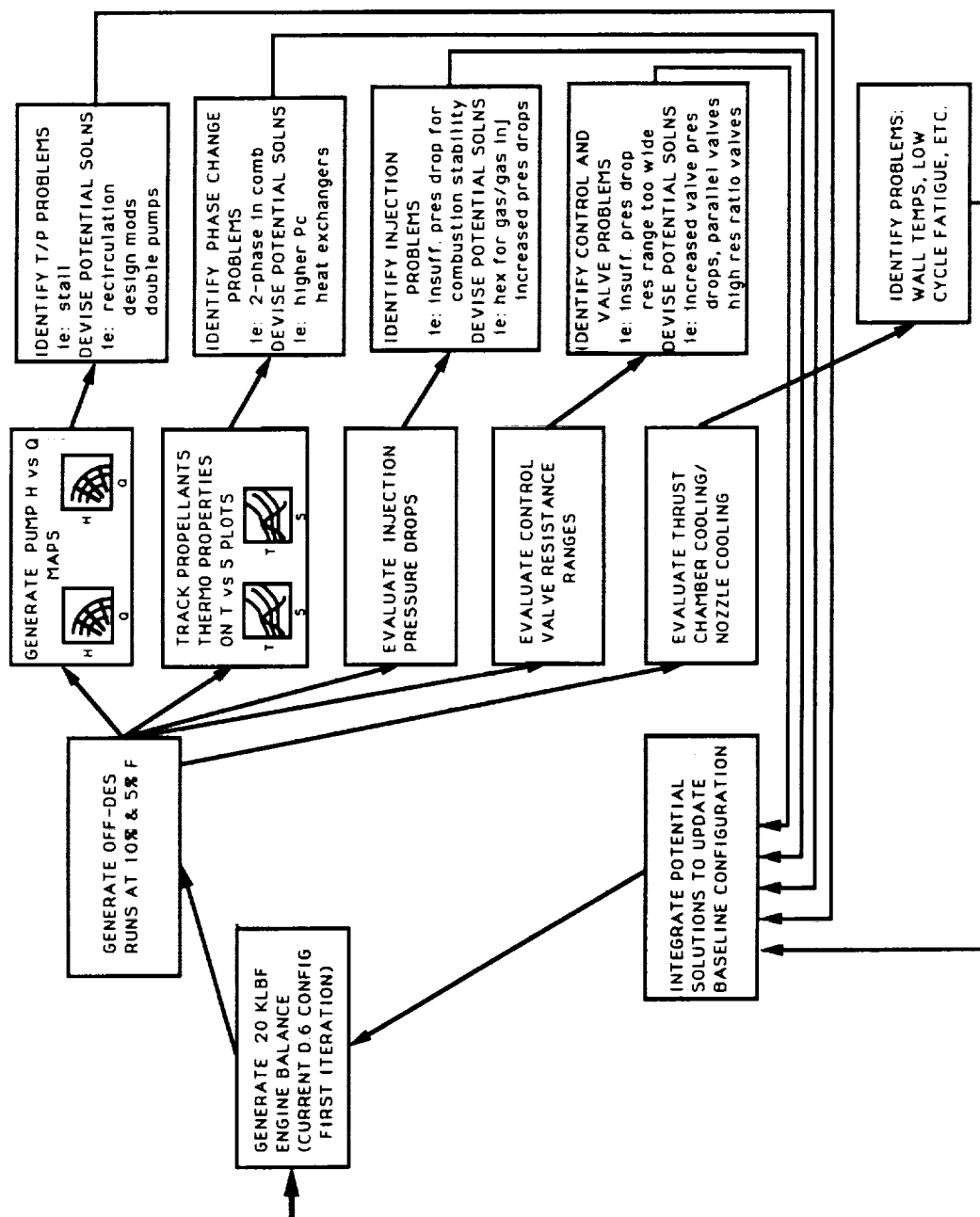


FIGURE 17. Advanced Engine Study, Task D.6 Engine Variation Studies - 20:1 Throttling

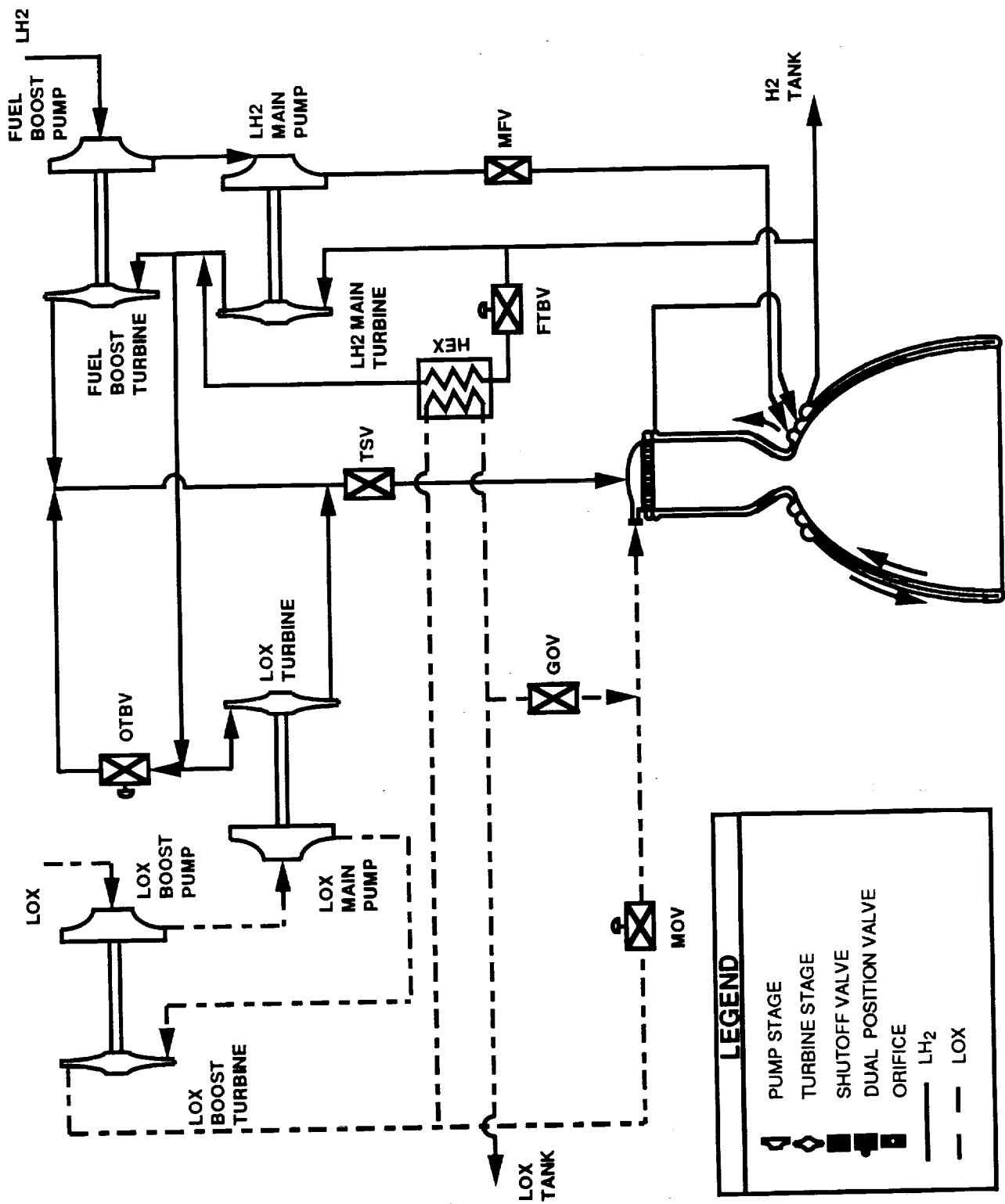


Figure 18: Revised OTVE Turbine Bypass Reroute Schematic for MR up to 12:1

engine were plotted on T-S diagrams to ensure two phase transition problems were avoided. Valve resistance ranges and system pressure drops were checked for violation of accepted limits. Thrust chamber and nozzle material temperatures were also tracked to ensure structural integrity.

Having defined the engine system, necessary technologies to be developed before the OTVE could be put into operation were identified. Demonstration requirements for these technologies were listed. Manufacturing issues and impacts to the engine system were also addressed.

TASK B - TURBOMACHINERY TECHNOLOGIES

In Task B, the most promising turbomachinery technologies for OTV sized engines were explored. These included two stage partial admission turbines (subtasks B.1 and B.4), high velocity ratio diffusing crossovers (subtask B.2), soft wear ring seals (subtasks B.3 and B.5), advanced bearing concepts (subtask B.6) and a fuel pump rotordynamic analysis (subtask B.7).

Two Stage Partial Admission Turbines

Performance of the small, high power, low pressure ratio turbines required for the expander cycle upper stage rocket engines of the future is crucial to meeting overall OTVE performance requirements. For this size high pressure fuel pump, a two stage turbine was found to be the best compromise between performance and life of the turbopump. Analysis found that partial admission also improved turbine performance by increasing the hub to tip ratio. The OTVE two stage partial admission turbine was designed as two single stage subsonic impulse stages with the kinetic energy of the first stage rotor discharged directly into the second stage nozzle to minimize staging losses. Because very little data on this turbine type existed, full scale testing was planned in subtasks B.1 and B.4.

The objectives of these subtasks were to (1) verify the two stage partial admission turbine analytical predictions by conducting laboratory tests using ambient (room temperature) gaseous nitrogen, (2) update analytical performance prediction methods for future designs of similar low thrust engine turbines and (3) provide baseline data for comparison with the

OTV MK49-F turbine for possible performance enhancement by minor hardware modifications.

Turbine design requirements were derived from an expander cycle engine balance using the MK49-F turbopump. In constructing the test apparatus, all available MK49-F turbine hardware, such as the turbine and exhaust housing, was used for ease of comparison and shortened fabrication time. In addition, most of the tester hardware was machined from aluminum to avoid design and fabrication complexities.

A layout of the turbine tester is shown in Figure 19 with major features labeled. To minimize test turnaround time and maintain good test-to-test performance correlations, a movable second stage nozzle remote-controlled system was devised to change the first to second stage nozzle angulation during a single test period. Nozzle arcs of admission were changed by plugging, or unplugging, discrete numbers of nozzles by the use of silicon rubber. Even numbers of nozzle passages were plugged 180 degrees apart from each other to prevent radial loads. Instrumentation locations to measure performance parameters on the tester are given in Figure 20.

A total of thirteen tests were conducted in three phases accumulating approximately 36 hours of run time on the rotor assembly. The original test matrix is presented in Table 9, but testing deviated somewhat from this plan to accommodate hardware and schedule modifications. The test objectives were still satisfied, but a slightly lesser range of nozzle angulation was tested, very low arcs of admission were investigated, and the laser velocimeter tests were canceled due to budget and schedule constraints.

In the new test series, nozzle angulations from plus 40 to minus 30 degrees from the designed nozzle angulation (40 degrees arc separation) were tested. First stage nozzle arc of admission variation ranged from a high of 37.4 percent (10 nozzle passages - 5 per side) to a low of 6.9 percent (2 nozzle passages - 1 per side). Second stage arc of admission varied from 84.4 percent (26 nozzle passages - 13 per side) down to 12.9 percent (4 nozzle passages - 2 per side).

An example of the resulting efficiency vs. velocity ratio (U/Co) graph generated for 0 degrees nozzle angulation is given in Figure 21. A sample equivalent flowrate vs. equivalent pressure ratio graph for the same test conditions is shown in Figure 22. Performance of the turbine at design conditions was approximately 7.9 percent higher than

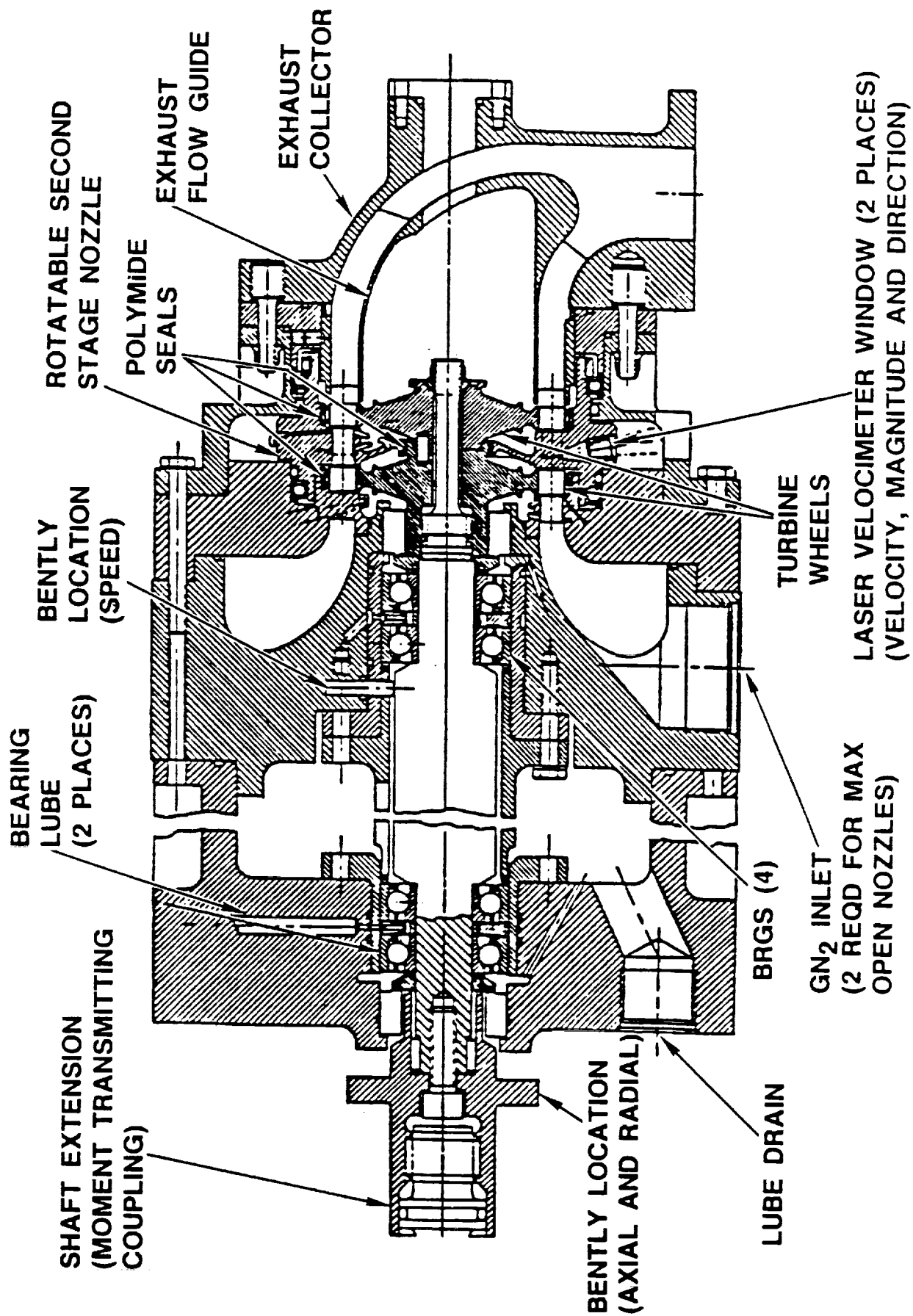


Figure 19: Two-Stage Partial Admission Turbine Tester

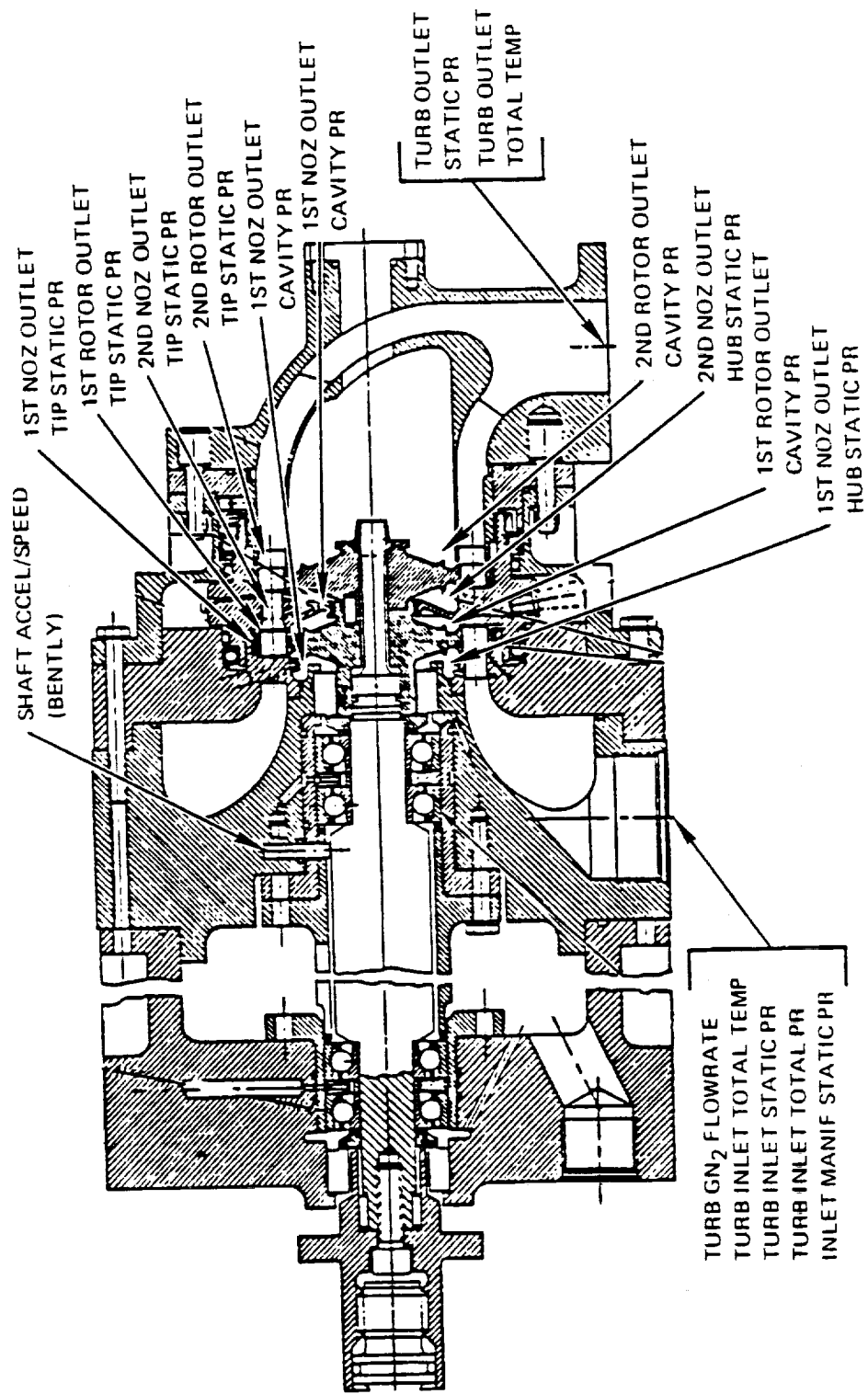
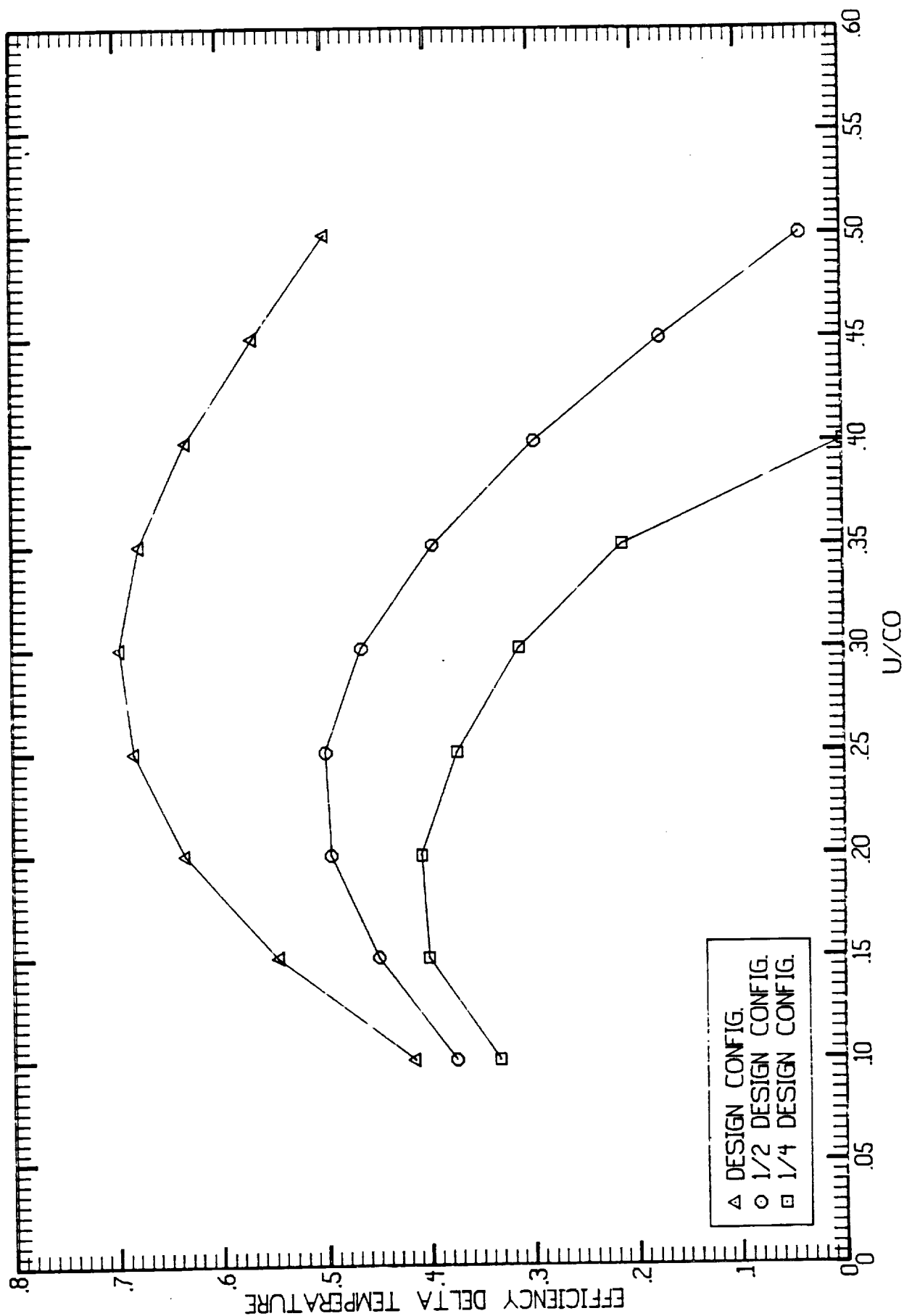


Figure 20: Turbine Tester Instrumentation Parameter Locations

Table 9: Two-Stage Partial Admission Turbine Test Matrix

TEST DAY	PHASE/TEST NO.	ARC OF ADMISSION		2ND STAGE NOZZLE POSITION VARIATION	PRIMARY OBJECTIVES		SECONDARY OBJECTIVES		REMARKS
		1ST STAGE	2ND STAGE		PRESSURE RATIO	ROTOR SPEED, KRPM	PRESSURE RATIO	ROTOR SPEED, KRPM	
1	1/1	34.5	45.2	0	N/A	21,31	N/A	10,15,25	TARE TEST WITH TURBINE REPLACEMENT DISC SYSTEM SAFETY, INSTRUMENTATION CHECKOUT
2	2/1	34.5	45.2	-40 TO +40	1.6,1.76	21	1.3,2.0	15,25,31	DESIGN ARCS OF ADMISSIONS, FLOWGUIDE REMOVED, PRESSURE RATIO MAPPING, NOZZLE ANGULATION MAP. PING, OPTIMUM NOZZLE ANGULATION – MAX EFFICIENCY
3	3/1	34.5	45.2	-40 TO +40	1.6,1.76	21	1.3,2.0	15,25,31	SAME AS 2/1 EXCEPT FLOWGUIDE INSTALLED
4	4/1	13.8	19.4	-40 TO +40	1.6,1.76	21	1.3,2.0	15,25,31	UNDERSIZE ARC OF ADMISSION, FLOWGUIDE INSTALLED, PRESSURE RATIO MAPPING, NOZZLE ANGULATION MAPPING, OPTIMUM NOZZLE ANGULATION – MAX EFFICIENCY
5	5/1	48.3	83.9	-40 TO +40	1.6,1.76	21	1.3,2.0	15,25,31	SAME AS 4/1 EXCEPT LARGER ARCS OF ADMISSION
6	6/1	34.5	45.2	TBD	1.6,1.76	21	1.3,2.0	15,25,31	LASER VELOCIMETER FLOW. FIELD MEASUREMENTS AT DESIGN ARC OF ADMISSION, PRESSURE RATIO MAPPING, FLOWGUIDE INSTALLED



**Figure 21: Two-Stage Partial Admission Turbine Efficiency vs. Velocity Ratio
(0 Degrees Nozzle Variation)**

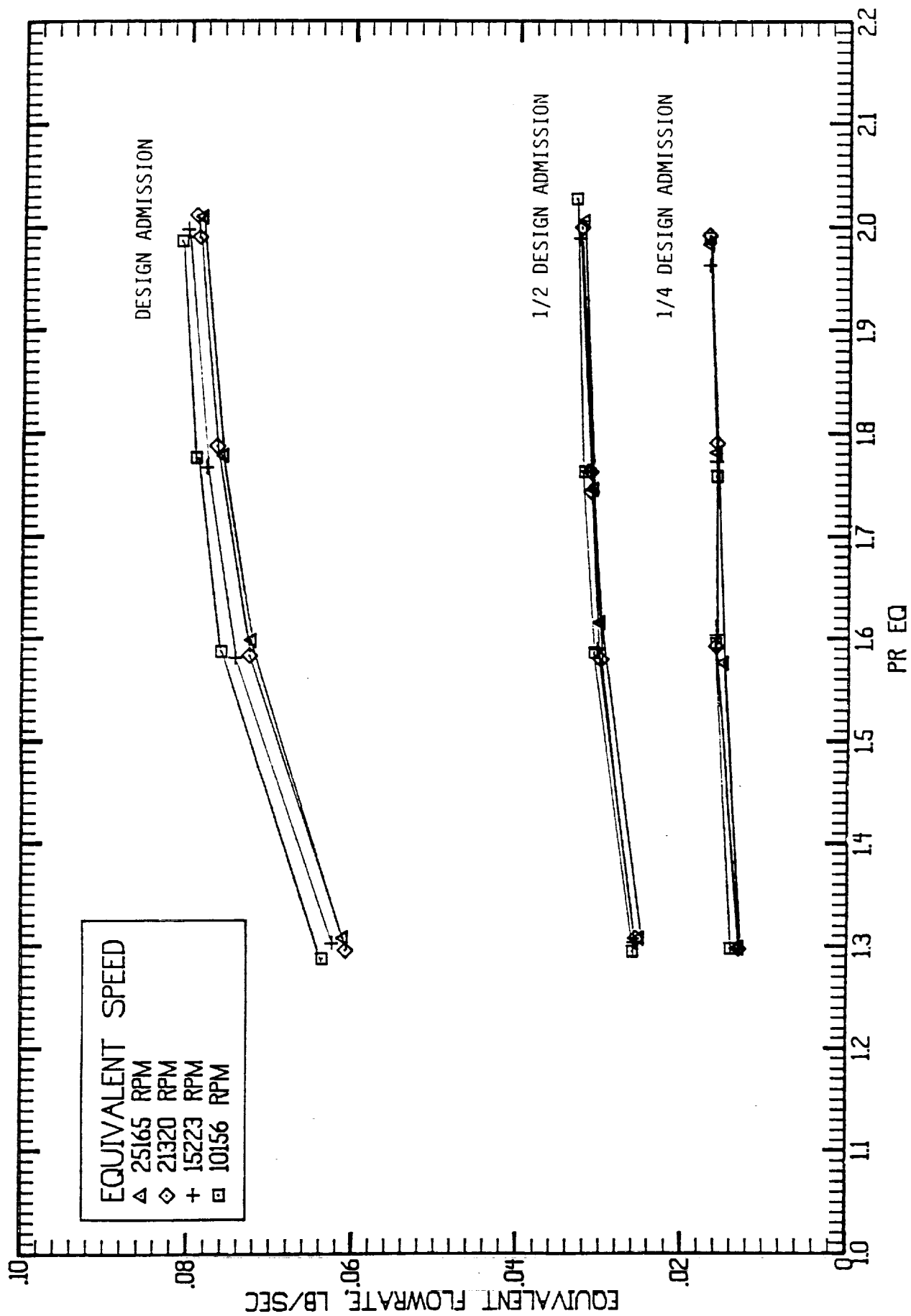


Figure 22: Two-Stage Partial Admission Turbine Equivalent Flowrate vs. Equivalent Pressure Ratio (0 Degrees Nozzle Variation)

originally predicted, probably attributable to a higher loss predicted for turbine windage losses. Effects and trends of nozzle arc of admission variation were generally as expected with the lowest performance coincident with the lowest arc of admission. In addition, large deviations from the design nozzle angle setting produced the lowest performance. Turbine pressure ratio variations (1.3 to 2.0) had little effect on the overall turbine performance.

The data generated in this subtask substantially verified the turbine performance prediction methods used at Rocketdyne. It was also found that minor nozzle to nozzle angulation changes could be made to attain the highest performance of the MK49-F turbine according to the test results.

High Velocity Ratio Diffusing Crossovers

Multistage pumps require the use of crossover passages to convey the fluid from the exit of one impeller to the inlet of the next. To develop the high discharge pressure necessary for the advanced expander cycle OTVE, a high impeller exit velocity was required. A relatively low velocity, however, was required at the inlet of the next impeller for the best overall performance. The solution was a large diffuser inlet to outlet velocity ratio through the crossover, such as in the MK49-F pump, a component of the 15,000 lbf OTVE which uses seventeen diffusion passages at a velocity ratio approaching the diffusion limit for stable design of 6.23.

With the MK49-F high diffusion rate, boundary layer flows had to be carefully controlled to preclude stall while operating over a wide range of pump flows. The design was based on advanced analysis anchored by tests of stationary two dimensional diffusers with steady flows. To accurately assess the design, however, a more accurate simulation of the impeller flow was necessary to correctly evaluate the unsteady, non-uniform flow fields and potentially large inlet boundary layers.

Subtasks B.2 and B.4 further investigated the performance of high velocity ratio diffusing crossovers used in the first and second stages of the MK49-F high pressure fuel turbopump. The crossover portion of this pump is pointed out in Figure 23. The different crossover sections are also labeled in Figure 24. With the diffuser inlet conditions generated by a scaled up model of the MK49-F inducer and impeller, the performance of these pumping elements and the high velocity ratio diffusing crossover were accurately

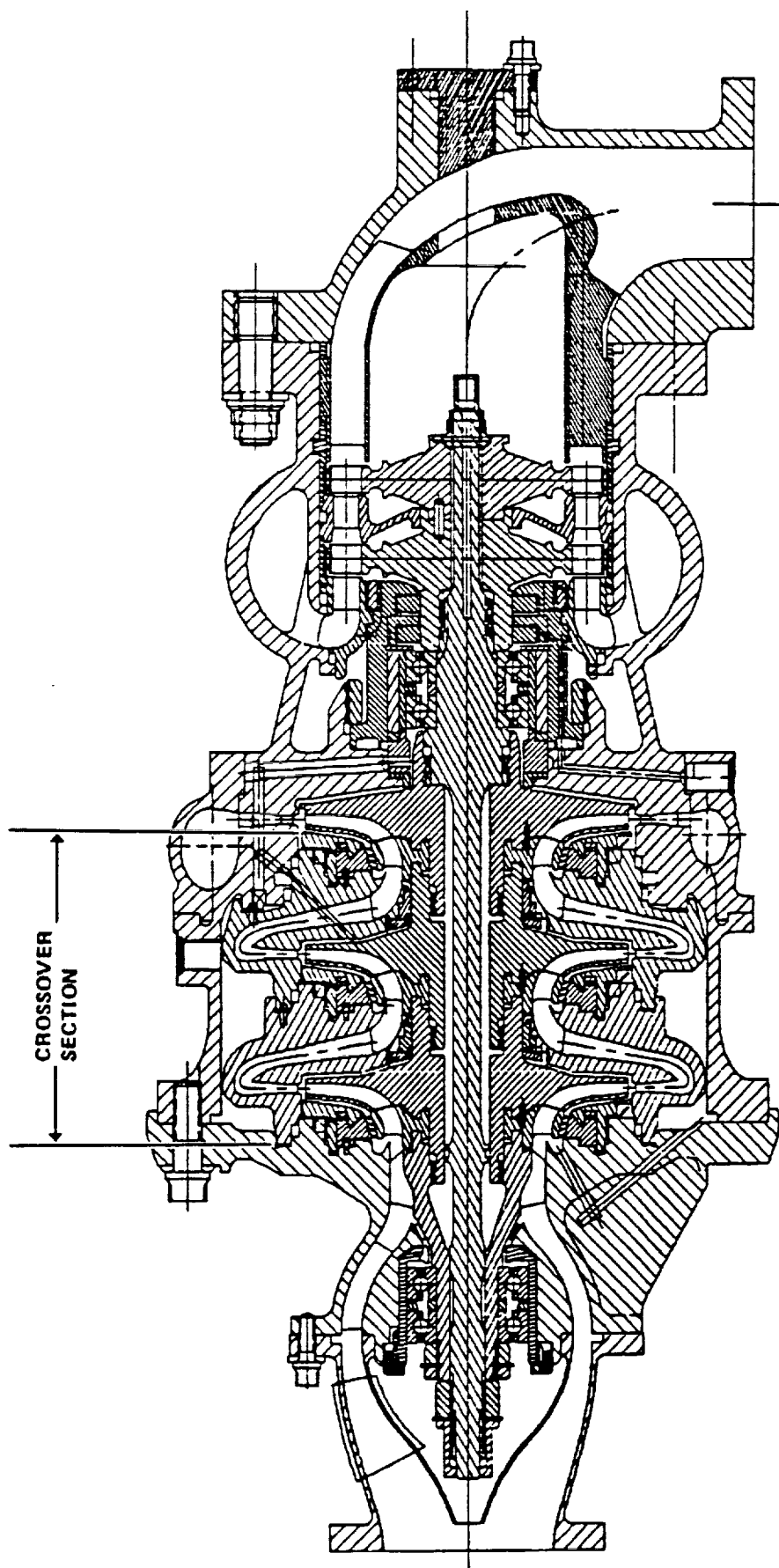


Figure 23: MK49-F High Pressure Liquid Hydrogen Turbopump Crossover Section

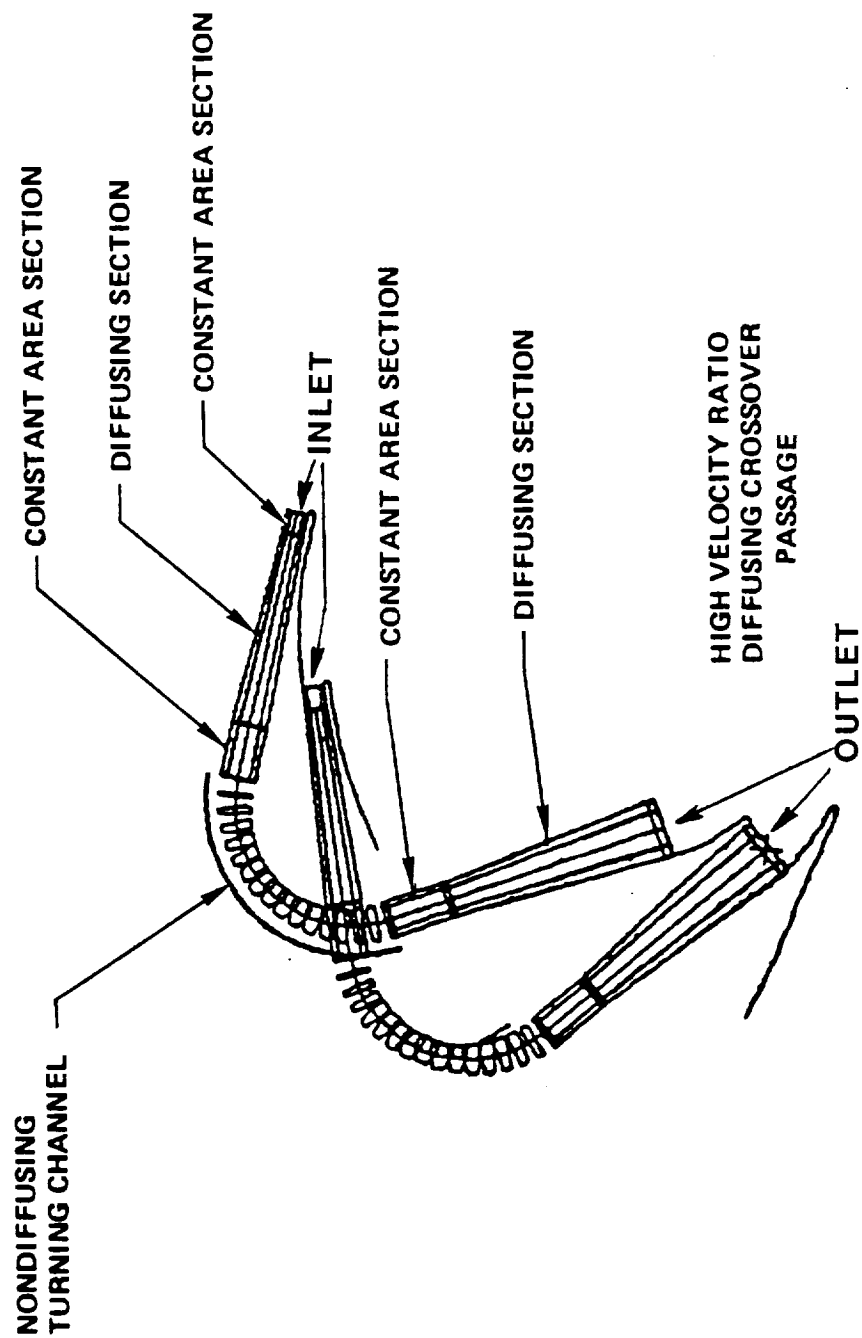


Figure 24: High Velocity Ratio Diffusing Crossover Passages

determined using water and air as the pumped fluids. The air tests were included to obtain performance data over a wide range of Reynold's number.

These performance surveys were planned in order to verify the design of the high velocity ratio diffusing crossover, and correct any design deficiencies. Since the MK49-F was tested prior to the completion of this test program, the data from the MK49-F was used as a comparison for the water and air test data.

Existing SSME HPFTP tester hardware was used to save design and fabrication costs. A scaled MK49-F inducer, impeller, and diffuser crossover system, were designed, fabricated, and integrated into the tester. Additional costs were saved by fabricating the new crossover tester components from aluminum, thus minimize machining complexities and procurement costs. A layout of the crossover tester showing instrumentation locations is depicted in Figure 25.

A total of nine tests were conducted. The first two tests of the diffusing crossover were conducted in air, while the remaining seven tests were conducted in water. Both, the air and water tests were conducted at 6322 rpm. A test matrix defining these experiments is presented in Table 10.

In air, the head versus flow (H-Q) test data determined that the upcomer diffuser in the crossover was stalled for all the flow conditions attempted. The stall was caused by increased boundary layer blockage due to the low Reynold's number resulting in the impeller discharge flow entering the diffuser inlet at an angle and velocity which would produce a flow separation in the diffuser. Air test data compared well with the analytic predictions and MK49-F hydrogen data for the impeller and inducer head performance, clearly showing that the stall was in the diffuser.

H-Q tests in water, from 65 to 140% of design flow, were conducted. The overall stage head measured in these tests was only 4% lower than the prediction as seen in Figure 26. Again, the performance of the inducer and impeller were compared with the available resources. During the H-Q tests, the upcomer diffuser stall point was determined to be at a somewhat lower flow than predicted, and the hysteresis region was clearly evident. The head loss during stall was not severe, which was indicative of a leading edge stall characteristic. Internal pressure distributions were also examined to evaluate the inducer, impeller, and various positions within the diffuser crossover system. Suction performance

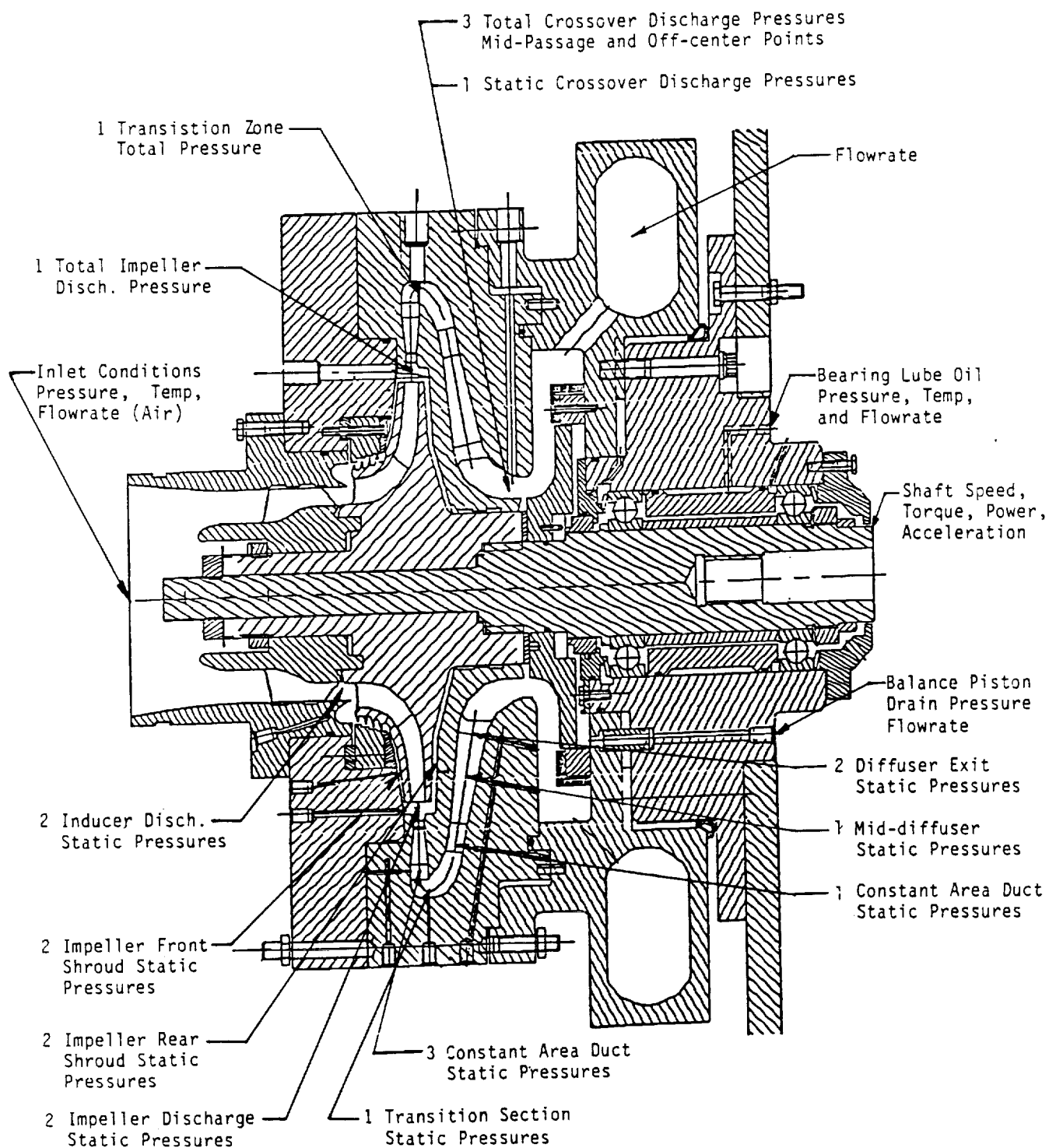


Figure 25: High Velocity Ratio Diffusing Crossover Tester Instrumentation

Table 10: High Velocity Ratio Diffusing Crossover Test Matrix

TEST NO.	TEST TYPE	TEST FLUID	FLOW (GPM)	TEST DESCRIPTION	SPEED (RPM)	DATA SAMPLING	PROBE TYPE
1	CHECK OUT	H2O	582	ESTAB AXIAL LOAD	6322	20 SCANS	KIEL
2	HEAD vs. FLOW	H2O	408-694	H-Q W/ PROBE	6322	20 SCANS	KIEL
3	H-Q STALL MAPPING	H2O	233-408	HQ 60-90%	6322	20 SCANS	KIEL
4	CAVITATION	H2O	582	NPSH @ 100%	6322	CONTINUOUS	KIEL
5	CAVITATION	H2O	640	NPSH @ 110%	6322	CONTINUOUS	KIEL
6	CAVITATION	H2O	698	NPSH @ 120%	6322	CONTINUOUS	KIEL
7	CAVITATION	H2O	523	NPSH @ 90%	6322	CONTINUOUS	KIEL
8	CAVITATION	H2O	465	NPSH @ 80%	6322	CONTINUOUS	KIEL
9	CAVITATION	H2O	407	NPSH @ 70%	6322	CONTINUOUS	KIEL
10	CAVITATION	H2O	349	NPSH @ 60%	6322	CONTINUOUS	KIEL
* 11	PROBE SURVEY POS#1	H2O	408-694	HQ 70-120%	6322	20 SCANS	YAW
* 12	PROBE SURVEY POS#2	H2O	408-694	HQ 70-120%	6322	20 SCANS	YAW
* 13	PROBE SURVEY POS#3	H2O	408-694	HQ 70-120%	6322	20 SCANS	YAW
TEST NO.	TEST TYPE	TEST FLUID	FLOW (CFS)	TEST DESCRIPTION	SPEED (RPM)	DATA SAMPLING	PROBE TYPE
14	HEAD vs. FLOW	AIR	0.91-1.56	H-Q W/ PROBE	6322	20 SCANS	KIEL

* These tests were later deleted

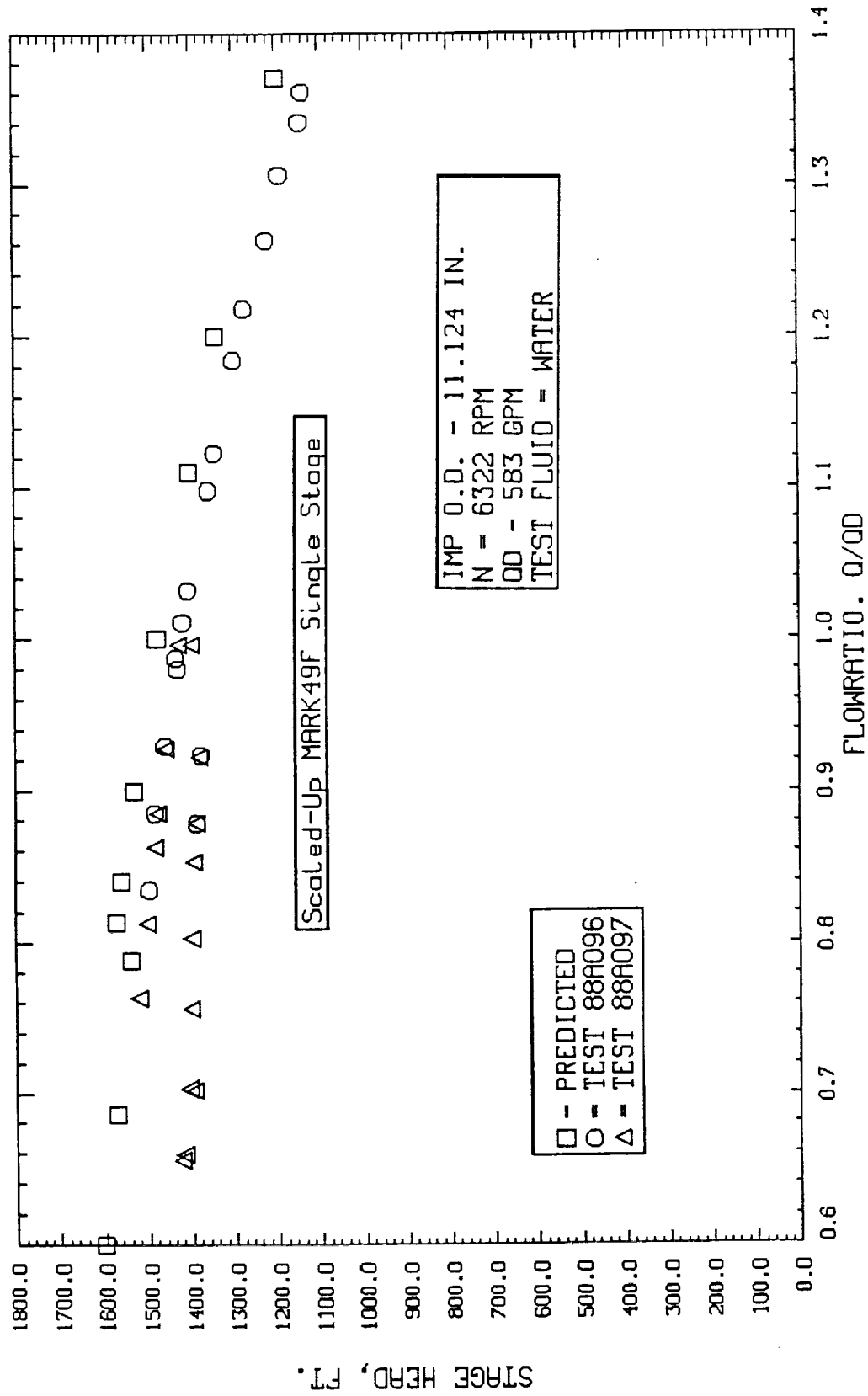


Figure 26: Scaled MK49-F Stage Head in Water vs. Flow Ratio

tests from 80% to 124% of design flow were conducted, which established the minimum inlet Net Positive Suction Head (NPSH). The performance was lower than the ideal potential, but a lower performance was expected with the design characteristics scaled from the smaller MK49-F. Test efficiencies vs. predicted values are shown in Figure 27. The performance of the tester exceeded the minimum design requirements of the MK49-F turbopump.

The test data showed 95% of the overall diffusion being accomplished by the upcomer portion of the crossover passage, as predicted. By calculating the required diffuser inlet boundary layer blockage to match the test data and using the Loss Isolation program to determine the vaneless area diffusion, the mean pressure recovery coefficient from the test data compared favorably with the predictions.

The technique generated to analyze the data will be beneficial for the design and analysis of future diffusing crossover passages. The data generated in this test program verified the methods used at Rocketdyne to design and predict the performance of pumping elements and high velocity ratio diffusing crossovers. The data generated will also be of value in further anchoring the predictive codes of other designs.

Soft Wear Ring Seals

The Soft Wear Ring Seal Development Program in subtasks B.3 and B.5 provided a systematic and comprehensive technical approach that explored new polymeric materials for cryogenic turbopump seals. The benefits of soft seals with their tighter clearances is evident from the MK49-F performance data in Table 11. The project plan included a total of five technical and one reporting efforts. The subtask B.3 efforts included:

- 1: Technology Assessment and Requirements Definition
- 2: Material Selection, Design, and Test Plans.

Seal locations within the OTVE pumps are likely to correspond to those in the MK49 turbomachinery. Seal positions for the MK49 fuel pump are shown in Figure 28 and MK49 oxidizer seal positions in Figure 29. Based on the operational requirements passed down from the OTVE systems and the mechanistics listed in Table 12, the turbopump dynamic seal environment required that the soft seal materials maintain certain mechanical,

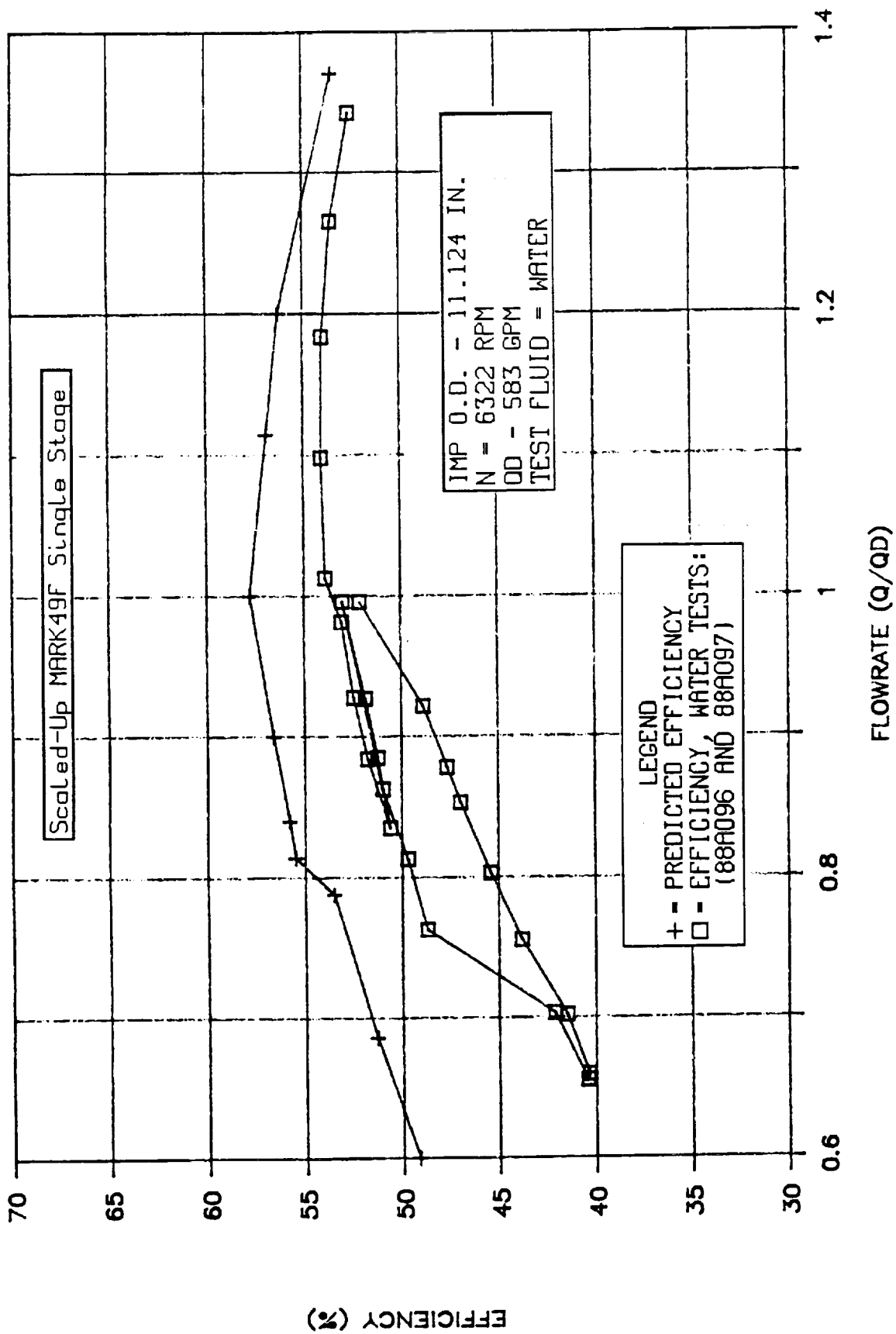


Figure 27: Scaled MK49-F Stage Efficiency in Water vs. Flow Ratio

Table 11: MK49-F Seal Clearance Influence on Performance

IMPELLER AND INTERSTAGE RADIAL SEAL CLEARANCE IN.	PUMP HEAD FT.	PUMP EFF. %	HORSEPOWER	TURB DRG FLOW GPM	BAL PISTON FORCE RANGE POUNDS
0.002	144,056	59.2	1085	14.2	13,606
0.003	130,853	56.8	1080	13.0	12,801
0.004	132,347	54.4	1074	11.4	12,042

NOTE: ROTATING SPEED = 110,000 RPM
DESIGN FLOW RATE

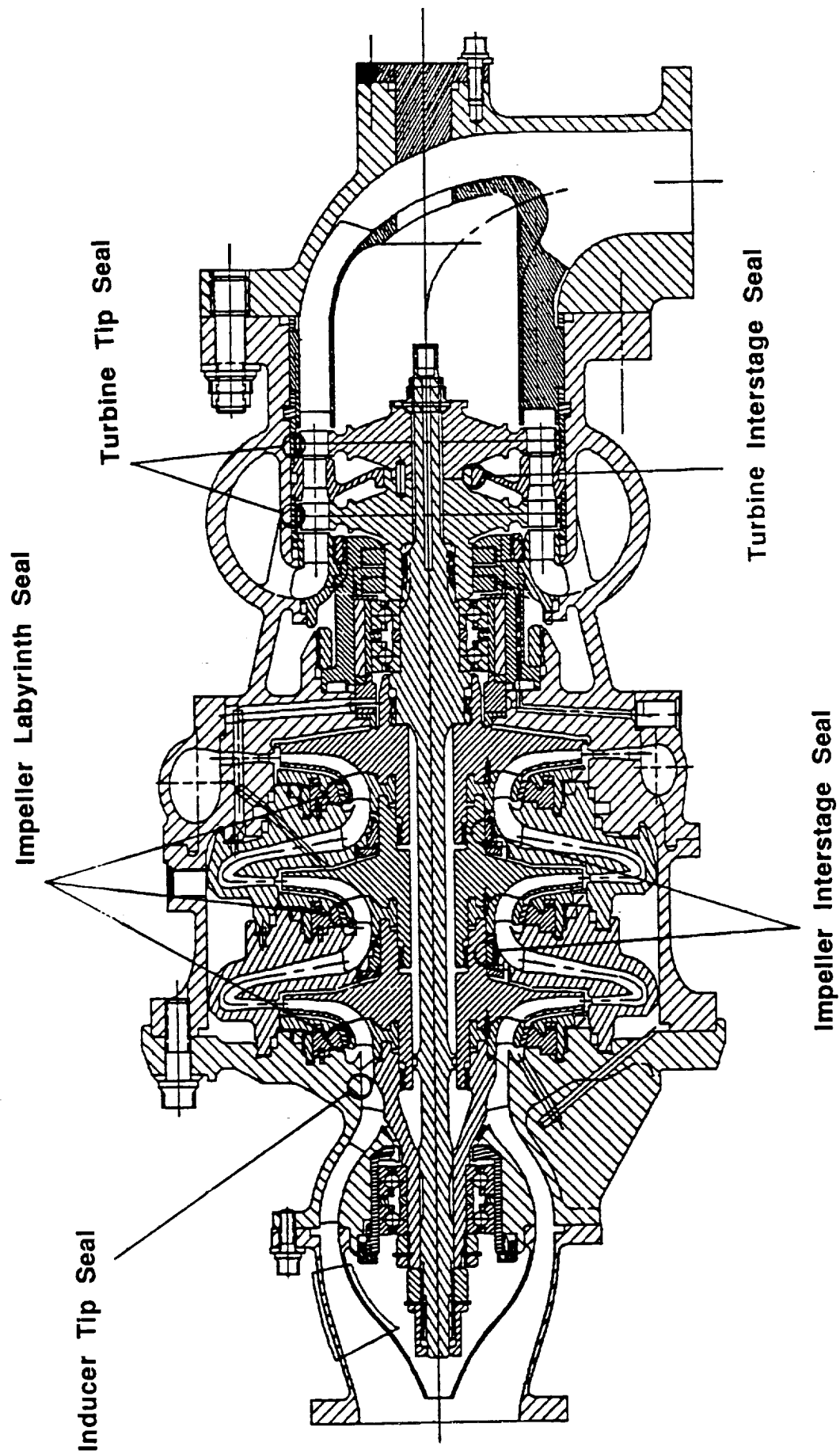


Figure 28: MK49-F Soft Seal Locations

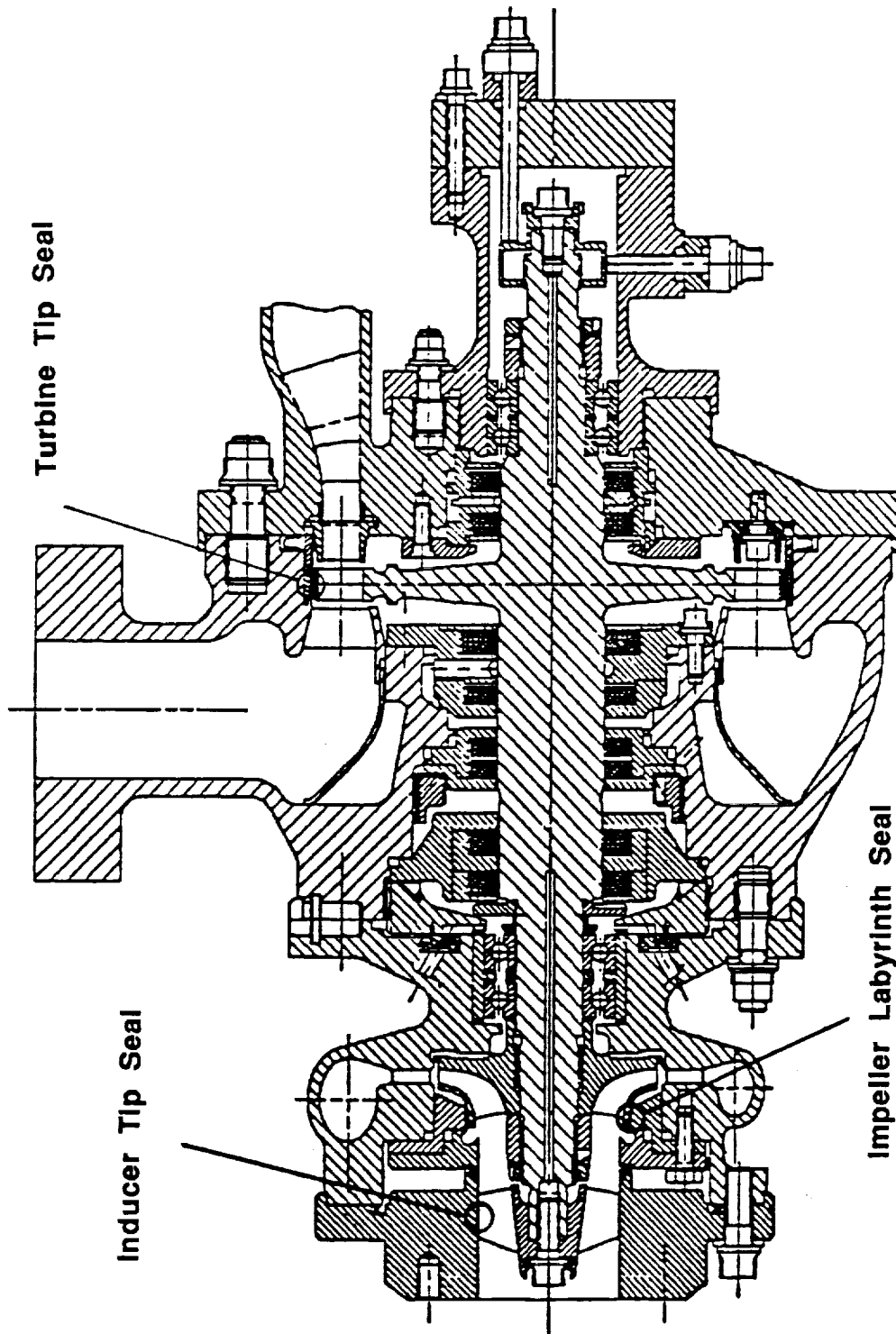


Figure 29: MK49-O Soft Seal Locations

Table 12: Soft Wear Ring Seal Operational Characteristics

THERMAL	RUB ENERGY				ROTORDYNAMICS
	WEAR/ABRASION	IGNITION	MATERIAL PROPERTIES		
CONVECTION	RUB SPEED	ENVIRONMENT	TENSILE STRENGTH	AMOUNT OF DEFLECTION	
FLUID PROPERTIES	DIAMETER	PRESSURE	HARDNESS	BALANCING	
FLOWRATE	RPM	TEMPERATURE	COEFFICIENT OF	CRITICAL SPEEDS	
MATERIAL	RUB AREA	MATERIAL	THERMAL EXPANSION	SUPPORT STIFFNESS	
CONDUCTION	TYPE OF CONTACT	MATERIAL PHASE	DUCTILITY	DAMPERS	
FLUID PROPERTIES	CONTINUOUS	GAS	USABLE TEMPERATURE	HOUSING MODES	
MATERIAL PROPERTIES	INTERMITTENT	LIQUID	RANGE / MELT POINT	ROTOR INCURSION	
RADIATION	RUBBING SWEEP	SOLID		MAXIMUM DEFLECTION	
MATERIAL TEMPERATURE	LOAD	PROPAGATION		OPERATING CLEARANCE	
	ROTOR INCURSION	AVAILABLE FUEL		CLEARANCE STIFFNESS EFFECTS	
	RATE	HEAT BALANCE		STIFFNESS	
	MATERIAL PROPERTIES	RATE OF REACTION		DAMPING	
	HARDNESS	RATE OF OXIDIZER		INCREASED POWER REQUIREMENTS	
	COEFF. OF FRICTION	TRANSPORT		RUBBING	
	STRENGTH	HEAT OF			
	PARTICLE GENERATION	COMBUSTION			
	SIZE				
	LIMITS				
	OPERATIONAL				
	DOWNSTREAM				
	HAZARDS				

thermal, and chemical characteristics to survive. The major Criteria and their importance are listed in Table 13.

Table 13: Major Seal Material Properties Needed

PROPERTY	IMPORTANCE
LOW COEFFICIENT OF FRICTION	LOW HEAT GENERATION
DUCTILITY (3 - 5%)	ABSORB IMPACT, WITHSTAND THERMAL SHOCK
COEFFICIENT OF THERMAL EXPANSION	AS CLOSE AS POSSIBLE TO HOUSING MATERIAL
TENSILE STRENGTH	10 - 20 KSI AT CRYOGENIC TEMPERATURE TO WITHSTAND SEAL PRESSURE GRADIENT, FLOW INDUCED SHEAR LOAD

Initial candidate soft seal materials and their material properties were summarized from tests conducted during and prior to subtask B.3. Based on the results of these tests, a down-selection was conducted, isolating those materials with superior properties in the various turbopump seal applications that had been identified. These selected candidate seal materials included Vespel SP211, Polybon MT747, and Torlon 4301. Kel-F was used as the baseline material for comparison, having already been implemented in the SSME LOX pump seal.

A soft seal Energy Dissipation Factor (EDF) model was formulated which rated these new seal materials based on their mechanical and thermal properties, the particular seal location, and the particular fluid medium. Subtask B.3 was completed when the soft seal test plan and the low speed and high speed friction and wear test rigs were designed.

Due to the sensitivity of LOX environments to heat generation, the test program focused on materials that were identified for a liquid oxygen environment. The test program was to establish the basic chemical compatibility and mechanical survivability attributes of the seal materials. To fully evaluate these candidate materials, autogenous ignition tests, promoted ignition tests, LOX impact tests and low speed friction and wear tests were conducted at

both high and low pressures. Additional tests were planned to evaluate liquid hydrogen turbopump and gaseous hydrogen expander cycle turbine configurations, however they were only partially completed due to test hardware malfunctions.

Upon completion of the technical effort of subtask B.3, the plans for subtask B.5 were formalized. The efforts performed during subtask B.5 included:

- 3: Hardware Fabrication
- 4: Testing
- 5: Data Correlation.

The LOX compatibility test series presented above, including the auto-ignition, promoted ignition, and LOX impact tests were conducted in the test rigs pictured in Figures 30, 31 and 32. These test series identified Kel-F, Vespel SP211, and Polybon MT-747 as demonstrating sufficient resistance to reaction. Torlon 4301 showed more reactivity during the LOX impact tests at 2000 psig, reaching only the 4 kg-m level, while all the other materials achieved at least the 8 kg-m level. Torlon 4301's poorer performance in these tests were grounds for eliminating testing with this material in the low speed friction and wear tester.

An existing frictional heating tester was modified and used to conduct the low speed friction and wear tests at the White Sands Test Facility (WSTF). This tester is pictured in Figure 33. Two types of friction and wear tests, static friction and running friction, were conducted to simulate the characteristics of the different seal operation approaches. A total of 28 tests were conducted at PV products (normal contact pressure times the sliding velocity) ranging from 4,000 to 21,000 psi-ft/sec. These low speed tests were used as a demonstration for the new seal materials as well as a concept verification. Material wear rate, debris size, and frictional heat management of the seal were of particular interest. High speed tests were planned as a final verification of the soft seal concept, but these efforts were not pursued under this contract.

To better correlate the interactions at the rubbing surface from the low speed test data, a 2-D axisymmetric frictional heating model was constructed. Temperature distributions measured within the seal specimen were compared with the output of the model. By adjusting the frictional heat rate input in the model, the seal temperature profiles were

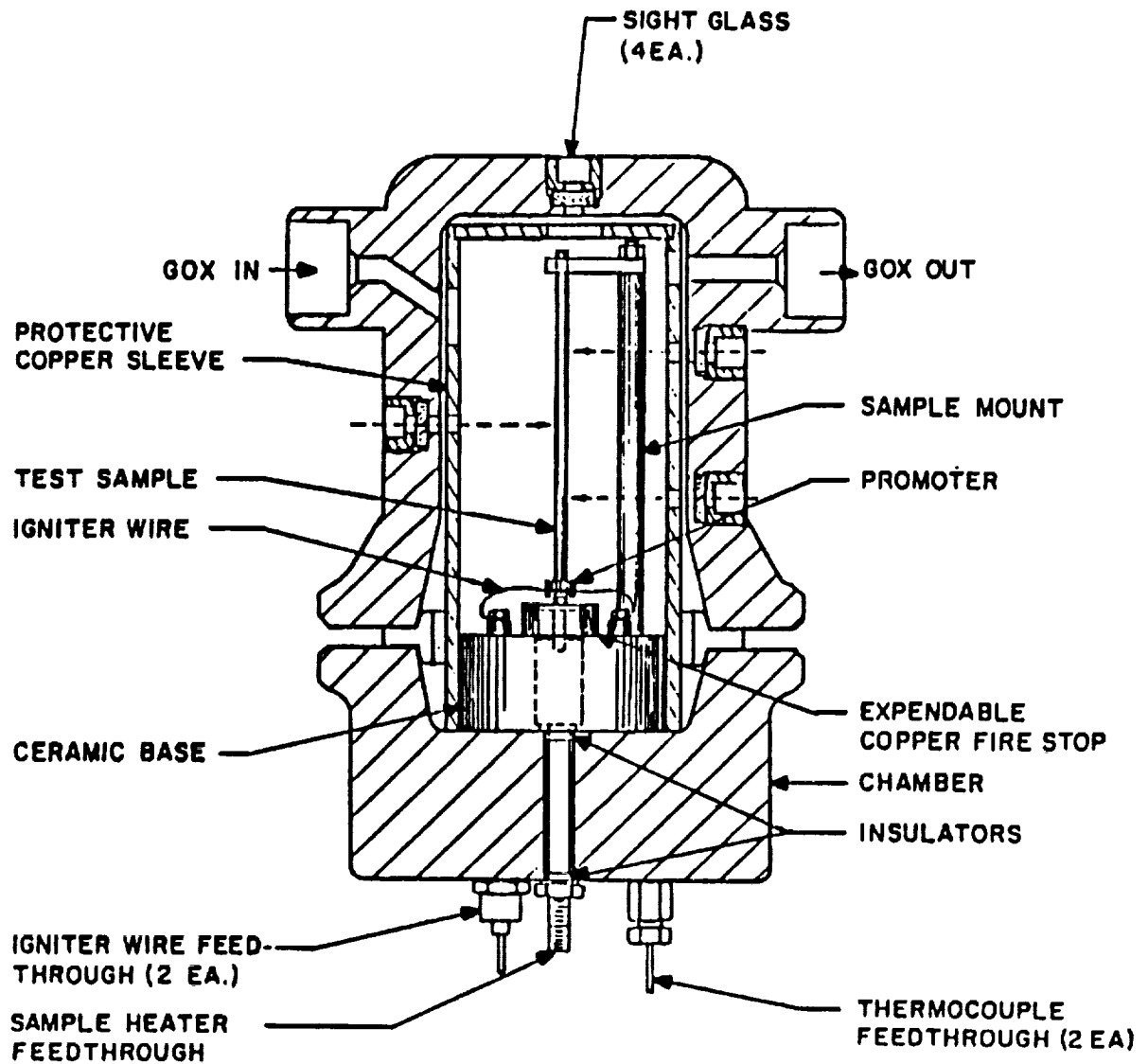


Figure 30: Promoted Ignition Tester

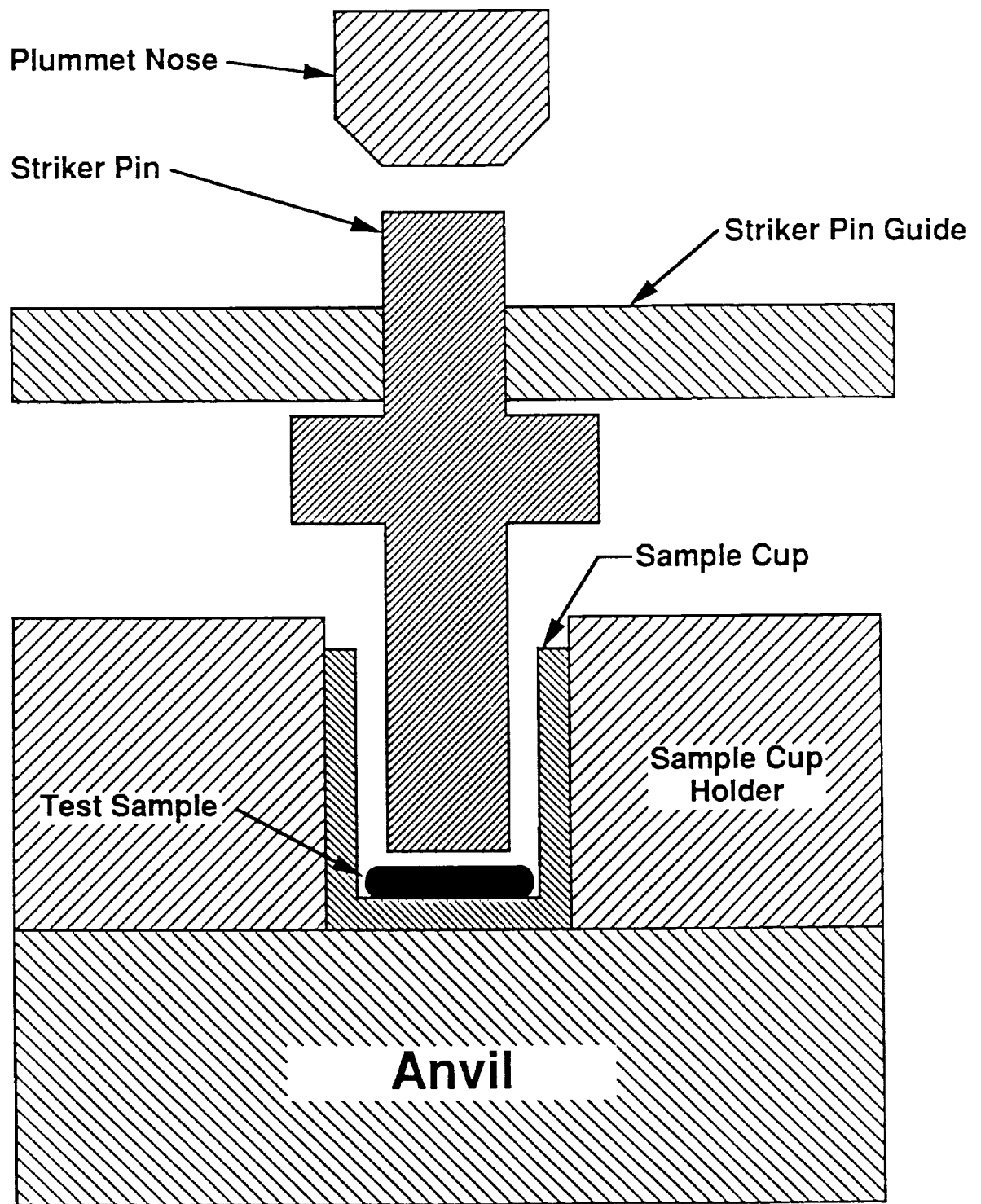


Figure 31: ABMA Oxygen Test Cell

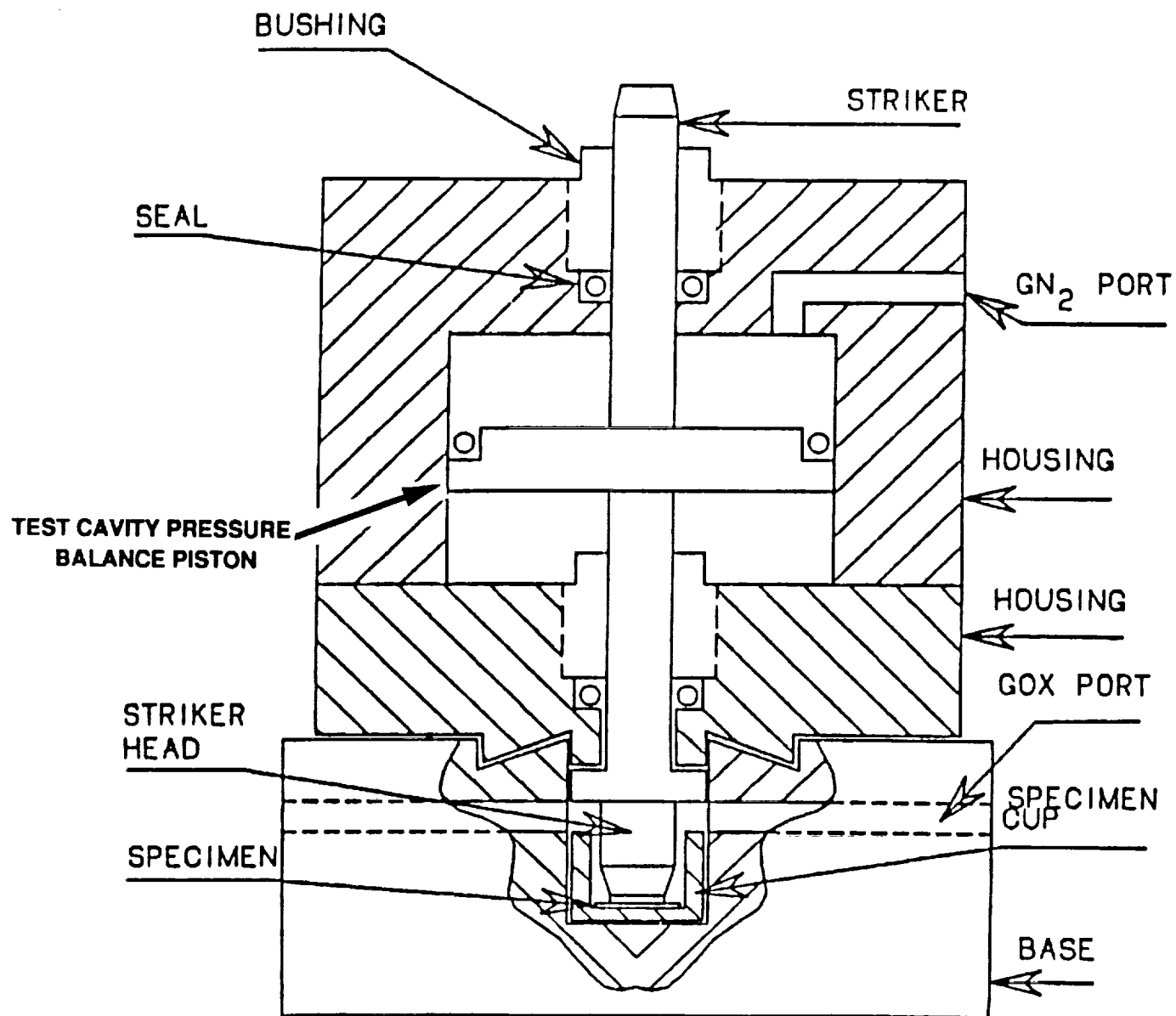


Figure 32: High Pressure LOX Impact Housing

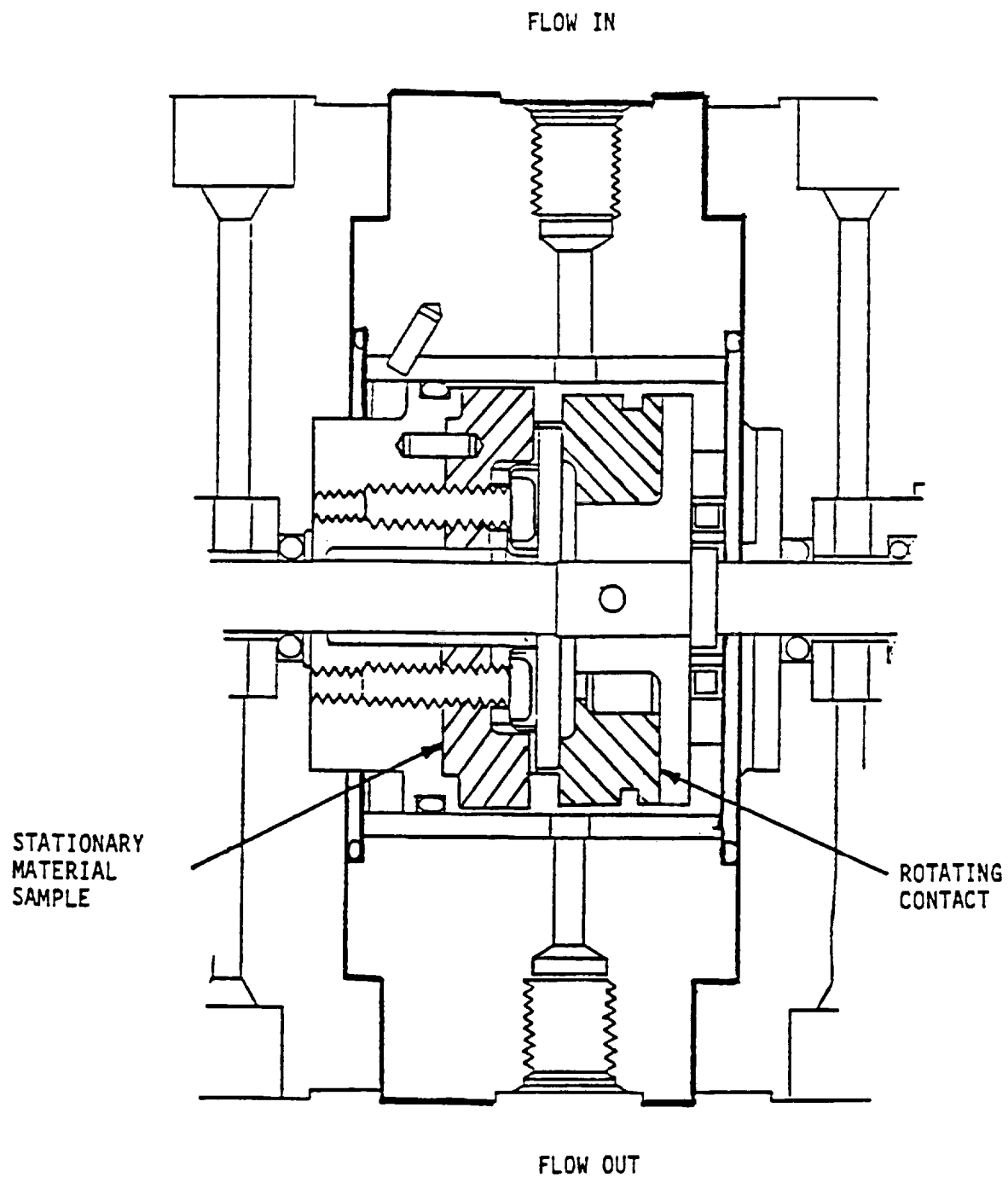


Figure 33: Friction and Wear Test Chamber

matched. This model was used to help isolate the energy dissipation mechanisms consistent with a rubbing contact.

Wear track depths were measured in the seal specimens, and the wear rate correlated with the surface temperatures predicted by the frictional heating model. Specific wear rates were also calculated from the wear track data and were compared with the literature. The specific wear coefficients calculated from the low speed friction and wear tests were an order of magnitude greater than the literature, possibly due to the higher sliding velocities (four orders of magnitude greater) and a highly oxidizing environment.

In general, the data generated by this program helped strengthen the understanding of the rubbing environment within a stationary polymeric seal ring. Due to the unique differences between the polymeric materials used in this program, interesting and varied heat generation and dissipation mechanisms were witnessed. Kel-F produced higher wear and essentially no internal temperature rise, while Vespel SP211 produced low wear and higher internal temperatures. The chemical complexity and differences between the polymers selected increased the difficulty in predicting the specific operational (PV) limitations of these materials. Most importantly, the friction and wear test program demonstrated that an interplay existed between the thermal, mechanical, and chemical characteristics of the soft wear ring seal materials. A quantitative method, however, could not be implemented to isolate the contributing mechanisms with the available data.

Advanced Bearing Concepts

The requirements for the OTV engine were derived from NASA-sponsored vehicle and engine studies. To achieve these requirements and the engine operating needs, the OTV Fuel Turbopump may be required to operate at nearly 230,000 rpm. In subtask B.6, conventional rolling element, hybrid, foil, and hydrostatic bearings were evaluated against turbopump imposed speed, as well as load, cryogenic environment, engine life and duty cycle requirements. The results of this study are summarized in Table 14.

This evaluation led to the selection of the hydrostatic bearings as the prime candidate design for the OTV Fuel Turbopump. Subsequently a program was conducted to design, fabricate, and assemble a hydrostatic bearing tester. A diagram of this bearing tester with major elements labeled is shown in Figure 34. It was planned to test the candidate bearings in a follow on program to quantify bearing wear rates and fluid flows required for the

Table 14: OTVE Turbopump Bearing Comparison Summary

BRG TYPE	LOAD CAPACITY RAD (LB)	STIFFNESS (LB/IN)	DAMPING $\left(\frac{\text{LB/SEC}}{\text{IN}}\right)$	LIFE (HR)	SPEED LIMIT (DN) $\times 10^{-6}$	BRK AWAY TORQUE (LB/IN)	LEAKAGE (LBM/S)	LIFT OFF SPEED (RPM)	REQD PRESSURE (LB/IN)
ROLLING ELEMENT (BALL)	150	200000 TO 600000	1.0	5.0	1.8	0.3	COOLANT FLOW =.05	0	MAINTAIN LIQUID OR HI DENSITY
ROLLING ELEMENT (ROLLER)	300	600000 TO 1.5×10^6	1.0	5.0	1.8	0.15	.05	0	MAINTAIN LIQUID OR HI DENSITY
FOIL	30-40 FOR 1" L X 1" D BRG @ SPEED	2K-10K	≤ 286	55000- 95000 IN ECU	UNKNOWN	< 2 IN-LB FOR 1" L X 1" D BEARING	FLOW THRU FOR COOLING < 1 ROLLING ELEMENT	$< 30\%$ SPEED LOWER WITH LESS PRELOAD	$\sim 10'$ PSI ΔP ACROSS FOR COOLING
HYBRID	150 OR .25 (ΔP)	100000	10	50	3.0	0.3	0.15 (H_2)	$\sim 10K$	~ 2000 (ΔP)
HYDRO- STATIC	.25 (ΔP)	400 (ΔP)	10	START LIMITED TO ∞	> 5.0	0.05 X ω	0.2 (H_2)	$\sim 10K$	~ 2000 (ΔP)

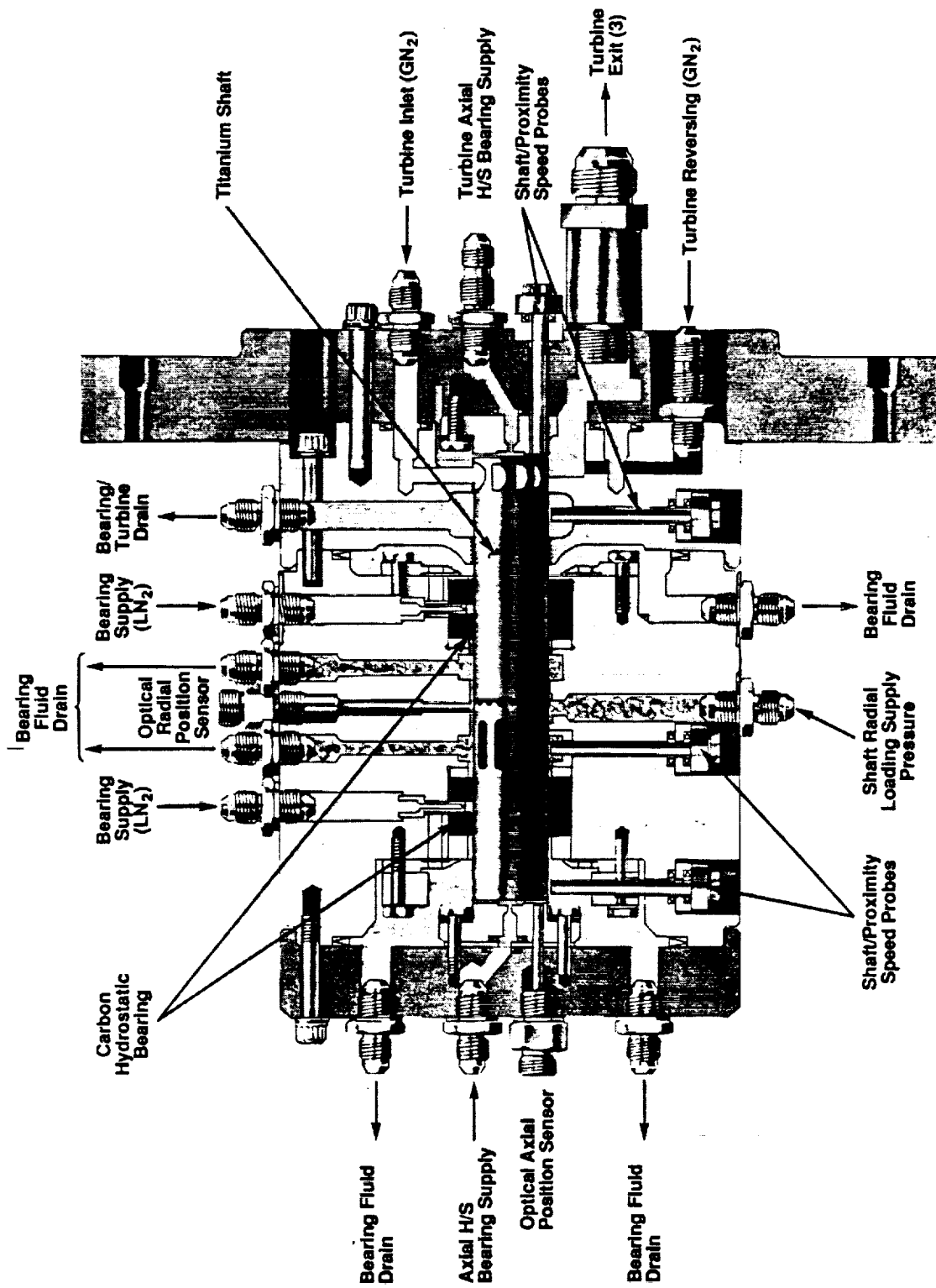


Figure 34: OTVE Hydrostatic Bearing Tester

selected hydrostatic bearing designs. Budget constraints, however, limited the scope of work at the time to the fabrication of the tester.

Rolling element bearings were evaluated for the OTVE high speed fuel turbopump with a design point shaft speed of approximately 200,000 rpm. Life calculation results of 5 hours for an appropriate bearing size of 25 mm, fell short of the OTVE requirement of 20 hours. The DN speed limit value of 1.8×10^6 also fell short of a DN goal of 5.0×10^6 for the turbopump. These limitations excluded rolling element bearings from further consideration.

Hybrid bearing configurations offered improved life (50 hours); however, these configurations had larger turbopump cross sectional requirements in both the radial and axial directions. This space requirement made these bearings less suitable for use in the small diameter OTVE high speed fuel turbopump. The rolling element bearing in the hybrid combination has the capability of reacting to transient axial loads but will continue to rotate and generate parasitic losses during steady state operation.

Foil bearings were reviewed for applicability to the OTVE high speed fuel turbopump. The four types of foil bearings reviewed include the multi-leaf type, the bumper supported, the tension type, and the multi-layer single leaf. The multi-leaf bearing has been applied in various aircraft for air-conditioning and heating needs and has gained the most experience to date. Under cryogenic turbomachinery conditions, however, there has been no experience with foil bearings. Additionally, the impact of foil bearings on minimal clearance soft seals remains undefined.

Significant attributes made the foil bearings attractive however. The foil bearings operate in a bath of fluid and generate little heat after lift-off from the foil and as a result require little cooling and minimal process fluid replenishment. They have demonstrated long life and reliability, and simplified rotordynamics. The characteristic foil bearing aspect ratio (journal diameter divided by bearing length approximately equal to one) also results in shafts of large diameter and increased shaft stiffness which could result in simplified rotordynamics. Foil bearings are worthy of investigation as turbopump bearings; however, uncertainty about their rotordynamic characteristics prompted the recommendation of a follow-on program to evaluate their application into high speed turbopumps pumping liquid propellants.

Hydrostatic bearings offer predictable stiffness and damping and unlimited DN. Bearing life, while predicted to be infinite, needs to be quantified and process fluid flow requirements need to be defined. The predicted attributes of long life, high reliability and operational experiences resulted in the selection of the hydrostatic bearings for use in the OTVE High Pressure Turbopump. Material candidates were chosen for future evaluation and testing and are listed in Table 15.

Fuel Turbopump Analysis

In subtask B.7, the High Pressure Fuel Turbopump (HPFTP) for the OTVE was sized and analyzed. A preliminary design of the turbopump was generated, taking into account the wide range of conditions corresponding to the engine operating parameters established in subtask D.5. A layout of the HPFTP is shown in Figure 35. A rotordynamic analysis was also performed to characterize pump operation over the entire range of expected loads and speeds.

First, the number of pump stages was decided and the impellers were sized to the required flow for the 7500 lbf engine. Performance was then calculated, incorporating effects of design elements such as hydrostatic bearings, high velocity diffusing crossovers and soft wear ring seals. Suction performance was also derived and was found to be well within the limits set by the available NPSH from the pressurized tanks.

The fuel turbopump was analyzed at off-design conditions as well as on-design. It was determined that the pump could achieve the required throttling level and remain within the stable operating range. Pump characteristics resulting from mixture ratio variations were also investigated and found to be within operational limits.

The rotordynamic analysis performed on the HPFTP included several finite element beam models. The models consisted of variations of the preliminary configuration, each including an inducer, four pump stages, two turbine stages, two hydrostatic bearings and the seal packages. Stiffness, damping and cross coupling for the seals and bearings were determined. From these models, natural frequency and stability maps were generated showing the critical speeds and mode frequencies. The models were refined until all critical speeds and stability modes were at safe values.

Table 15: Hydrostatic Bearing Material Candidates

MATERIAL	NAME AND MANUFACTURER	E psi x 10^6	α in/in°F	σ bend ₂ ksi	σ comp ksi	$\frac{k}{Btu/ft/}$ hr/°F	$\frac{K_{IC}}{ksi\sqrt{in}}$	$\frac{K_{IC}}{E \alpha}$	$\frac{K_{IC}^k}{E \alpha}$	PV psi-ft/min
Carbon- Graphite	P-5N Pure Carbon	3.0	2.4 E-6	12.5	40	~5	1.8	250	1250	500,000
SiC	PS-9242 Pure Carbon	53.0	2.5 E-6	55 (4) 68 (3)	400	85	3	23	1925	500,000
PSZ	Nilsen	29.7	5.0 E-6	94 (3)	175	1.27	~8	54	68	
Si ₃ N ₄	NC-132 Norton	45.0	1.9 E-6	~150 (3)		18.5	~5	58	1080	
WC + Ni	K801 Kennametal	89.6	1.8 E-6	315 (3)	690	47.4	3	18	870	
Polyimide	Vespe1 SP211 DuPont	0.2	30 E-6	10.0	--	.44	--	--	--	100,000
TiC + Ni/Mo	K1628 (Kennatium) Kennametal	59.0	4.1 E-6	235 (3)	610	11.1	9.6	77	860	
Carbon- Carbon	S.A.I.C.1	18.6	1.5 E-6	45	--	18	3.1	114	2106	

NOTES: 1 Scientific Applications International Corporation
2 Number in parentheses indicates 3- or 4-point bend test

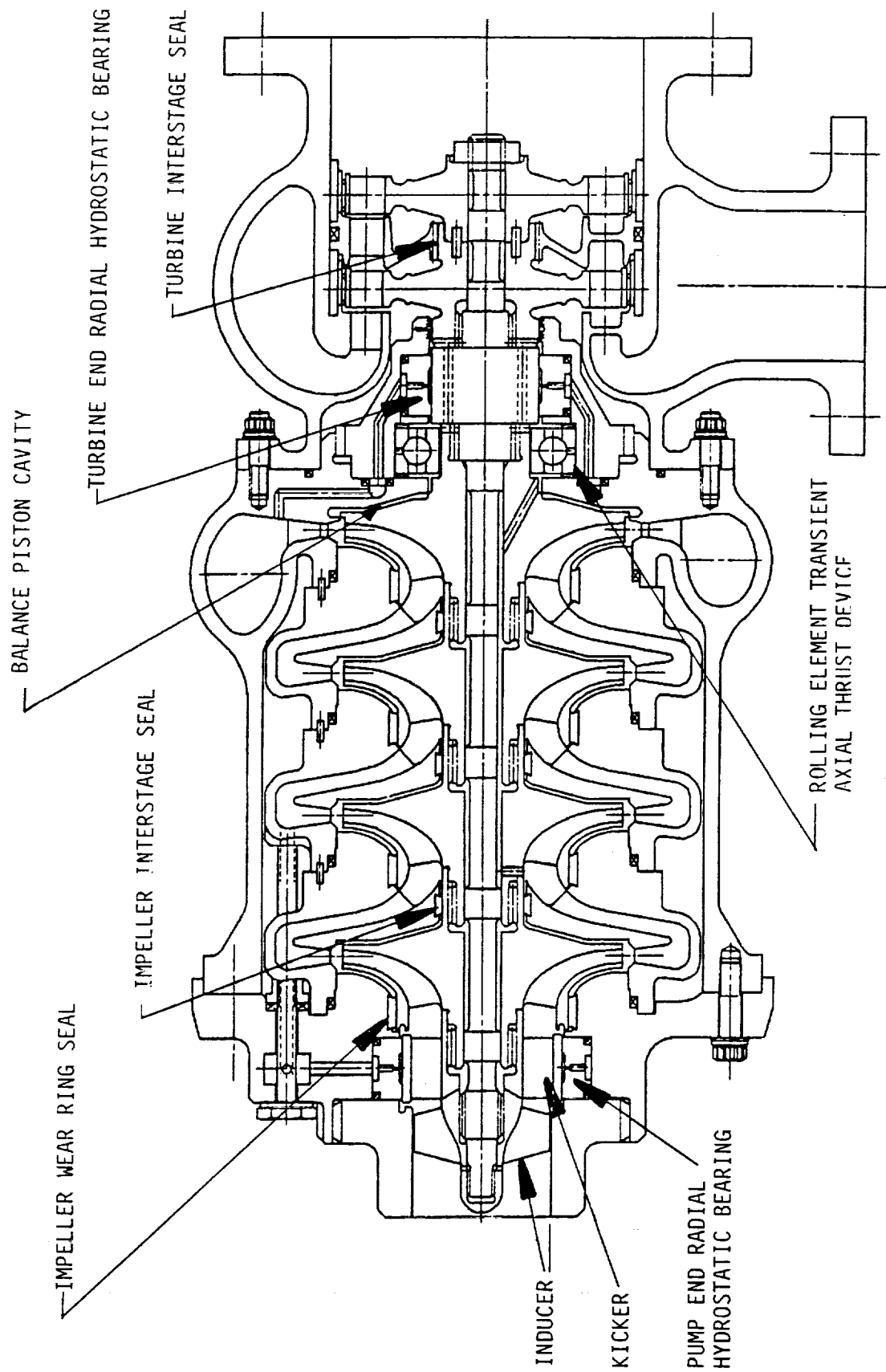


Figure 35: OTVE High Pressure Fuel Turbopump

TASK C - COMBUSTION CHAMBER TECHNOLOGIES

In order to increase chamber pressure and in turn increase engine performance, more heat energy needed to be extracted from the OTV coolant circuit to drive the turbomachinery. Increased heat energy maximizes the efficiency of turbomachinery operation and reduces the size and weight of the engine. In the past, increased heat energy requirements of the turbopumps required longer combustion chambers. Size limitations created the need for a different method to increase heat extraction. This requirement was fulfilled by increasing the area exposed to the hot-gas by using combustor ribs. The ribs increased the total area exposed to the hot-gas by 80%, and thus increased the enthalpy in the coolant working fluid. Task C efforts proved the validity of the ribbed combustion chamber concept, determined the optimal rib and channel configuration, and tested the configuration to verify the heat load enhancement factor predicted.











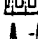

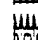







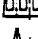
Ribbed Wall Flow Tests

The overall objective of subtask C.1 was to assess the use of ribbed walls to increase the heat extraction capability of an expander cycle engine combustor. Supporting objectives were: screen appropriate rib configuration candidates; evaluate flow characteristics around the candidate ribs; compare the designs under hot gas conditions; and select the best designs for hot-fire test evaluation.

A matrix of candidate rib configurations was formulated based on preliminary studies conducted at Rocketdyne. The matrix featured ribs with varying heights, widths, pitches (spacing), and base geometries (sharp or curved). These candidates were screened analytically for heat transfer enhancement, boundary layer risk, producibility, and structural/life considerations. The required heat transfer and boundary layer analyses were conducted with two dimensional computer models using a uniform heat transfer coefficient for all surfaces. Results of these analyses for the candidate matrix and the weighting factors used are given in Table 16.

Rating of each rib type with respect to heat transfer enhancement was based on comparisons against a conventional smooth walled combustor. This evaluation was conducted using two-dimensional finite difference Differential Equation Analyzer Program (DEAP) combustor models of the various rib geometries. The results for these models were in the form of two-dimensional "slices" of the hot-gas wall and combustor liner at

Table 16: Hot Gas Side Rib Selection Matrix

RIB GEOMETRY	HEIGHT		HEAT TRANSFER 30 WEIGHTED		BOUNDARY LAYER 30 WEIGHTED		PRODUCTIVITY 15 WEIGHTED		STRUCTURE/ LIFE 25 WEIGHTED		WT'D SUMS	RANK	OTHER FACTORS	SEL RANK
			RAT'G	WT'D	RAT'G	WT'D	RAT'G	WT'D	RAT'G	WT'D				
IA. STANDARD RIB														
RIB OVER LAND .040 BASE WIDTH .0785 PITCH .020 TIP	.040		6	1.8	8	1.8	10	1.5	8	2.25	7.25	1	EXPAND DATA BASE FOR ADV. MAT'L DEV	1
	.060		7	2.1	8.5	1.65	10	1.5	4	1.0	6.25	3		2
	.080		8.5	2.55	5	1.50	8	1.2	0	0	5.25	8		8
	.120		10	3.0	4	1.20	5	.8	0	0	5.10	11		
IB. STANDARD RIB														
RIB OVER LAND .060 BASE WIDTH .0785 PITCH .020 TIP	.040		5	1.5	5	1.5	10	1.5	8	2.25	8.75	2	DUPLICATION: CHANGE IN BASE WIDTH TO BE COMPARED AT .080 HT	—
	.060		6	1.8	4.5	1.35	10	1.5	4	1.0	6.85	7		4
	.080		7.5	2.25	4	1.2	8	1.35	0	0	4.80	13		
	.120		9	2.7	3	.8	7	1.05	0	0	4.85	14		
II. SKIP RIB														
.040 BASE WIDTH .1570 PITCH .020 TIP	.060		3	.8	8	2.4	8	1.2	5	1.25	8.75	6	TECHNICAL BREADTH	3
	.080		4.5	1.35	8	2.4	7	1.05	0	0	4.80	12		
	.120		8	1.8	6	2.7	5	.75	0	0	6.25	10		
III. HALF PITCH RIB														
.020 BASE WIDTH .0385 PITCH .010 TIP	.040		—	—	0	0	5	.75	—	—	.75	20	HEAT TRANSFER AND LIFE NOT ANALYZED DUE TO EXTREME BOUNDARY LAYER RISK	
	.0785		—	—	0	0	3	.45	—	—	.45	21		
IV. RIB/CHANNEL SH														
RIB OVER CHANNEL .040 BASE WIDTH .0785 PITCH	.060		7	2.1	8.5	1.65	10	1.5	4	1.0	6.25	4	DUPLICATION: HOT GAS WALL IDENTICAL TO IA/.060	—
V. RADIUS .020														
.0785 PITCH .020 TIP	.040		8.5	1.65	4	1.2	7	1.05	8	2.25	6.15	5	DUPLICATION: CHANGE IN THROUGH GEOMETRY TO BE COMPARED AT .060 HEIGHT TECHNICAL BREADTH	—
	.060		8.5	1.65	4	1.2	7	1.05	5	1.25	6.45	6		5
	.080		8	2.4	3	.8	5	.8	0	0	4.25	15		
	.120		9	2.7	2	.8	4	.8	0	0	3.80	17		
VI. RADIUS .060														
.1570 PITCH .020 TIP	.060		2	.6	4	1.2	6	.8	5	1.25	3.95	16		
	.080		3.5	1.05	5	1.5	5	.75	0	0	3.30	18		
	.120		5	1.5	4	1.2	3	.45	0	0	3.15	19		

discrete axial stations. Rib designs were rated in terms of a heat transfer "enhancement factor", relating rib potential compared to a smooth wall liner, and the steady state temperature profile. Rating of ribs in this category resulted, as expected, in the taller ribs being rated highest, due mainly to increased hot-gas surface area.

A comparison of heat transfer enhancement was made for orientation of the rib over the land area or over the coolant channel. No difference in enhancement was noted. therefore, from a heat transfer standpoint the cases are equivalent and can be interchanged. Structural considerations will be used to select the best approach.

Boundary layer risk was evaluated based on a best estimate of boundary layer growth over combustor wall length, taking into account the insulating effect of a "filled" rib contour, and rib corner effects on boundary layer formation. Results reflected that wider spacing of the ribs is best, yielding the most effective boundary layer contour with minimized risk of heat flux degradation due to boundary layer build-up.

Producibility risk addressed the difficulty in machining complex liner geometries. Rib complexity is driven by aspect ratio, scale and multiple contours. As expected, the larger and simpler rib geometry types rated higher.

The structural and life considerations were based primarily on material property degradation with increased temperature. Comparison data was obtained from the DEAP steady state temperature profiles. These were relative temperature comparisons, since some rib tip temperatures went well beyond material limits. Potential advances in material and cooling technology were considered in selecting cases to be tested. Evaluation of ribs in this category showed that the taller ribs rated lowest, due mainly to excessive material temperatures. Again, there was essentially no difference in the rib over land and rib over channel configurations.

A rib sensitivity study was conducted to evaluate how potential variations in hot-gas wall film coefficient (H_g) due to boundary layer effects would impact rib temperature and heat transfer enhancement. The results showed that H_g variations do affect heat transfer enhancement directly, but due to a parallel effect of lower material temperature may allow the use of taller ribs. Additionally, a study was made to determine the effect on H_g of large temperature gradients from rib tip to trough. Results showed only a 12% change in H_g for

a 1000 F temperature gradient, which fell well into the Hg range covered in the sensitivity studies described above.

Of the twenty-one candidates, six best rib configurations were selected for the two lab tests planned; 1) the hot-air calorimeter panel tests, and 2) the cold-air flow boundary layer mapping tests. Final rib selection was based on total weighted scores for each rib type in the four categories, plus "other factors", such as duplication of data, and broadening of the data base. Both boundary layer risk and heat transfer were weighted highest, due to their direct influence on rib effectiveness. Producibility was weighted low due to the relatively narrow range of influence it has, considering that all ribs analyzed were within the state-of-the-art for machining processes. Structure/life considerations, though important, played a much larger role in structural analysis studies farther along in the program. The overall weighted rating scores gave a prioritized ranking of the candidates for the four quantified evaluation criteria.

The selected concepts included ribs of 0.040, 0.060, and 0.080 inches in height. Two base width values were selected for the 0.060 high rib to evaluate the impact of this parameter. A twice-nominal pitch configuration, the 'skip rib' case, was included based on its overall ranking and low boundary layer growth risk. Finally, a radius based design rated highly and was also selected for technical breadth.

The six rib candidates were tested using a hot air test chamber, the components of which are pictured in Figure 36. The test chamber was designed to test four ribbed or smooth panels at a time to speed testing. Each panel made up a longitudinal quarter section of the tester and had its own coolant circuit. The hot air test setup is shown in Figure 37. Typical measured temperature rise results for each rib candidate and a smooth wall baseline are given in Figure 38. As expected, the taller ribs produce the greatest temperature difference.

Cold flow laser velocimeter testing was also performed for the various rib configurations in order to evaluate boundary layer velocity profiles between the ribs. These tests were performed in the two dimensional tester shown in Figure 39. Seen in Figure 40 is the complete test setup. The tester was designed for easy test element replacement to reduce time between test runs. As is shown in Figure 39, multiple configurations could also be tested without changing the test element. Figure 41 gives the nondimensionalized scaled results of the the velocimeter tests for each of the rib height and spacing configurations. From these, Stanton numbers were calculated by the Reynolds analogy with a Prandtl

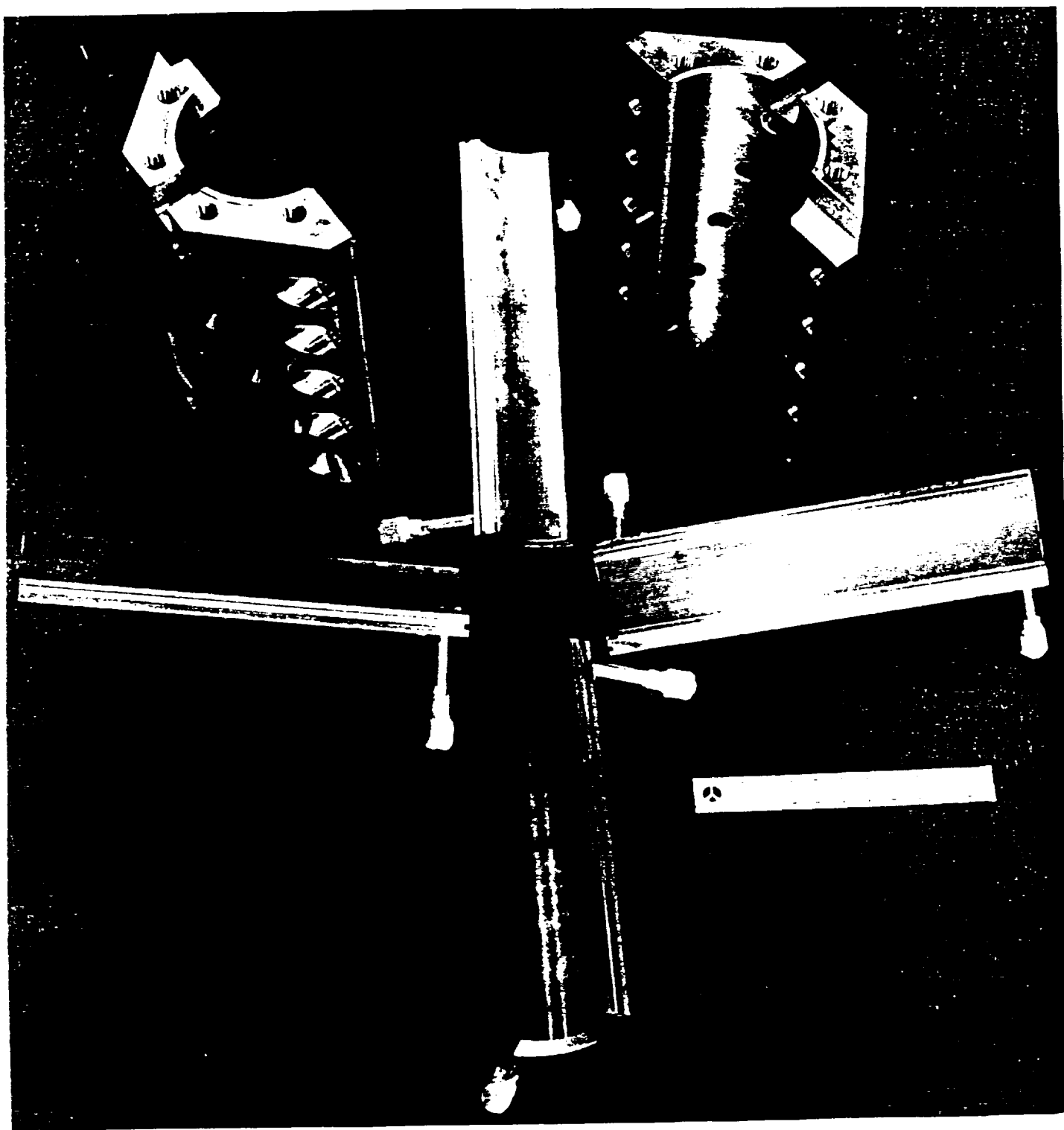


Figure 36: Hot Air Test Chamber Components

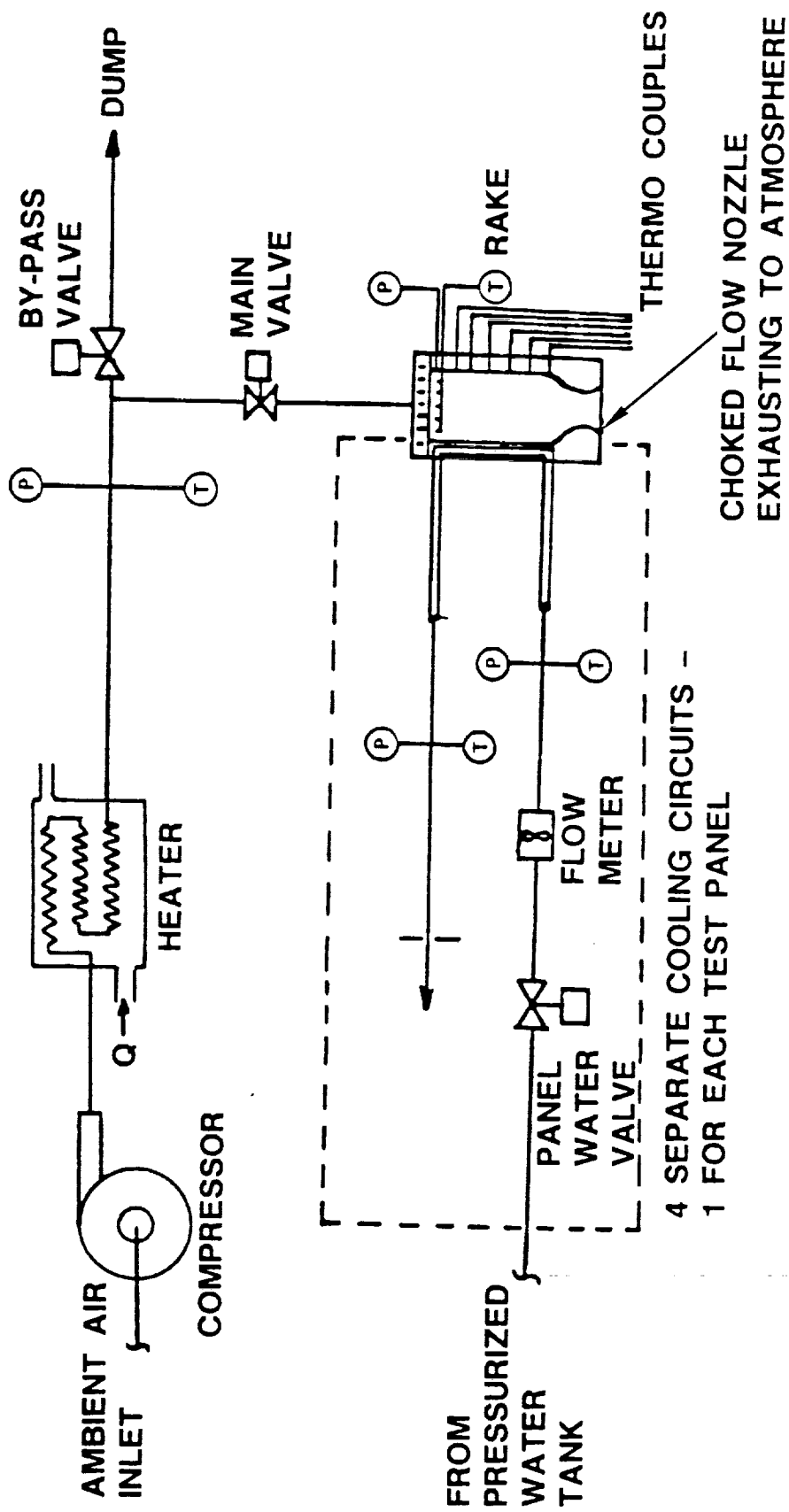


Figure 37: Hot Air Test Setup Schematic

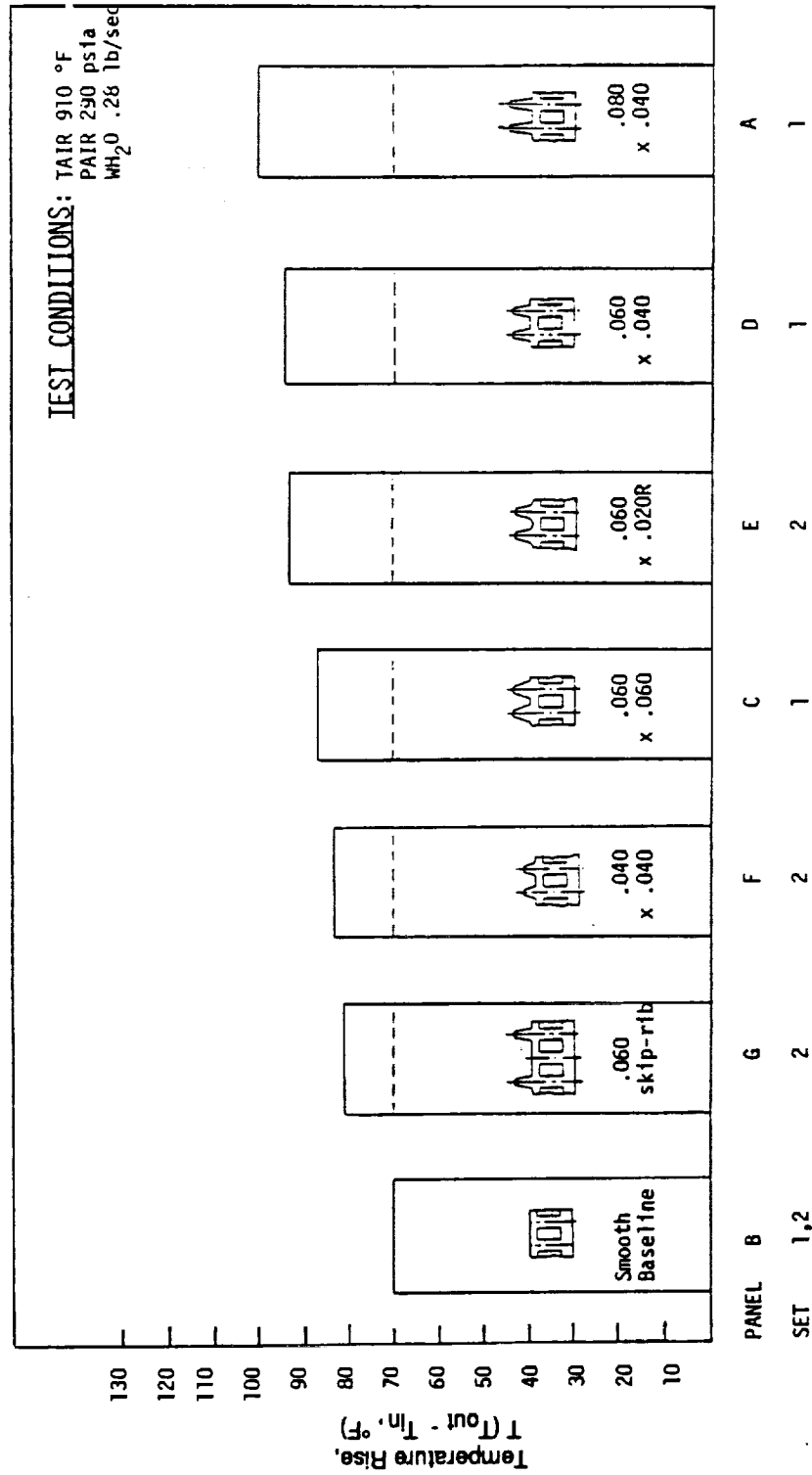


Figure 38: Typical Measured Panel Temperature Rise

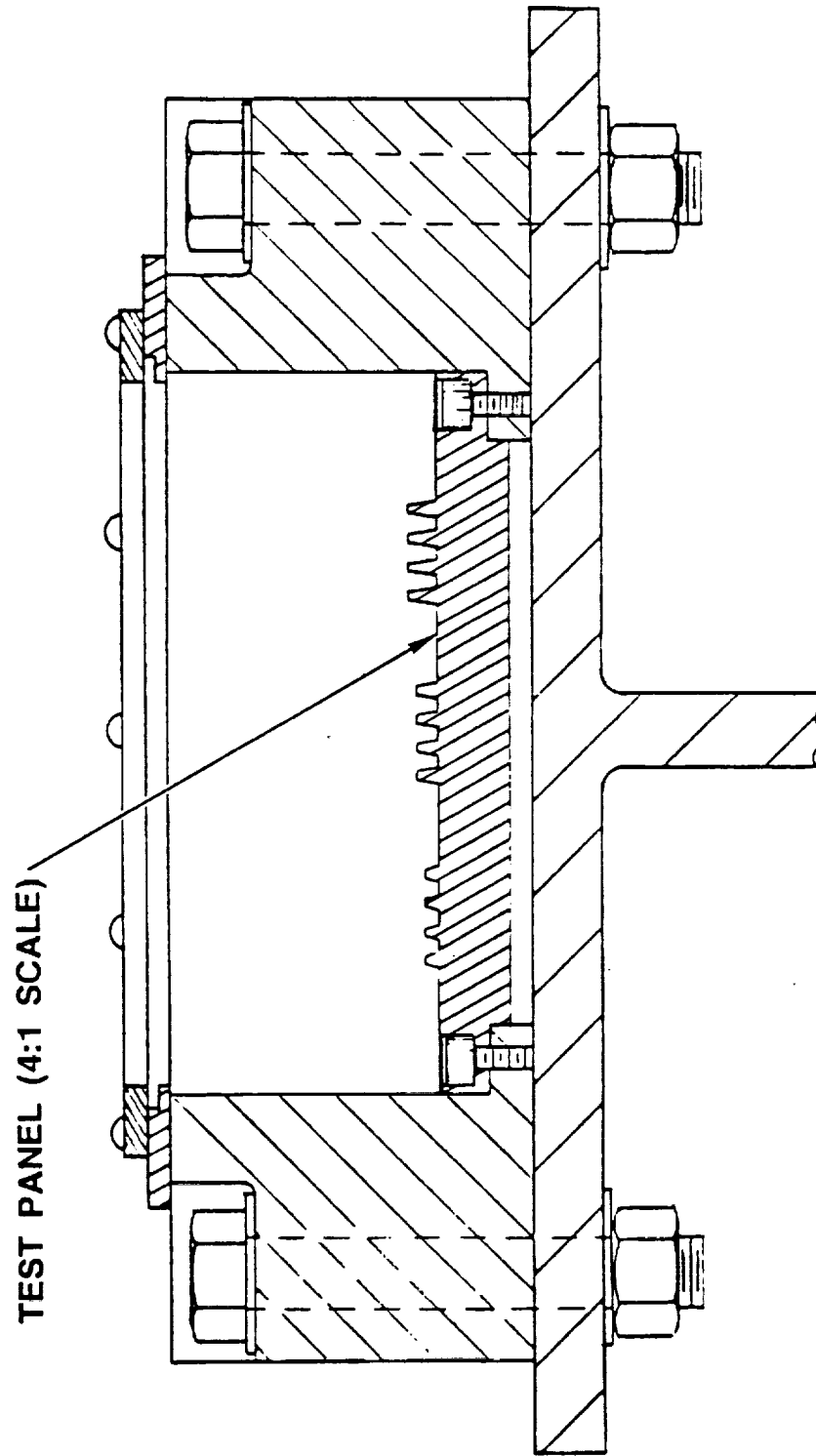


Figure 39: Cold Flow Test Fixture - Hot Gas Rib Configuration

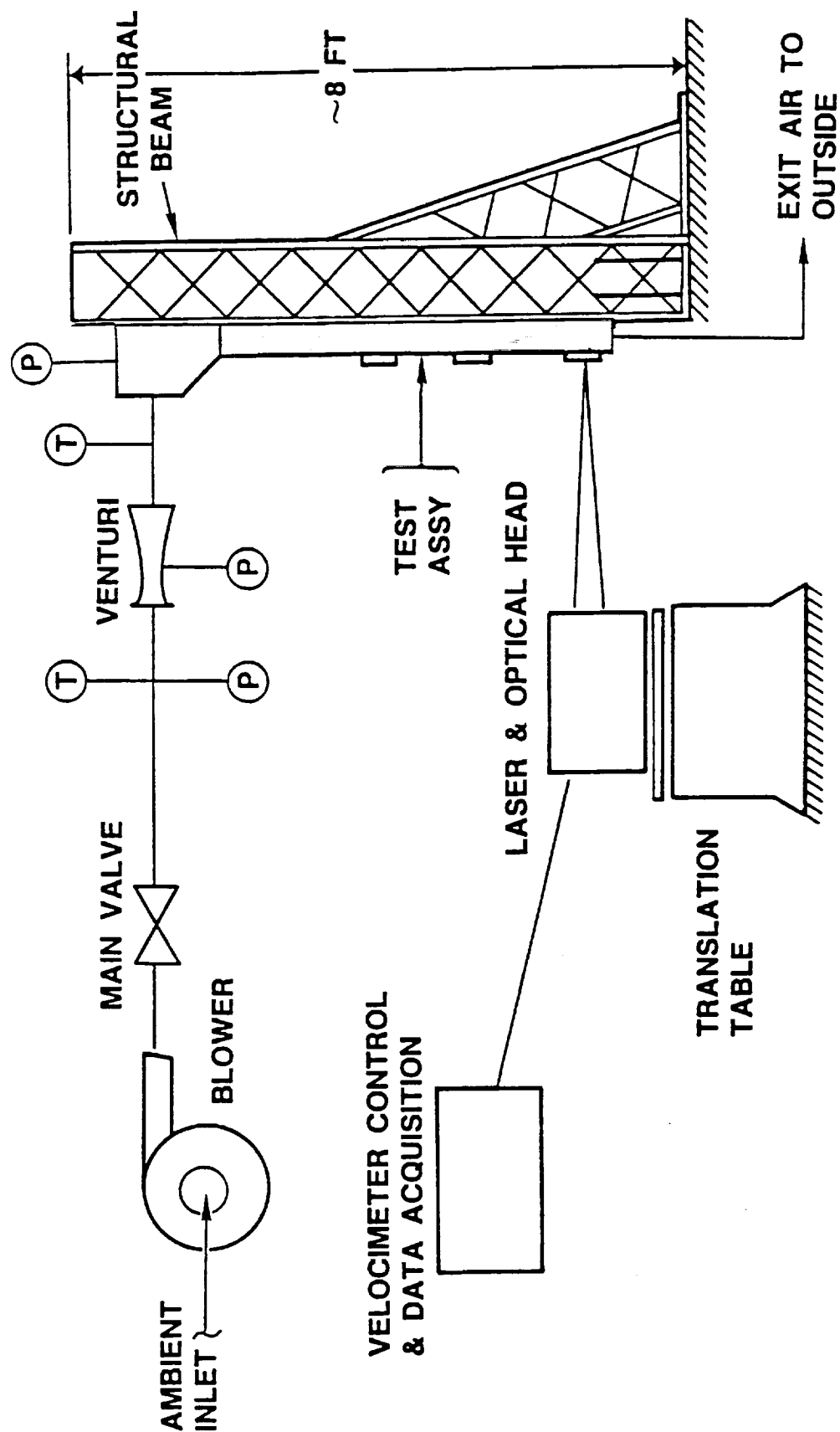


Figure 40: Cold Flow Test Setup Schematic

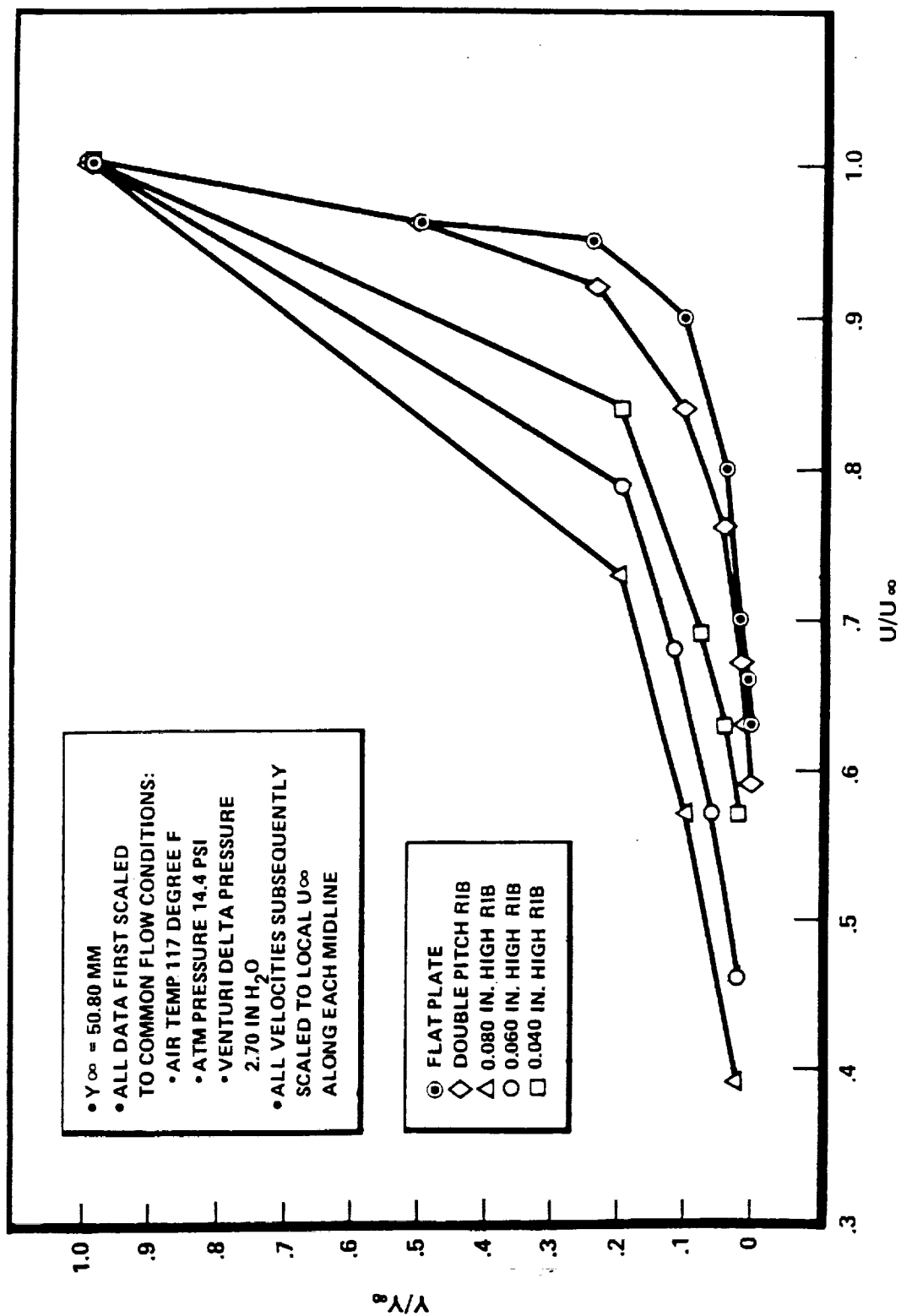


Figure 41: Nondimensionalized Scaled Velocities Along Midline Between Ribs

correction using flat plate turbulent boundary layer equations to determine skin friction factors. An area integration of the Stanton numbers produced heat transfer coefficient profiles for candidate comparison.

Resulting combustor heat transfer estimates for the rib candidates from four predictive sources are tabulated in Figure 42. The first column represents the unscaled cold flow test results. The second column gives the hot air calorimeter test numbers. The last two columns are predicted results from the DEAP code at hot air test and hot fire test conditions. The hot air and cold flow test results show good agreement. The DEAP hot air model results are lower because of cold flow Stanton number effects, and the hot fire DEAP model shows lower values because it includes the non-isothermal rib effect predicted for the higher actual heat fluxes.

Scaling analysis results from the cold flow velocimeter data led to the selection of the preferred rib configuration. The highest performance was predicted for a 0.040 inch high, 0.040 inch base truncated triangular rib with a 0.020 inch tip width and a pitch of 0.0785. Wall temperatures for this configuration were projected to be acceptable and fabricability was demonstrated during the hot air test chamber fabrication. This recommended rib pattern along with an alternate derived from the test data are shown in Figure 43.

Combustor Coolant Channel Selection

The objective of subtask C.2 was to evaluate alternate combustor coolant channel geometries that would enhance the combustor liner service life. The design objective was to maintain an acceptable wall temperature with the increased heat extraction due to hot-gas wall ribs without excessive coolant circuit pressure drop or adverse structural efficiency. The design approach taken was to screen appropriate channel candidate configurations, evaluate the flow characteristics in the channels, compare the designs at hot-fire conditions, and select the best designs for hot-fire test evaluations.

A matrix of candidate channel configurations was developed based on previous design studies at Rocketdyne. The matrix featured channels with base fins, high aspect ratio rectangular channels, rounded corner channels, and channels with interrupted flow fins. The base fins were of varying width, aspect ratio, shape, and number (one or two). A summary of these configurations is shown in Table 17.

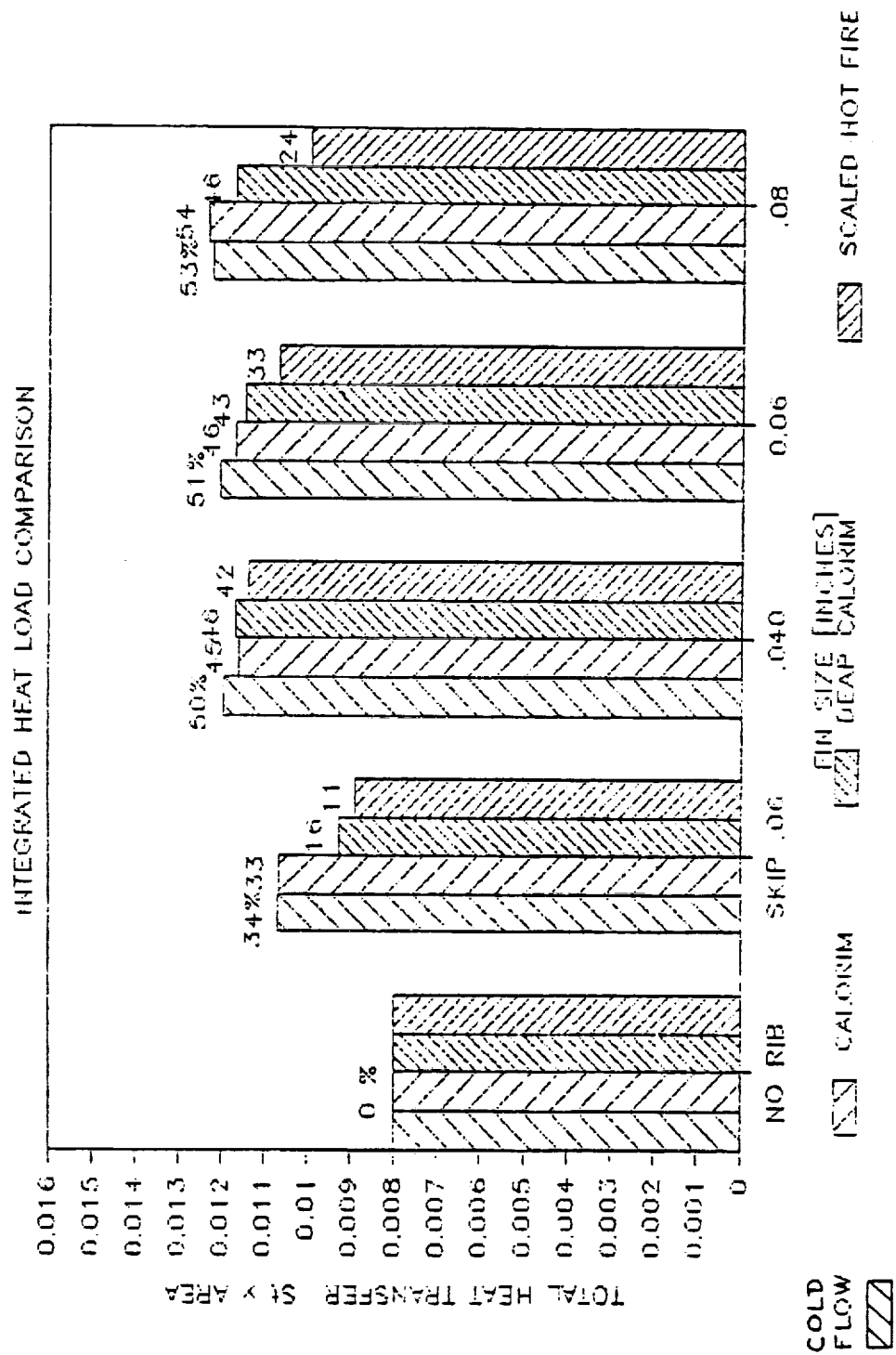
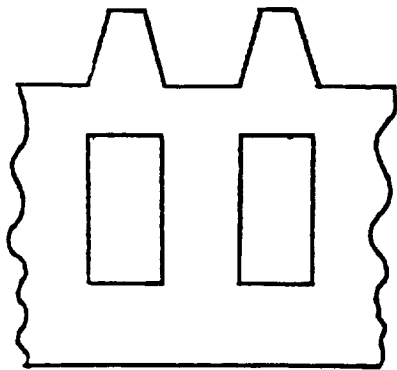


Figure 42: Ribbed Combustor Heat Transfer Results



0.040 tall - 0.040 base rib with
0.020 tip width - 0.0785 pitch

0.030 tall - 0.040 base rib with
0.020 tip width - 0.0785 pitch

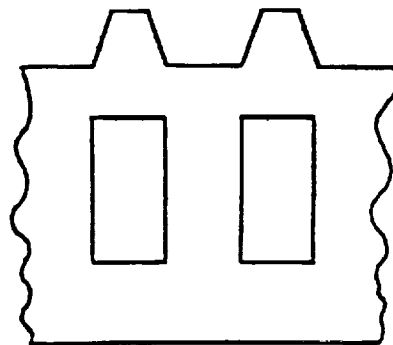




























Figure 43: Selected Rib Configurations

Table 17: Coolant Side Channel Geometry Selection Matrix

CATEGORY	CHANNEL GEOMETRY	STRUCTURE/ LIFE		COOLANT ΔP		BOUNDARY LAYER		PRODUCIBILITY		HEAT TRANSFER		WEIGHTED SUM	WEIGHTED RANK	SELECTION RATIONALE	SELECTION RANK		
		35 WEIGHTED	25 WEIGHTED	35 WEIGHTED	25 WEIGHTED	35 WEIGHTED	25 WEIGHTED	35 WEIGHTED	25 WEIGHTED	35 WEIGHTED	25 WEIGHTED						
ASPECT RATIO		AR		RATG		RATG		RATG		RATG							
O80 HEIGHT		0.040	2.0	0	0	8	2.25	8	1.80	10	1.00	0	0	4.86	18	BASELINE CHANNEL FOR COMPARISONS	8
		0.036	2.67	2	70	3	75	7	1.40	10	1.00	8	60	4.45	22		
		0.026	3.2	2	70	6	0	8	1.20	8	80	8	80	3.60	24		
		0.020	4.0	0	0	6	0	8	1.00	8	80	8	80	2.80	26		
120 HEIGHT		0.040	3.0	0	0	10	2.50	8	1.80	10	1.00	0	0	6.10	14		
		0.030	4.0	0	0	8	2.25	7	1.40	8	80	4	40	4.86	18		
		0.025	4.8	0	0	6	1.80	8	1.20	8	80	6	80	4.10	20		
		0.020	6.0	0	0	6	0	8	1.00	8	80	8	80	2.80	27		
160 HEIGHT		0.040	3.75	6	8	10	2.50	8	1.80	10	1.00	0	0	6.10	16		
		0.030	5.0	0	0	10	2.50	7	1.40	8	80	4	40	6.10	16		
		0.025	6.0	0	8	6	2.00	8	1.20	8	80	6	80	4.60	21		
		0.020	7.5	0	0	3	75	8	1.00	8	80	8	80	3.16	26		
IIA SINGLE FIN STANDARD O80-040 CHANNEL TAPERED FIN	FIN GEOM. AR															NARROW FINS ALSO IN DUAL FIN GEOM'S (CAT. IIB) BEST OF SINGLE FIN WIDE FIN STUDY TAPERED FIN STUDY	3 7 4 6
		0.16x.016	1.5	7	2.46	7	1.75	4	80	7	70	4	40	6.10	7		
		0.24x.016	2.4	8	2.80	6	1.80	3	80	6	80	4	40	6.40	8		
		0.16x.016	1.0	8	2.80	7	1.75	3	80	7	70	4	40	6.26	8		
		0.24x.016	1.6	8	2.80	6	1.25	2	40	6	80	4	40	6.45	13		
		0.24x.016/ 0.10 TYP	1.87	8	2.80	6	1.80	4	80	6	80	4	40	6.00	8		
IIB DUAL FIN O80-060 CHANNEL		0.16x.016	1.8	10	3.60	8	2.25	3	80	4	40	8	80	7.28	1	BEST OVERALL	1 2
		0.24x.016	2.4	10	3.60	8	2.25	2	40	4	40	8	80	7.15	2		
III CORNER RADIUS O80-040 O20R O16x.010 FIN O05-010R		0.040 O20R		6	0	8	2.25	8	1.80	8	80	0	0	4.86	20	FLOW STUDY	6
		0.16x.010 FIN O05-010R		7	2.46	7	1.75	4	80	4	40	4	40	6.80	11		
IV COMBINATION STANDARD O80-040 CHANNEL 2 CHANNELS/RIS. FIN UNDER RIS ONLY	FIN GEOM.															FLOW EFFECTS CHARACTERIZED IN CATEGORY I, IIA & IIB SELECTIONS	
		0.16x.016		7	2.46	8	2.00	4	80	7	70	4	40	6.38	4		
		0.24x.016		8	2.80	7	1.75	3	80	8	80	4	40	6.15	8		
		0.16x.016		8	2.80	8	2.80	3	80	7	70	4	40	6.50	3		
	0.16x.024		8	2.80	7	1.75	2	40	8	80	4	40	6.95	10			
IV INTERRUPTED "SAWTOOTH" VARIATION OF SINGLE FIN				8	2.80	4	1.80	4	80	6	80	4	40	6.00	17	PRODUCIBILITY	

These candidates were screened by relative rating for temperature reduction capability (life), pressure drop, boundary layer build-up risk, producibility, and heat transfer enhancement. Heat transfer analyses were conducted using a two-dimensional computer model using fully developed flow characteristics in the channels. Results of the thermal analyses, and evaluations in the other categories, were used to select the eight configurations labeled in Table 17 for laboratory testing.

A cold flow velocity profile mapping test series, using the same fixture as the cold flow rib series, was conducted for the chosen channel configurations. The test fixture in the coolant channel configuration is shown in Figure 44. The air flow velocity data were analytically scaled to hot-fire conditions to evaluate channel performance. Predicted liner temperature changes for four configurations plus a reference smooth wall case are seen in the graph in Figure 45.

Three enhanced channel configurations were selected for possible hot-fire evaluation in the next program phase. Two were evaluated as part of the eight coolant channel candidate test matrix. They were the single high fin and the single low fin. Another channel concept, a high aspect ratio channel, was analyzed concurrently with those in the test matrix. It was not tested, but by analytical calculations was found to have a lower pressure drop. For that reason it was also recommended for further investigation. The three chosen channel types are pictured in Figure 46.

Combustor Calorimeter Experiments

A combustor calorimeter was fabricated to determine the heat transfer enhancement factor of a ribbed wall combustion chamber in subtasks C.4 and C.5. Results from subtask C.1 were used to define the geometric rib configuration for maximum heat transfer at acceptable life and structural limits. An existing Integrated Component Evaluator (I.C.E.) thrust chamber assembly was modified to accept the calorimeter and was installed into a test stand at the Advanced Test Propulsion Facility of Rocketdyne's Santa Susana Field Laboratory. A layout of this test assembly is depicted in Figure 47. The actual ribbed calorimeter section is pictured in Figure 48.

The 0.040 in. ribbed combustor calorimeter underwent a total of four steady state tests both in ribbed and smooth wall combustor configurations. The tests were conducted at 800 and 1000 psia chamber pressures with mixture ratio excursion sweeps between 5.0 and 7.0.

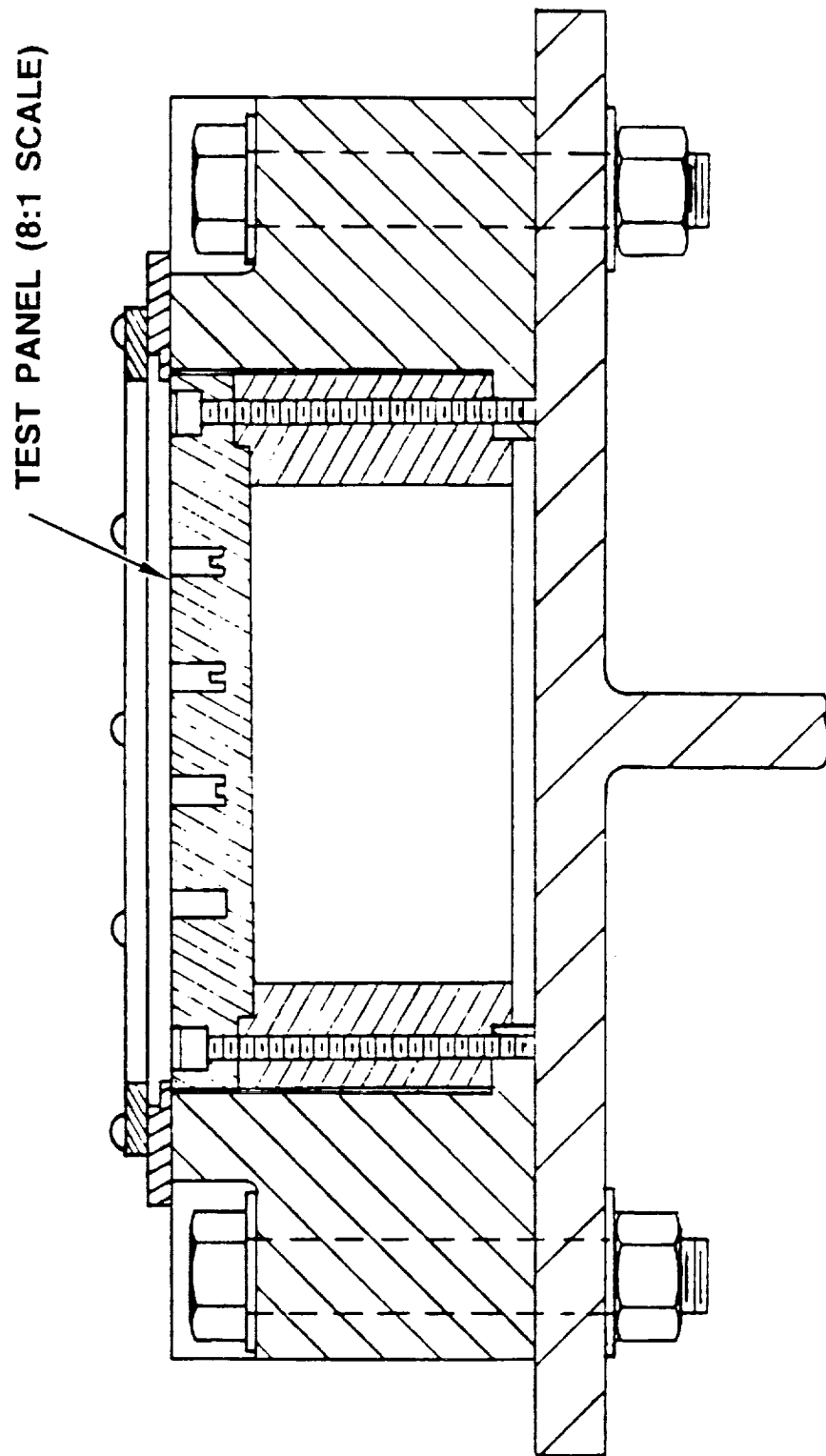


Figure 44: Cold Flow Test Fixture - Coolant Channel Configuration

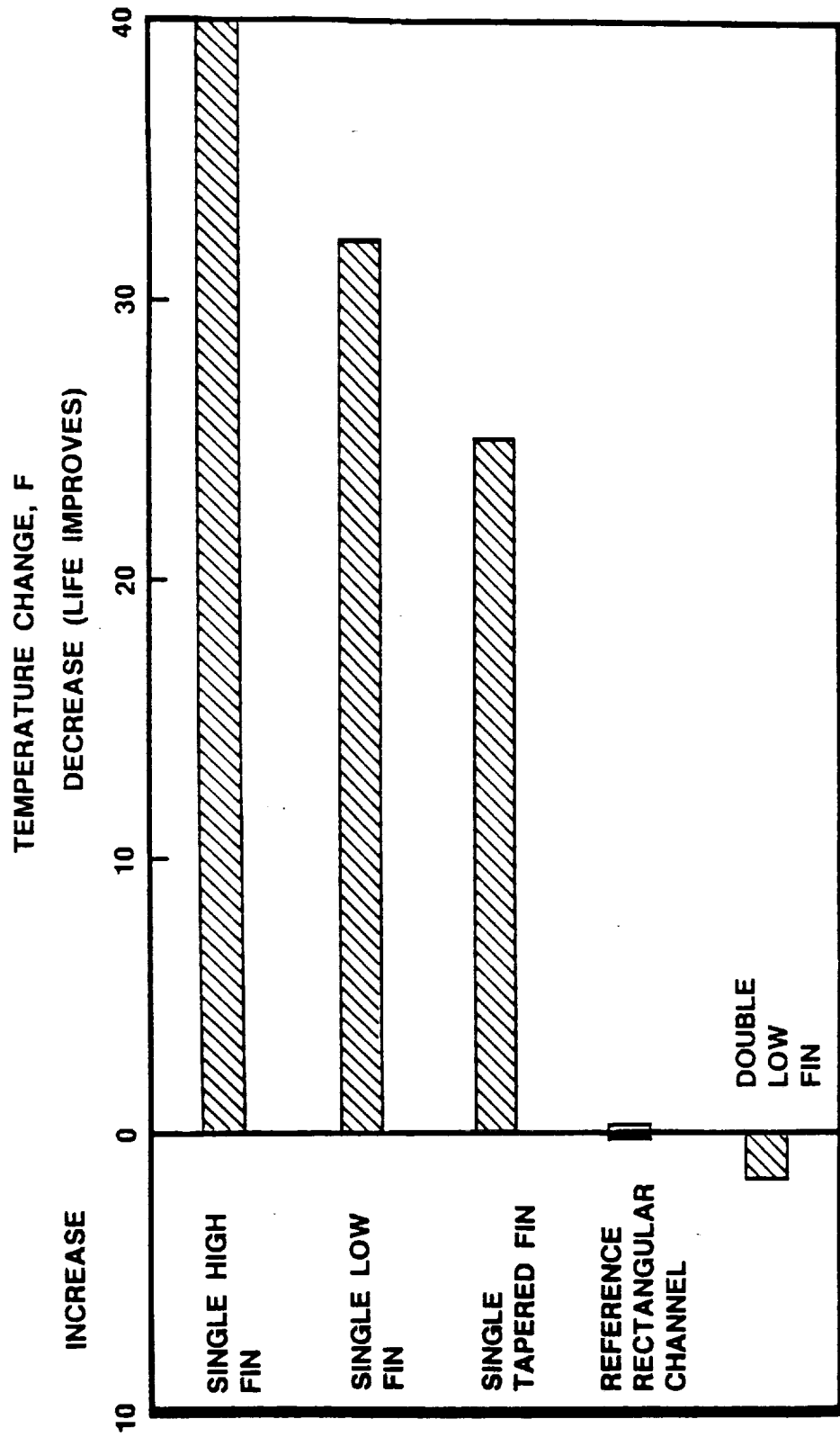
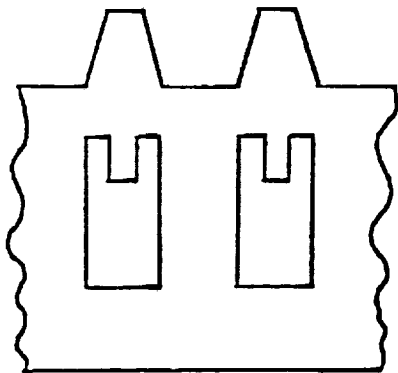
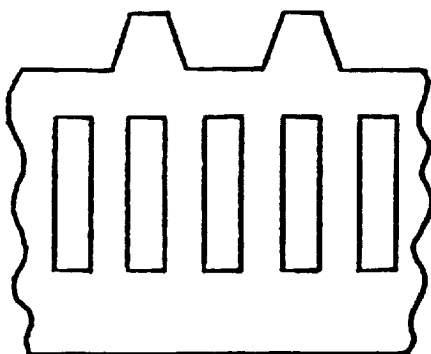
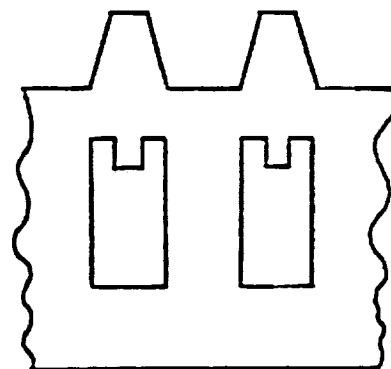


Figure 45: Predicted Liner Temperature Change With Enhanced Channels



0.040 wide - 0.080 tall channel with
0.015 wide - 0.024 tall fin

0.040 wide - 0.080 tall channel with
0.015 wide - 0.015 tall fin



0.020 wide - 0.080 tall high aspect
ratio channel

Figure 46: Selected Channel Configurations

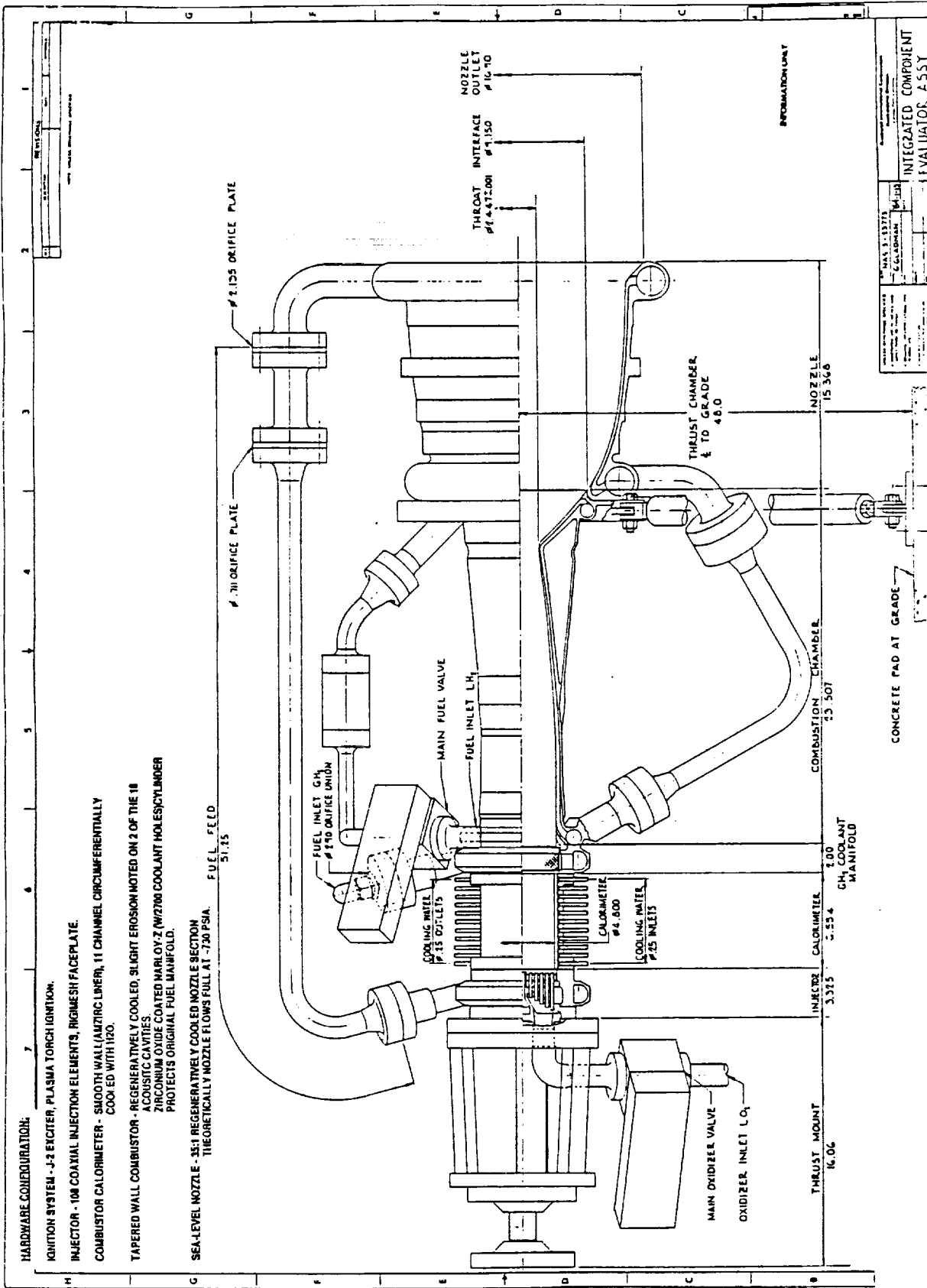


Figure 47: Integrated Component Evaluator (I.C.E.) Thrust Chamber Assembly - Enhanced Heat Transfer Combustor Configuration

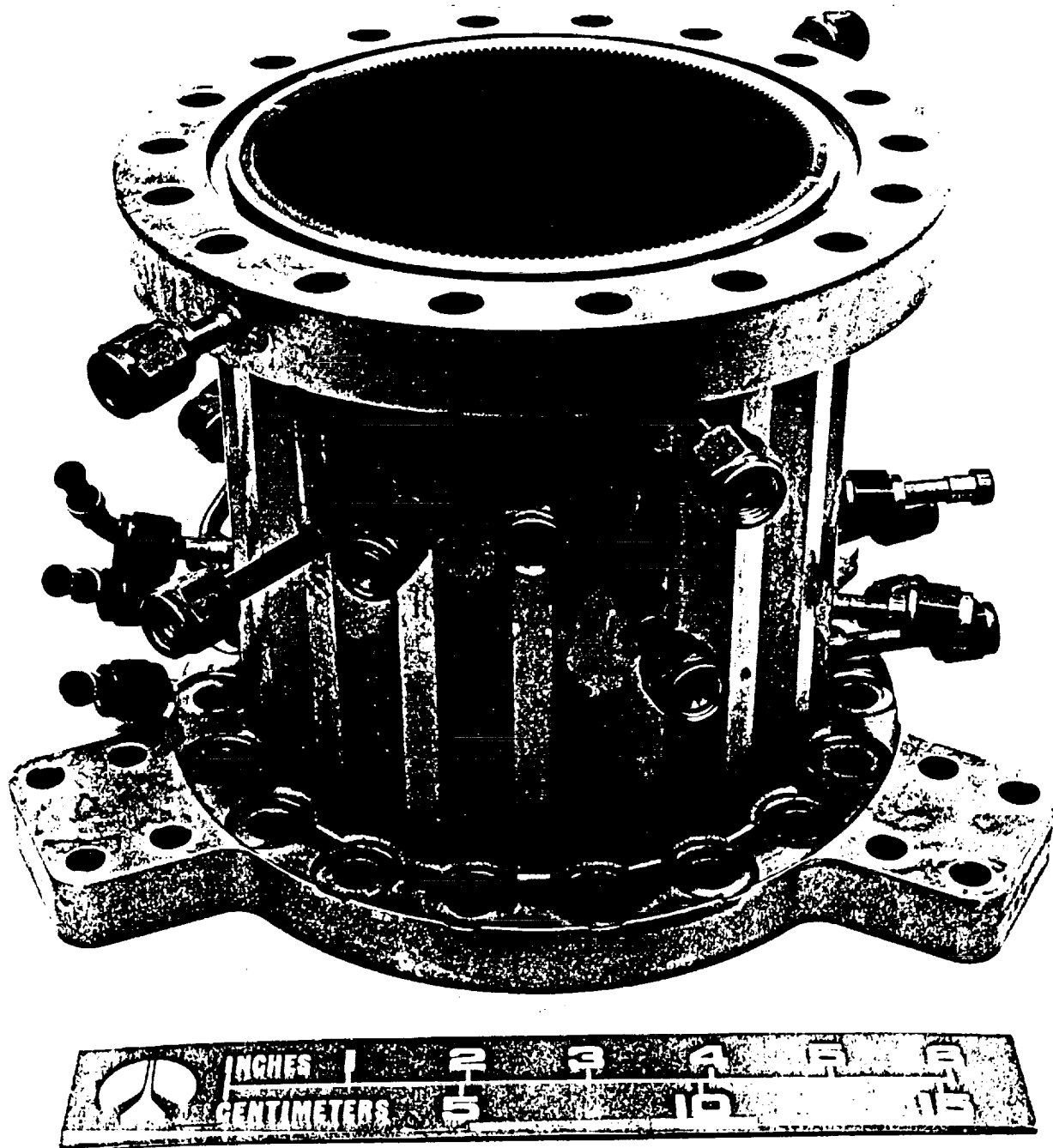


Figure 48: 0.040 Inch Ribbed Circumferentially Cooled Calorimeter

The heat transfer results from the ribbed calorimeter 800 psia P_c test indicated that the mixture ratio excursions affected heat loads significantly. The mixture ratio varied from 4.0 to 5.6 and increased heat loading approximately 1.92 BTU/in²-sec. per mixture ratio change of 1.0 (O/F). This data is given in Figure 49.

The heat transfer data from the 1000 psia P_c testing indicated that the heat load rate, although greater, followed the same pattern as the 800 psia P_c tests. The calorimeter test results indicated that the ribs caused a 50% increase in heat transfer for 800 psia chamber pressure and a 40% increase at 1000 psia (normalized for mixture ratio, the 1000 psia test enhancement is greater than that of the 800 psia P_c test). The heat loads vs chamber position for the ribbed and smooth calorimeters can be compared in Figures 50 and 51.

The projected enhancement from the ribs for a 16 in. long cylindrical combustor at 15 klbf nominal thrust level, was a 58% increase in heat transfer rate, which translated to a 46% increase for a full size 15k combustor. The Enhancement factors for these hot fire results are compared with the corresponding two dimensional enhancement factors in Figure 52. Enhancement factors for a 16 inch ribbed barrel and a 20 inch full combustor are projected in Figure 53 from the hot fire data for a range of chamber pressures at a mixture ratio of 6:1.

TASK E - ICHM AND PREFLIGHT METHODS

The objectives of Task E dealt with control and maintenance systems for the OTVE. After a preliminary design of the OTVE, a control scheme was devised for engine operation including start-up and shut-down sequencing. Methods of thrust and mixture ratio control were decided, and the necessary valves were incorporated into the system in the Task D efforts. Health monitoring functions were also introduced into the control system for greater reliability and more timely maintenance. Elements of the ICHM system were identified and component development costs were calculated for each element. Some of the condition monitoring processes were then developed through test programs. Methods of preflight engine checkouts with varying degrees of sophistication were also evaluated.

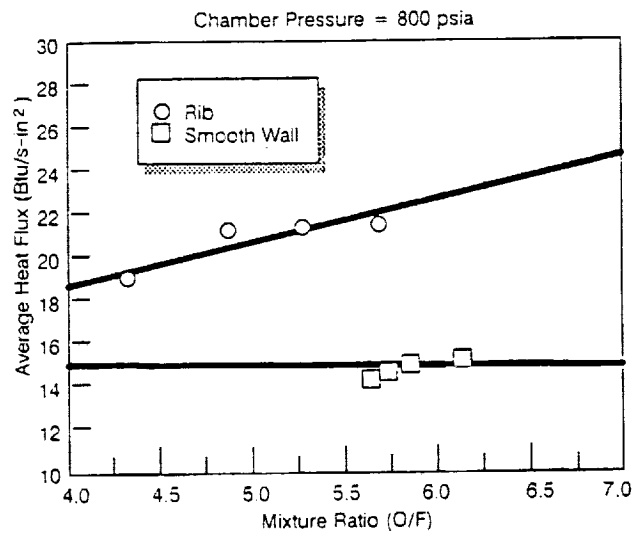


Figure 49: 800 psia Pc Heat Flux vs. Mixture Ratio

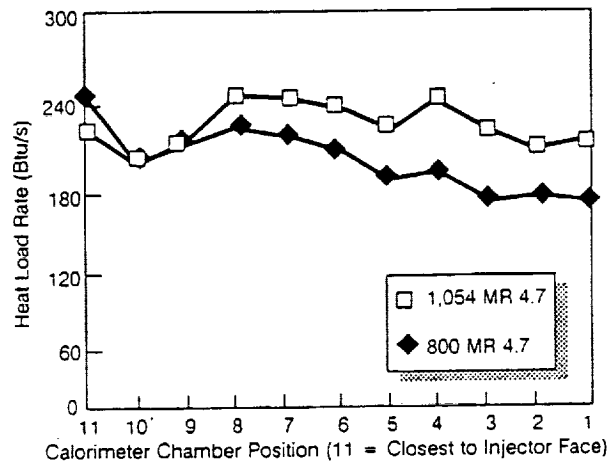


Figure 50: 0.040 Inch Ribbed Calorimeter 800 and 1000 psia Pc Test Results

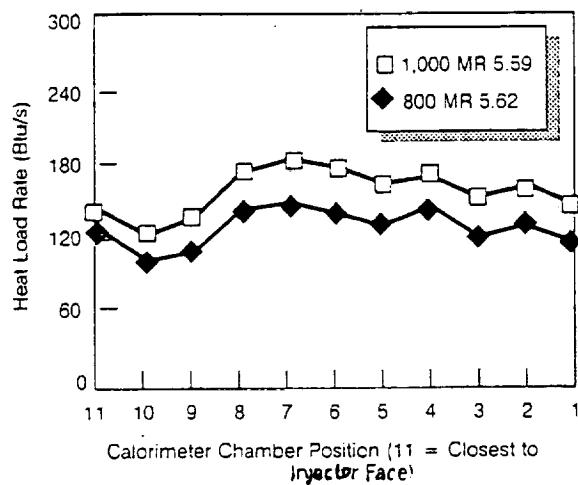


Figure 51: Smooth Wall Calorimeter 800 and 1000 psia Pc Test Results

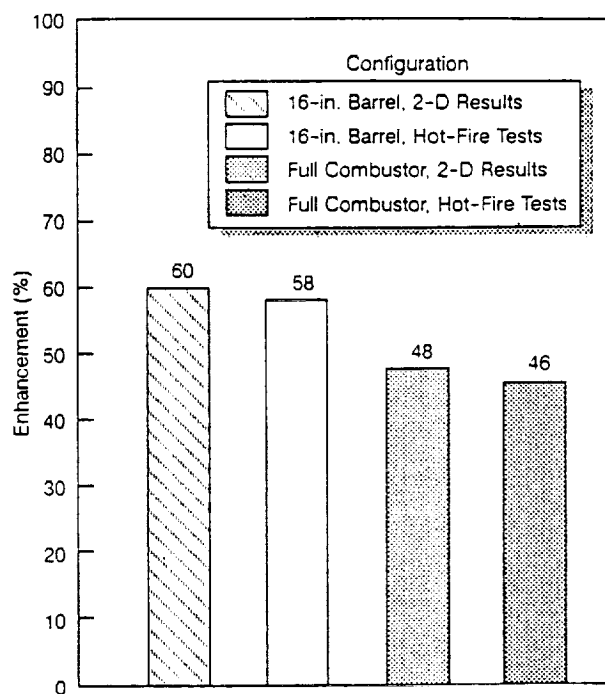


Figure 52: Heat Transfer Enhancement Comparison - 15 klbf Engine

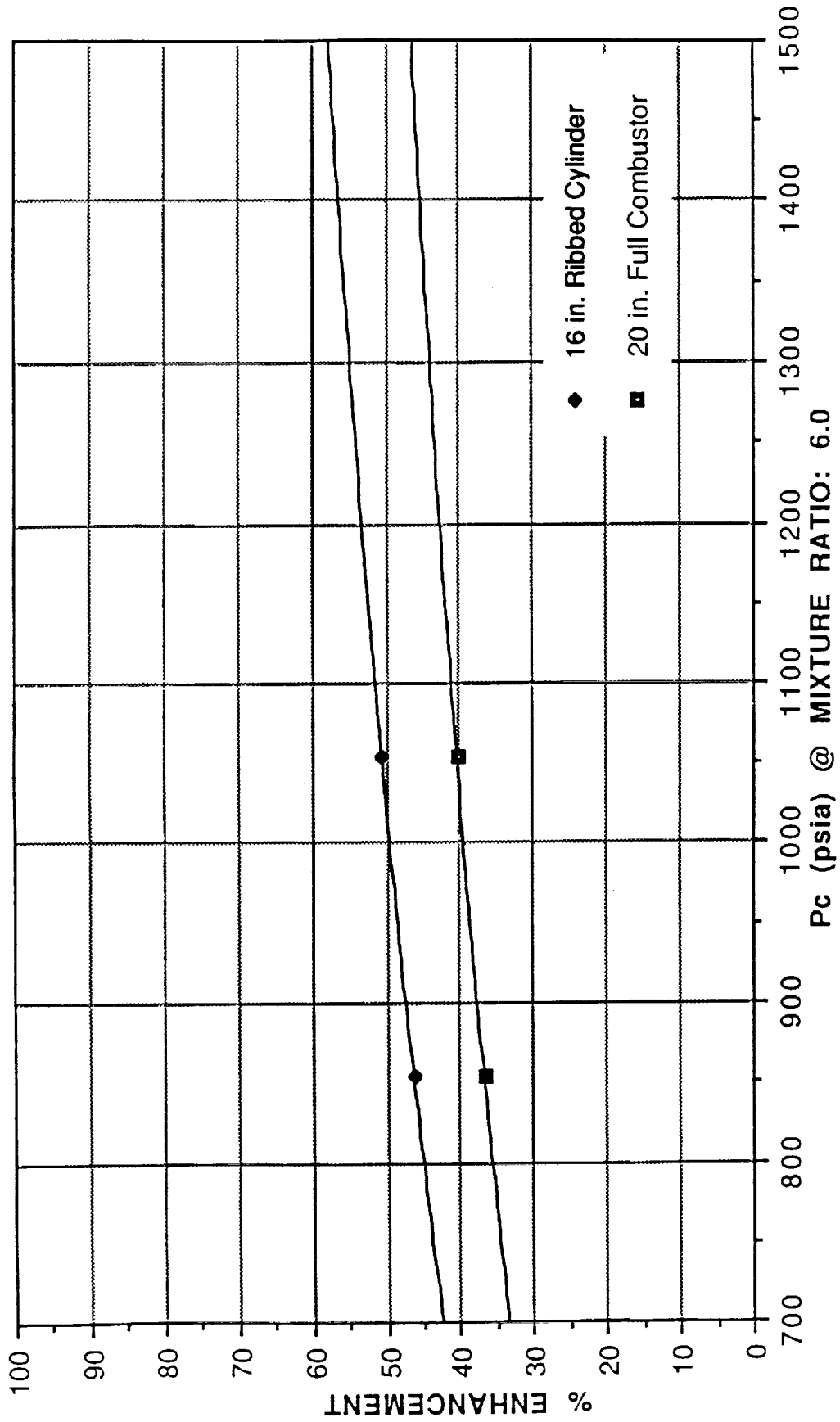


Figure 53: Heat Transfer Enhancement vs. Pc for 16 Inch Cylinder and 20 Inch Full Combustor

Fiberoptic Shaft Monitoring

Shaft dynamic behavior is a critical parameter in evaluating rocket engine turbopump component condition. Wear, erosion, spalling, pitting, and other surface degradation processes result in measurable changes to shaft dynamic motion. The measurement and interpretation of characteristic shaft motions can provide vital data for determining which components may be degrading, and to what extent the degradation has progressed.

In subtask E.5, a turbopump shaft monitoring system using fiberoptic sensors was designed. The system was intended to monitor shaft axial displacement, shaft orbit and shaft speed at up to 200,000 rpm. To provide these optical measurements, a method was developed to use a surface pattern on the shaft to modulate light as a function of shaft axial and radial motion, and speed. A fiberoptic deflectometer was adapted for use as the optical sensor. A suitable pattern was found to be eight triangles of non-reflective material whose change of reflectivity from that of shiny titanium shaft modulates the light intensity received by the deflectometer. This pattern is shown in relation to deflectometer position in the demonstrator schematic given in Figure 54. The modulation in light intensity, and the associated time periods of the change in intensity, indicated shaft axial and radial position and shaft speed. The method of displacement detection is explained in Figure 55. Extraction of these measurements was accomplished in a series of tests by a signal processing unit. The signal processor was designed to take the output of two orthogonal fiberoptic deflectometers which view this pattern, and to provide real-time voltages related to the amplitude of x,y and z motions, as well as speed.

This project required: (1) adaptation of the deflectometers to be used as the optical pickup, (2) development of a technique for economically applying a precision pattern on the shaft, (3) selection of an appropriate shaft surface treatment for placement of the pattern, and (4) development of an electronic signal analyzer to process the modulated deflectometer signal for extraction of the shaft motion and speed information.

Tests demonstrated the shaft monitoring system up to 10,000 rpm. The optical sensors were constructed for use in a 200,000 rpm LH₂ environment, and are ready for turbomachinery testing. The only remaining concerns are degradation of the reflection pattern due to oxidation or abrasion, and reflection intensity variations due to transmission through a two phase medium.

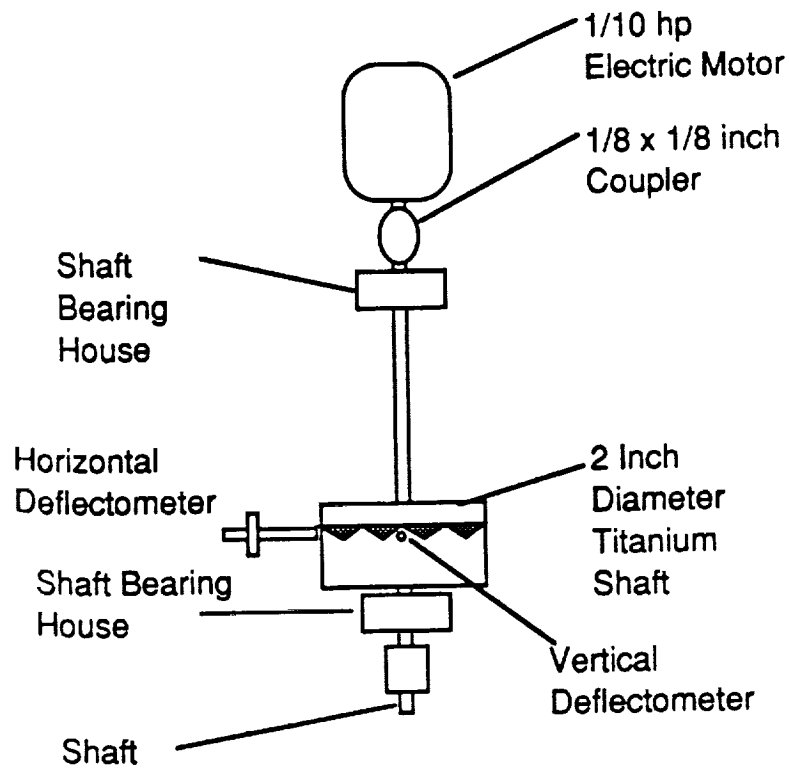


Figure 54: Rotating Hardware Demonstrator Configuration

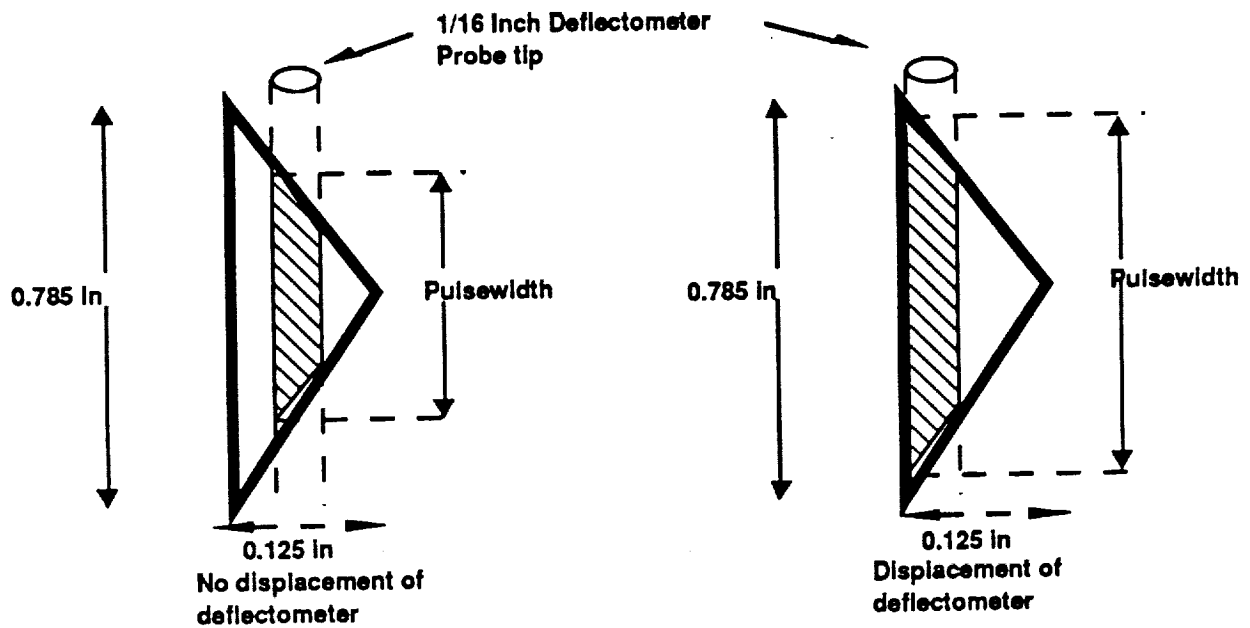


Figure 55: Probe View of Pattern

Combustor Wall Condition Monitoring

The scope of this additional subtask E.5 effort was to identify and evaluate condition monitoring technologies capable of nondestructively measuring wall thickness and the extent of cooling channel "doghousing" in test specimens emulating conditions which may exist in the throat region of the OTVE main combustion chamber after multiple firings. These measurements could then be correlated to the remaining combustor life, and be used to predict the overhaul schedule and requirements.

A literature search was performed resulting in thirteen candidate sensor technologies, which were initially evaluated against wall thickness measurement criteria such as thickness range, thickness and channel resolution, accuracy, and the simplicity of the measurement. From these criteria, three technologies -- ultrasonics, eddy currents, and electromagnetic acoustic transduction (EMAT), a noncontacting, couplant-free ultrasonic technique -- were selected for laboratory testing.

Transducers for measuring up to a 20-mil thick wall of copper with single channel resolution, were custom-designed and procured. Transducer fixtures were also designed and fabricated to provide for accurate, automated scans of the test specimens. Additionally, electromechanical translators were designed and fabricated to move the transducers at selected speeds across the specimens, and to monitor time and amplitude signals. Automated scans were then performed on a curved SSME combustor segment and channeled copper and Narloy-Z plates with 20-mil land/channel widths and wall thicknesses simulating OTVE combustor throat conditions.

Conventional ultrasonics easily distinguished between good channels, lands, and cut-through channels, providing a high-contrast amplitude signal. However, in its present configuration, its immersion or liquid couplant requirements inhibit its implementation for space-based applications. The test apparatus necessary for the ultrasonic testing is sketched in Figure 56. Output correlations with a test sample are shown in Figure 57.

Eddy current techniques were then tested and found to readily resolve a 0 - 10 mil thick wall thickness, and up to a 20-mil thick wall when not adjacent to thin-walled channels. This technology also provides a high-contrast signal for wall thickness measurements, and has the added feature of not requiring couplants. Eddy current traces for copper and Narloy-Z test pieces show strong signals at thin walled areas in Figures 58 and 59.

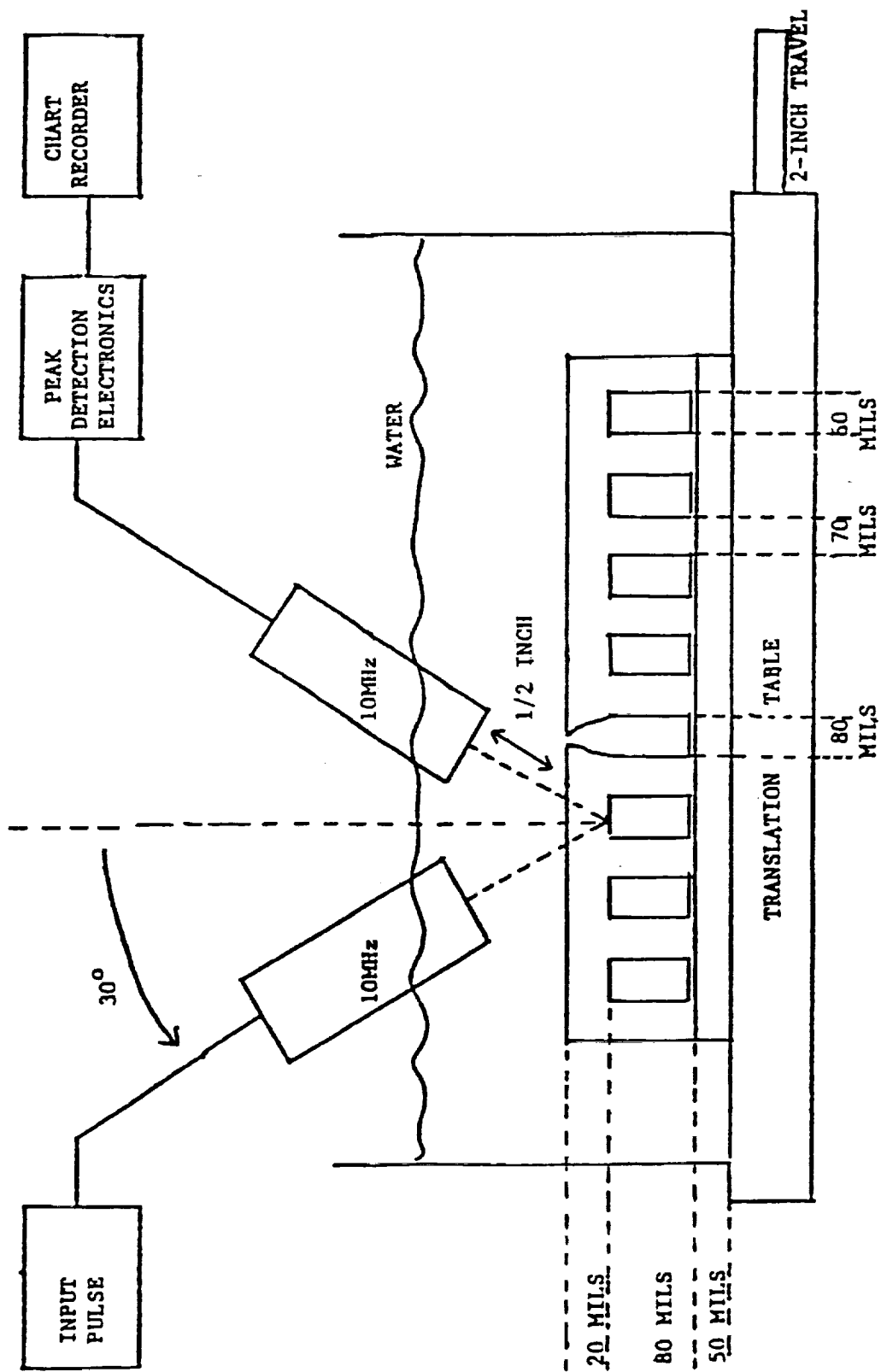


Figure 56: Ultrasonic Test Apparatus

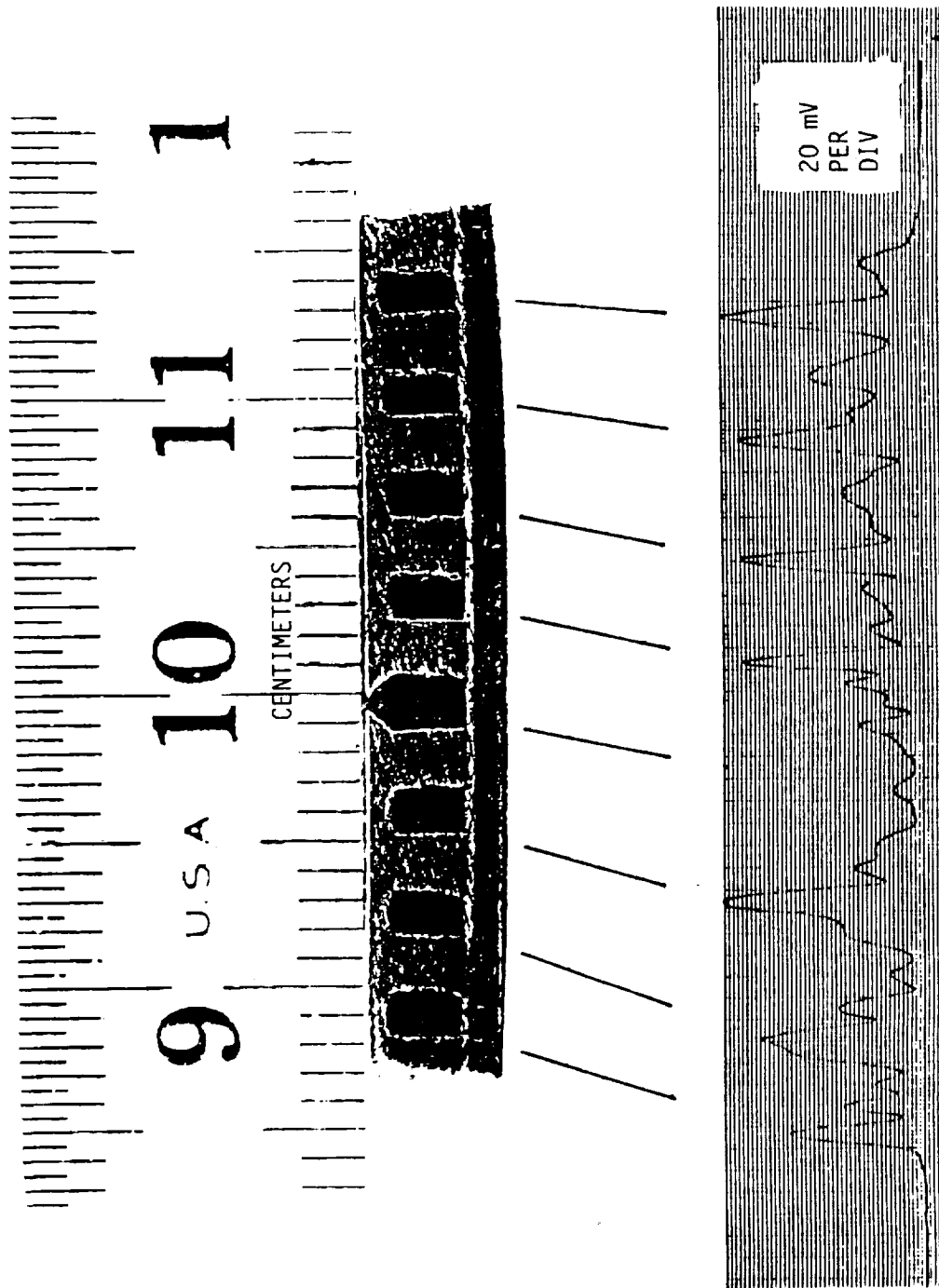


Figure 57: Ultrasonic Test Results

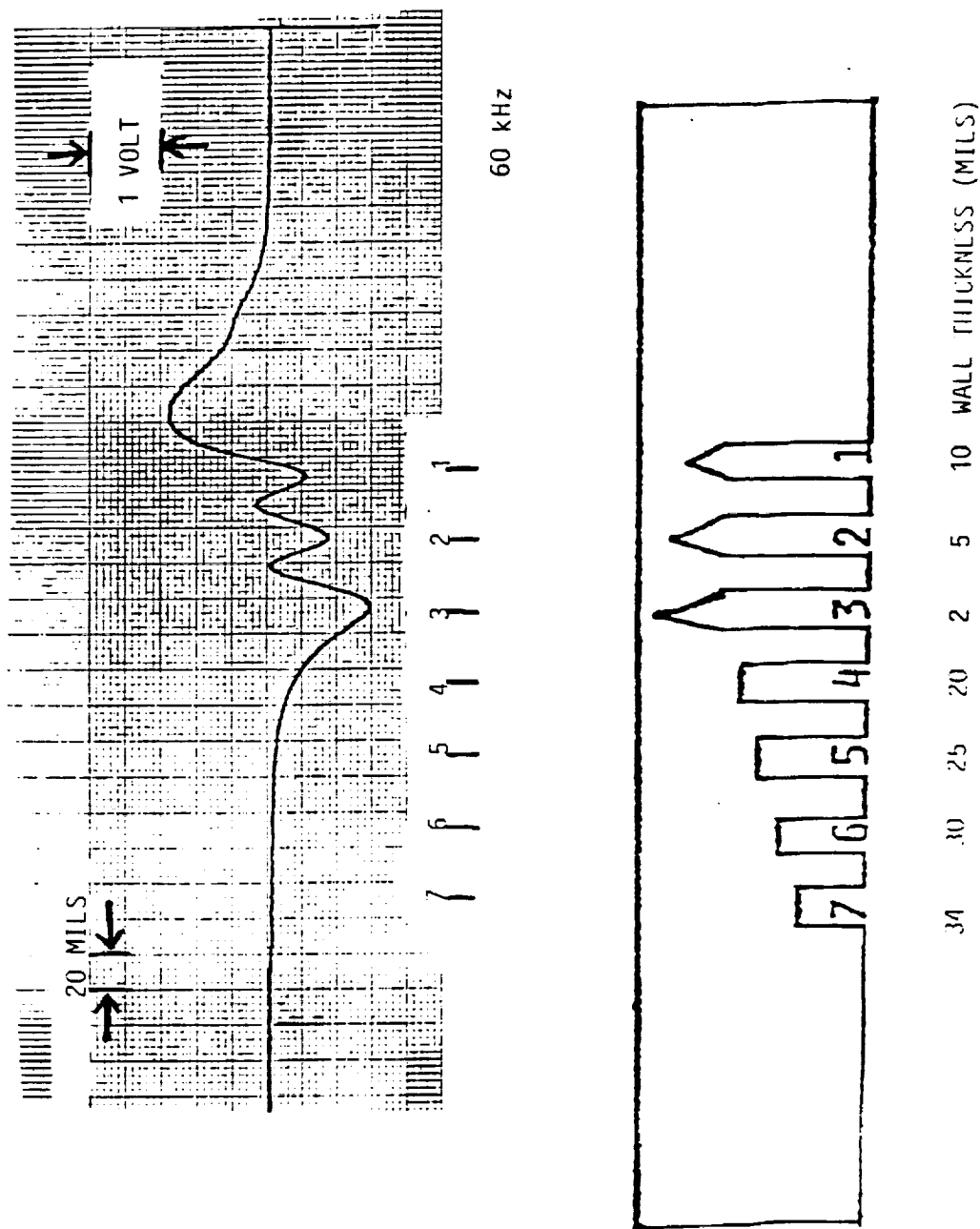


Figure 58: Experimental Trace of an Automatic Pitch/Catch Eddy Current Scan of a Copper Test Piece with 20-Mil Land/Channel Widths

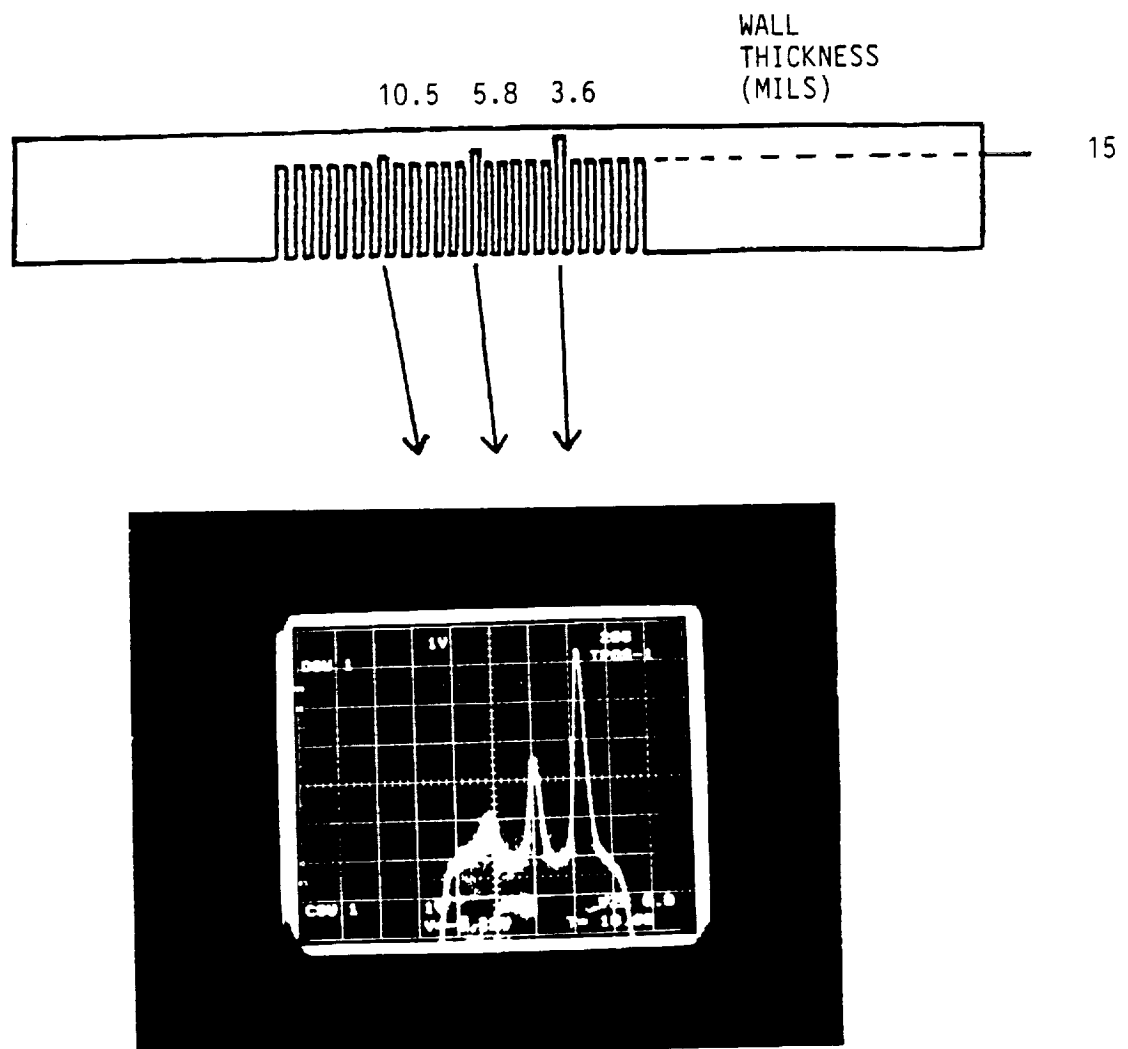


Figure 59: Differential Eddy Current Scan Showing Strong Signals From Three Thin Wall Channels

The couplant-free ultrasonic EMAT technology was also tested. A cutaway view of an EMAT is seen in Figure 60. Results showed that the EMATs could easily resolve signals from a single channel, but that additional data processing algorithms are required to correct for acoustic interference caused by multiple, consecutive channels. This effect is illustrated in Figure 61. Once this is performed, EMAT signal amplitude can be correlated with wall thickness to provide a second couplant-free combustor wall thickness measurement technique.

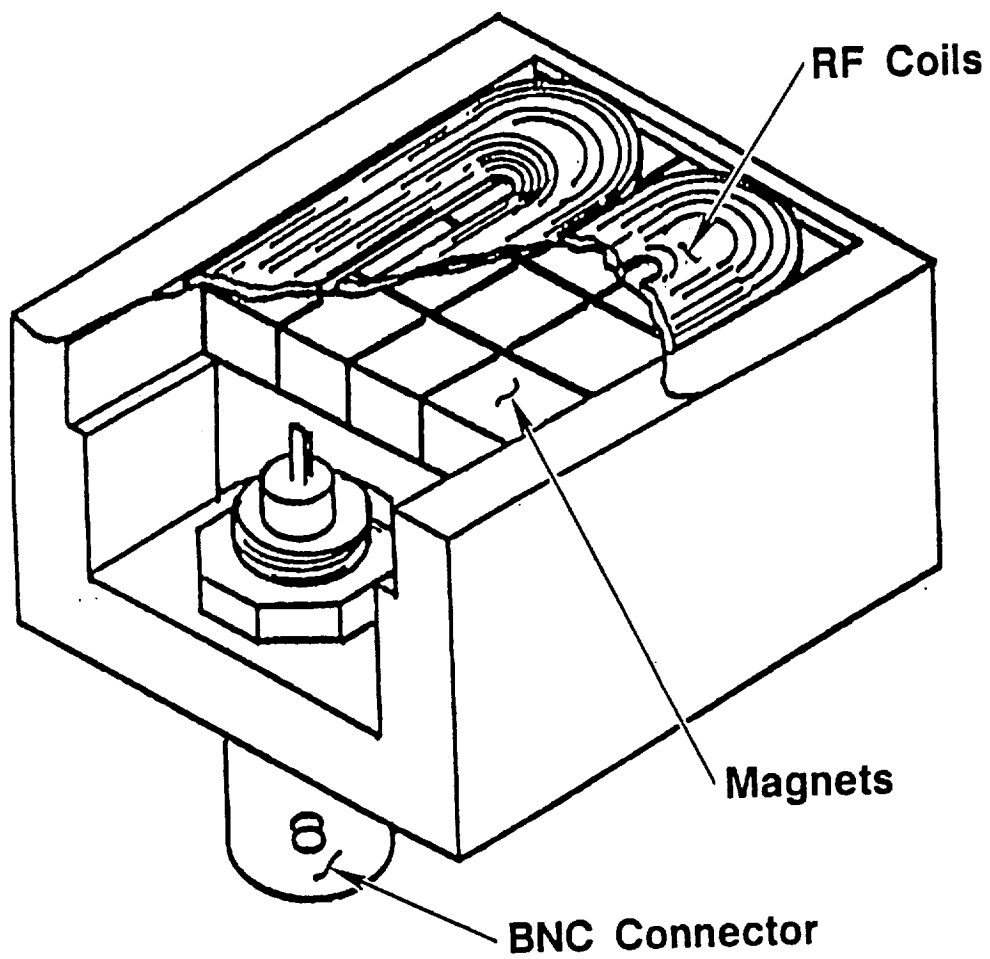
ICHM Elements

The ICHM system was to provide comprehensive control and monitoring capabilities in support of overall OTVE mission requirements. OTVE missions included requirements for long duration space exposure and multiple, zero gravity engine starts, as well as the capability for deep throttling for landings. A list of ICHM requirements and the minimum ICHM system functions from which they were derived are listed in Figure 62. More specifically, reusability requirements dictated a service-free life of 20 missions, with 100 starts and a total engine operational time of 4 hours. The overall system life (with service) requirement is established as 100 missions, with 500 starts and engine operational time of 20 hours.

The resulting ICHM system was defined in subtask E.6 and included control and condition monitoring electronics, sensing elements, software/algorithms and effectors. Effectors were those components of the ICHM which were commanded by the controller electronics to operate the OTV engine. These included valve actuators, nozzle extension and gimballing actuators and igniters. The ICHM architecture incorporating all these elements is depicted in Figure 63.

Individual sensor types were chosen to fulfill the specific ICHM functions. The sensor technologies selected for each of the sensor types are given in Table 18 along with their various attributes. Locations on the OTVE where these sensors are used by the ICHM system are labeled in Figure 64.

The technical readiness and development costs of the ICHM system were also calculated in subtask E.6. The minimal ICHM system was derived from a flowdown of engine requirements into system functions. These were evaluated and translated into a minimum set of ICHM elements (sensors, actuators, electronics, and software) to meet the



**Figure 60: Cutaway View of an
Electromagnetic Acoustic Transducer (EMAT)**

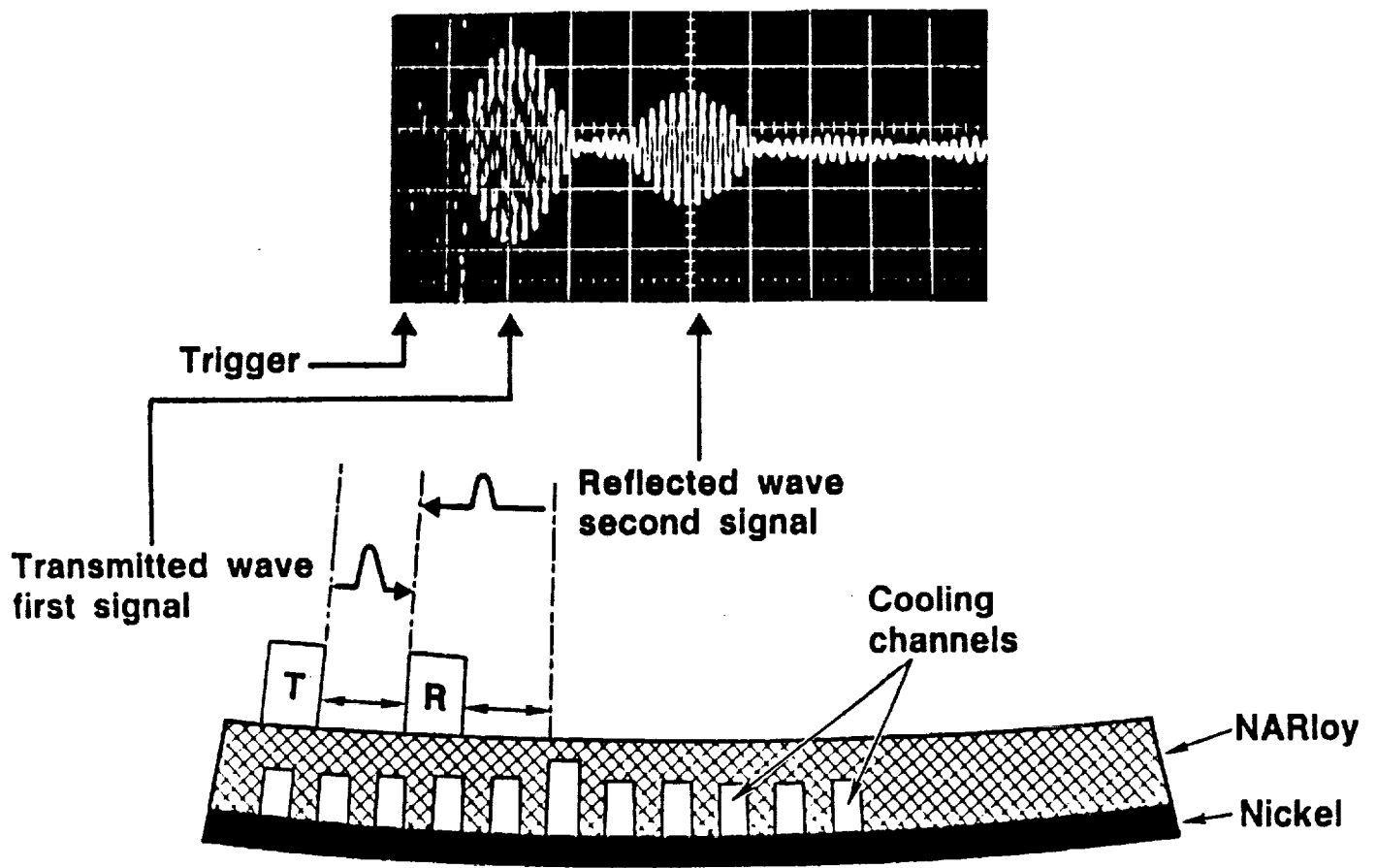


Figure 61: Thin Wall Channel Detection in Test Specimen Using EMAT Technology

ICHM Minimum Functions		ICHM Requirements							
		Nominal Engine Operations	Start and Cutoff in Zero-G	Throttling	Performance Requirements	Single Engine Reliability	Dual Engine Reliability	Service Free Life	Space Based
Start	Pre-Start Checkout	●							●
	Engine Conditioning	●							
	Start Ready Verification		●						
	Tank Head Sequence		●						
	Tank Head OK Verification		●						
	Pump Idle Ready Verification		●						
	Pump Idle Sequence		●						
	Pump Idle OK Verification		●						
	Main Stage Ready Verification		●						
	Main Stage Transition		●						
	Main Stage OK Verification		●						
	Start Transient Abort Sequences		●						
	Closed Loop, Proportional Thrust Control		●	●	●				
	Closed Loop, Proportional MR Control		●	●	●				
Mainstage	Multi-Variable (Coupled) Thrust/MR Control		●	●	●				
	Propulsion Level Thrust Vector Control					●			●
	Management of Coolant Resources				●	●	●		
	Mainstage Cutoff Sequence		●						
Shutdown	Engine Safing	●							
	Passive Cutoff System	●							
	Retractable Nozzle Control	●							
Safety Monitoring	Redline Monitoring					●	●		●
	Failure Detection/Accom Algo/Model					●	●		●
Condition Monitoring	Maintenance Algorithms					●			●
	Control System Fault Detection					●		●	
	Post Hot-Fire OK Verification					●		●	

Figure 62: ICHM Requirements and Corresponding Functions

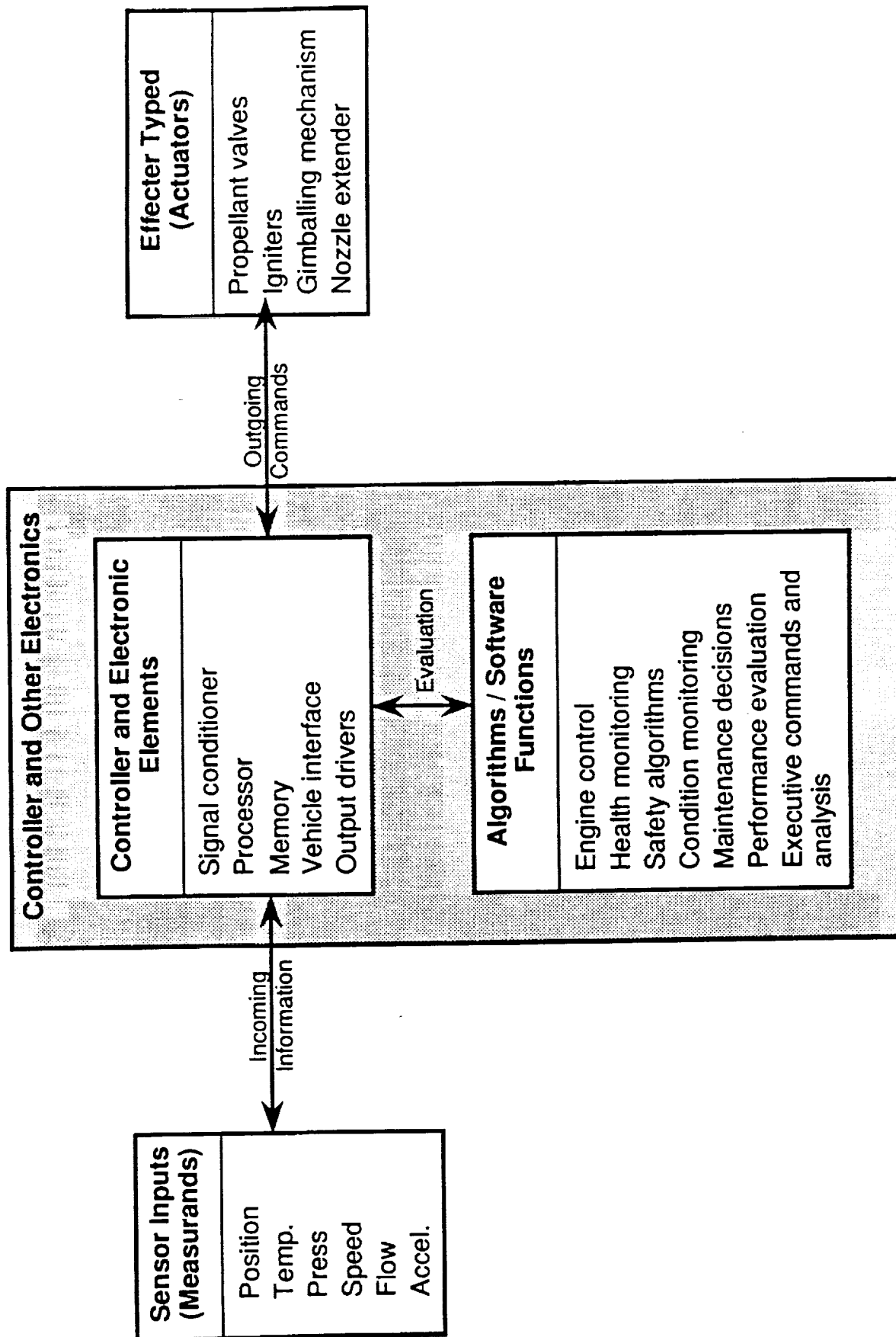


Figure 63: OTVE ICHM Element Architecture

Table 18: Sensor Technology Selections

MEASURE- MENT TYPE	STATIC PRESSURE	STATIC TEMPERATURE	FLOW	SPEED	DISPLACEMENT (continuous)	POSITION (on/off)	ACCELER- ATION
RECOMMENDED TECHNOLOGY	Silicon on Sapphire	Resistive Temperature Device	Turbine	Variable Reluctance	Resolver	Eddy Current	Piezoelectric
OPERATING RANGE	0/9000 PSI	LH2/+1400 °F	0/40 Lbm/sec	0/200,000 RPM	0/90 degrees	n/a	0/100,000 g
MEASUREMENT UNCERTAINTY	0.5% full scale	0.1% full scale	1.0% full scale	0.5% full scale	0.25% full scale	TBD	TBD
NOMINAL OUTPUT	0/50 mV d.c.	Bridge- dependent	Computed quantity	TBD V a.c.	TBD	5 V d.c. max	100,000 pC
OPERATING TEMPERATURE	0/1000 to 1500 R	20/1500 R	30/1500 R	0/1000 to 1500 R	30/1500 R	30/1500 R	20/1500 R
OPERATING PRESSURE	25/4000 PSIA typical	10/4000 PSIA	100/11,000 PSIA	10/10,000 PSIA	100/11,000 PSIA	100/4000 PSIA	100/10,000 PSIA
ALTERNATE TECHNOLOGY #1	Piezoresistive		Ultrasonic	Torque meter	L.V.D.T. *	Limit Switches	
ALTERNATE TECHNOLOGY #2						Proximity Switches	
COMMENTS AND LEGEND	Extremes range from 0 to 11,000 PSIA	Element is 50/5000 ohm	Need pressure and tempera- ture to compute	May combine with torque measurement	* Linear Variable Displace-ment Transformer		pC = pico- Coulombs, R = Rankine

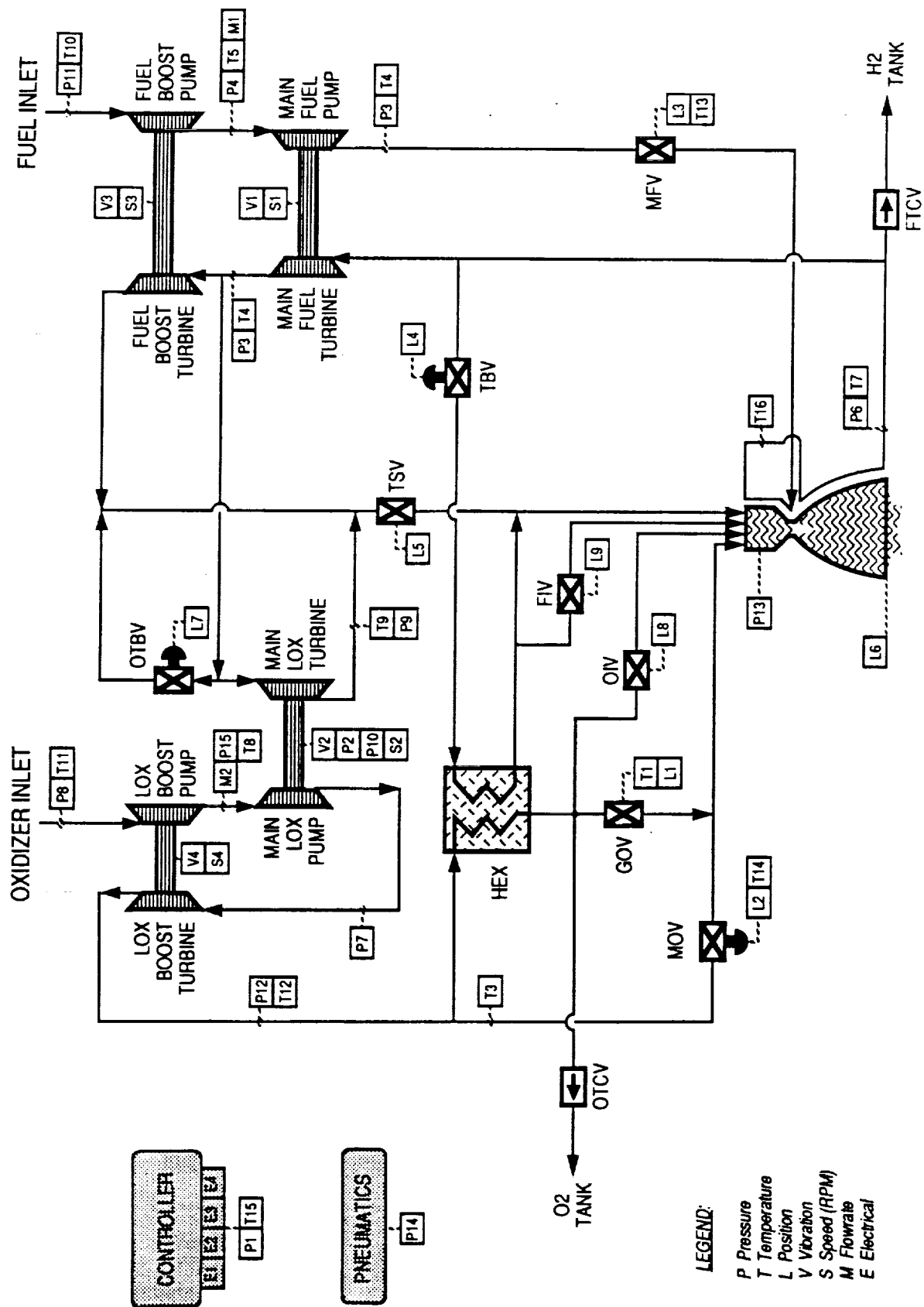


Figure 64: OTV Engine with Sensor Locations

requirements with the highest possible technology readiness. A baseline design for each of these elements was then described in enough detail to estimate the technology readiness and development costs of the minimum system. These costs are tabulated in Table 19.

Automated Preflight Checkout

A space-based chemical propulsion system capable of multiple starts and varied mission scenarios would require extensive preflight checkouts to assure crew safety and mission success. An automated approach for a space-based OTVE preflight checkout system was highly desirable from the standpoints of reliability and feasibility. Such a system was analyzed in subtask E.7.

Approaches to automating preflight readiness checkouts depended heavily on condition monitoring technology to provide the information required to assess the engine's readiness to fire. Condition monitoring sensors would permit remote monitoring of critical components as the engine fires during normal operation. Based on the flight data obtained from these sensors, an assessment could be made on the condition or health of a particular component which in turn would dictate the need for maintenance procedures or replacement. This study evaluated various methods of preflight readiness checkouts in the context of a space-based system. Where required, methods incorporated advanced Integrated Control and Health Monitoring (ICHM) technologies enabling rapid and remote engine turnaround.

Preflight readiness verification requirements were established for the engine. Requirements were based on previous logistics studies including the preliminary FMEA and the flow task analysis report. The requirements are listed in Table 20. This work supported previous efforts to establish the operational flow of the engine and identify the applicable maintenance tasks for both current and advanced technology hardware. The operational flow tasks of interest to this study were those executed after delivery to the space station and before return to earth. Maintenance tasks were reviewed in light of the SSME Operations and Maintenance Requirements and Specifications Document which reflected the current inspection and checkout philosophy evolved from the Challenger incident. Thirty six preflight readiness verification requirements were identified for the engine. Requirements included 14 functional checks, 10 leak checks, 10 inspections, and 2 servicing tasks.

Table 19: OTV ICHM Cost Estimate Summary

ELEMENT CATEGORY	MANHOURS	LABOR COST	HARDWARE	TOTAL	DURATION-MONTHS
SENSORS	3710	\$241,150	\$236,000	\$477,150	54
ELECTRONICS	354160	\$23,020,400	\$3,016,000	\$26,036,400	60
EFFECTORS (INCL VALVES)	117344	\$7,627,360	\$6,593,000	\$14,220,360	48
SOFTWARE	86396	\$5,615,740		\$5,615,740	60
				GRAND TOTAL	
				\$46,349,650	

Table 20: OTV Preflight Requirements

Functional Checks	Inspections
<ol style="list-style-type: none"> 1. Valve Actuator Check 2. Sensor Checkout/Calibration 3. Pneumatic Component Checkout 4. Operational Sequence Test (FRT) 5. Control System Redundancy Verification 6. Controller Memory Verification 7. Controller Pressurization Verification 8. HPOTP Torque Check 9. HPFTP Torque Check 10. LPOTP Torque Check 11. LPFTP Torque Check 12. Turbopump Axial Shaft Travel Check 13. Extendible Nozzle Travel Check 14. Igniter Operation 	<ol style="list-style-type: none"> 1. Exterior of Components for Damage/Security, etc. 2. T/C Assembly for Evidence of Coolant Passage Blockage 3. HPFTP Turbine Wheel/Blades for Cracks, Fatigue, and Damage 4. HPOTP Turbine Wheel/Blades for Cracks, Fatigue, and Damage 5. LPFTP Turbine Wheel/Blades for Cracks, Fatigue, and Damage 6. LPOTP Turbine Wheel/Blades for Cracks, Fatigue, and Damage 7. HPOTP Bearings for Damage 8. T/C Assembly Injector Faceplate, Igniter, and Lox Post Tips for Erosion, Burning, and Contamination. 9. Gimbal Bearings and TVC Attach Points for Evidence of Bearing Seizure and Fatigue. 10. Heat Exchanger for Cracks, Evidence of Wear, and Damage
Leak Checks	
Servicing Tasks <ol style="list-style-type: none"> 1. Combustion Zone Drying <ol style="list-style-type: none"> a. Igniter Valves b. P_c Sensors 2. HPOTP Lox/Turbine Drive Gas Seal Pre-Start Purge 	<ol style="list-style-type: none"> 1. HPOTP Primary Lox Seal 2. HPOTP Lox/Turbine Drive Gas Seal 3. Oxidizer Inlet Valve and MOV Ball Seals 4. Fuel Inlet Valve and MFV Ball Seals 5. Propellant Valves Primary Shaft Seals 6. Pneumatic Control Assembly Internal Seals 7. Heat Exchanger Coil Leak Test 8. Heat Exchanger Coil Proof Test 9. Thrust Chamber Assembly Outer Walls 10. Combustion and Propellant System Joints

Several approaches for remotely performing readiness checkouts in space were outlined for each preflight requirement. The range of approaches reflected a variety of method sophistications. Three approaches for remotely obtaining data were considered: (1) preliminary power-up, in which the engine is fired for a short time to acquire real time data, (2) automated component pre-cycling, in which engine components are cycled in an inert gas medium to assess component integrity without hot firing the engine, and (3) automated static checkout, in which an analysis of historical data and static checks are used to assess the engine's readiness to fire without the cycling of any components.

Issues and benefits were generated for each of the three preflight checkout approaches. Sensors and flight hardware, alternate component designs, and general approach were all addressed. Issues and benefits were categorized into space basing, vehicle infrastructure, and engine system impacts.

The technology readiness levels of the three preflight checkout methods were also evaluated as shown in Table 21. The scale used for comparing the methods was that used by the NASA office of exploration for evaluating options for future mission choices, given in Table 22. Estimates were also made for the remaining cost to advance the technology for each method to a level 6, where the system validation models have been demonstrated in a simulated environment. These costs are itemized in Table 23 and totaled for the different methods and technology levels in Table 24.

Table 21. Method Readiness Assessment

	Average Sensor Readiness	Minimum Sensor Readiness	Overall System Readiness
Preliminary Power Up	5.0	4	5
Automated Component Pre-cycling	4.9	4	4
Automatic Static Checkout	5.0	4	4

TASK F - ENGINE TEST FIRINGS

A 15,000 lbf thrust, pump-fed liquid oxygen/liquid hydrogen, advanced expander cycle rocket engine identified as the RS-44 Integrated Component Evaluator, was designed and

Table 22: Technology Readiness Level Definitions

Level 7	System validation model demonstrated in space; system ready for space-based applications
Level 6	System validation model demonstrated in simulated environment; test of an equivalent of the final system configuration
Level 5	Component and/or breadboard demonstrated in relevant environment
Level 4	Component and/or breadboard demonstrated in laboratory
Level 3	Analytical and experimental proof-of-concept for critical function and/or characteristic; conceptual design test
Level 2	Technology concept/application formulated; conceptual design drafted
Level 1	Basic principles observed and reported

Table 23: Element Development Costs

Summary of Development Cost Elements by Task*		(M\$, 91)
Sensor Development		0.5 to 8.0
Delta Software Development		
Maintenance Data Base • Optimized engine		3.5
• Not optimized engine		4.6
Process Software • Optimized engine		2.4
• Not optimized engine		3.6
Delta Computer Hardware Development		2.5
Soft Simulation		0.7
Hard Simulation		8.0
Integrated Sensor/Computer System Brassboard		4.0
OTVE Modification (for Cat. 2 only)		2.3
AETB Test Support		2.4

* These costs are not additive. The proper elements are combined for 4 different cases as shown in Table 24.

Table 24: Development Program Costs (M\$, 91)

	Engine Optimized for Space Base Operations				Engine <u>Not</u> Optimized for Space Base Operations			
	Max. Use of Current Sensors (Cat. 1, 2, 3)	Max. Use of Advanced Sensors (Cat. 1)	Max. Use of Advanced Sensors (Cat. 2, 3)		Max. Use of Current Sensors (Cat. 1)	Max. Use of Advanced Sensors (Cat. 1)	Max. Use of Advanced Sensors (Cat. 2)	Max. Use of Advanced Sensors (Cat. 3)
Sensors	2.5	4.0	5.5		5.5	2.5	7.5	5.5
Δ Software	← 5.9	→	→		← 8.2	→	→	→
Δ Computer	← 2.4	→	→		← 2.4	→	→	→
Soft Simulation	← 0.7	→	→		← 0.7	→	→	→
Hard Simulation	← 8.0	→	→		← 8.0	→	→	→
Integrated Brassboard	← 4.0	→	→		← 4.0	→	→	→
Engine Modifications	← —	→	→		← —	→ 2.3	→	→
AETB Test Supp.	← 2.4	→	→		← 2.4	→	→	→
Total	\$25.9M	\$27.4M	\$28.9M		\$31.2M	\$29.5M	\$28.2M	\$31.2M

Note: Preflight checkout category (1) = preliminary power up, (2) = automated precycling, (3) = automated static checkout

fabricated between the years 1982 to 1985 using Rocketdyne discretionary funds. The ICE system was conceived to demonstrate the performance and operational characteristics of an advanced expander cycle rocket engine and its components.

During the year 1985, component testing of the ICE turbomachinery was accomplished with Rocketdyne funds to characterize the individual pump performance capabilities as well as startup transient control of the turbopumps. The turbomachinery employed in the ICE were the Rocketdyne MK49-F high pressure liquid hydrogen and the MK49-O high pressure liquid oxygen turbopumps shown in Figures 65 and 66 respectively. The MK49 turbopumps were installed on the ICE during the component tests with propellants bypassed to overboard drains and burn stacks. This scheme permitted the installation of the entire engine system, requiring little down time to convert from turbopump component testing to engine testing.

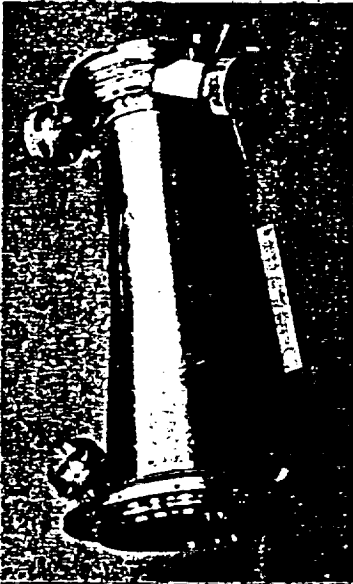
Nineteen successful turbomachinery checkout tests were conducted, including head versus flow excursions at various power levels. Transition data from these tests determined the component start sequence transients. A balance piston capability issue also surfaced during the MK49-F hydrogen turbopump component testing. The balance piston position calculations indicated a progressive closing position as the speed increased, therefore the safe rotor speed limit of the MK49-F turbopump for balance control was set at 87,000 rpm.

Once the turbopump testing was accomplished, testing of the ICE under Task F of this contract, NAS3-23773, began. An engine sub-system checkout methodology was employed to gradually transition into full engine test operations. Thirteen tests from early in 1986 to January 1987 were performed. For these engine system tests, the turbopump propellant discharges were routed into the ICE thrust chamber assembly instead of the drains and burn stacks previously employed. Figure 67 shows the elements comprising the ICE thrust chamber assembly; the tapered combustor, the sea level 35:1 area ratio test nozzle, the plasma torch igniter and the coaxial injector elements. Figure 68 shows the complete ICE engine installed in the NAN stand of the Advanced Propulsion Test Facility at the Rocketdyne Santa Susana Field Laboratory.

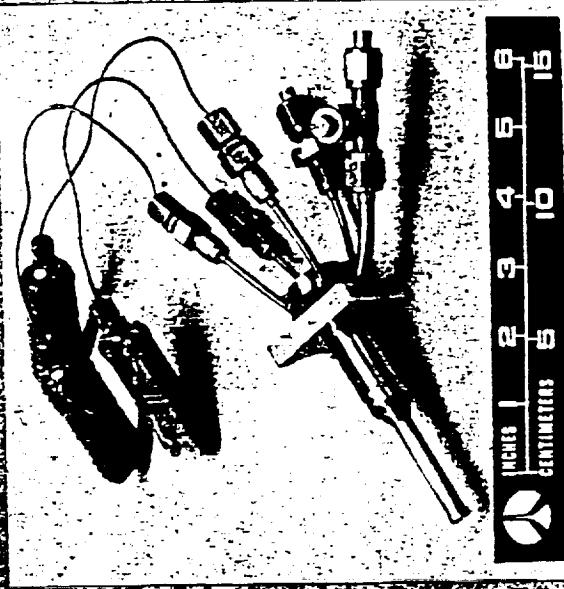
A summary of the first seven tests conducted under Task F is presented in Table 25. Igniter valve sequencing was based on the results of a previously conducted igniter test program. The sequencing resulted in nearly simultaneous entry of the GO_2 and GH_2 into



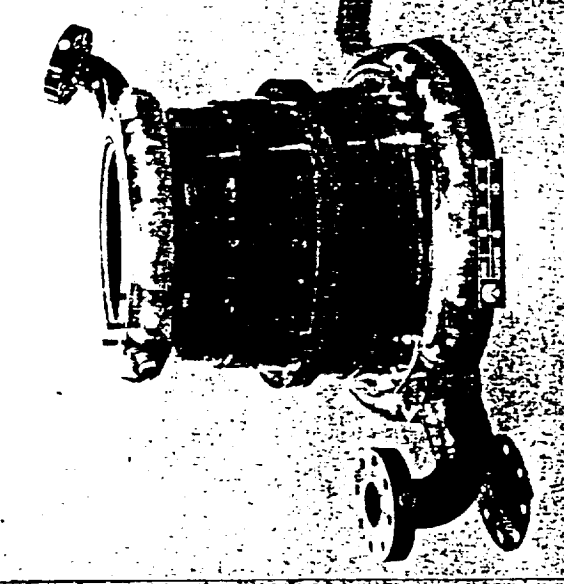
INJECTORS



COMBUSTOR



IGNITER



NOZZLE

LC490-398



Rockwell International
Rockwell International
Rockwell International

Figure 65: I.C.E. Combustion System Components

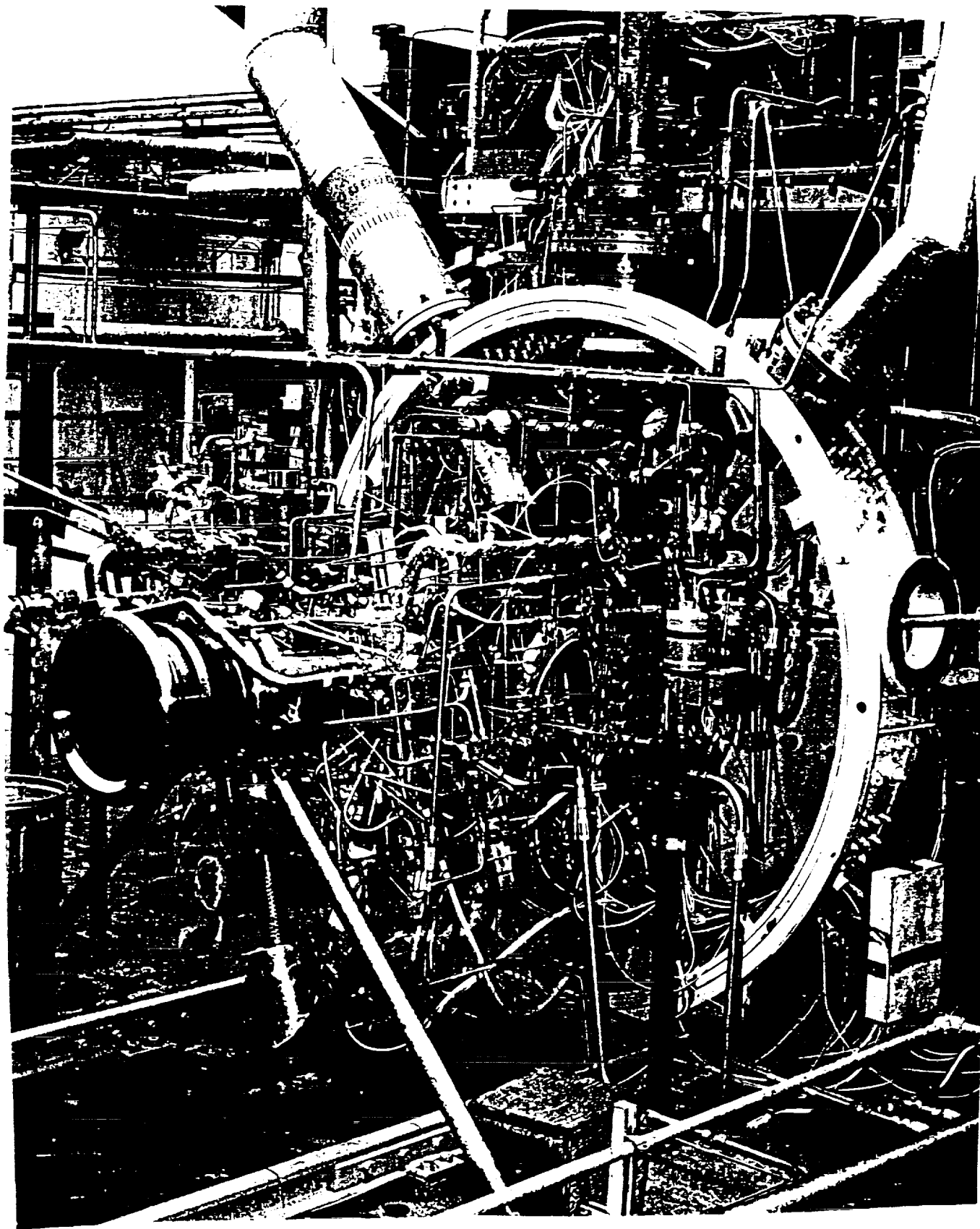


Figure 66: Installed I.C.E. Engine

Table 25: Integrated Component Evaluator Test Log

TEST (DATE)	OBJECTIVES (CUTOFF)	COMMENTS
017-001 (4/04/86)	LH ₂ BLOWDOWN (MANUAL)	MOV COMMAND SIGNAL NOT RECORDED. PRETEST TIME FROM COMMAND TO 50% MOV POSITION WAS 360ms. TEST TIME FROM 50% MOV TO LH ₂ INJECTOR PRIME WAS 170ms. COMMAND TO PRIME WAS ~530 ms.
017-002 (4/04/86)	1) IGNITER FIRING 2) LH ₂ BLOWDOWN	PRETEST: LH ₂ CHILL FASTER THAN T/P TESTS: NO OSCILLATION WHEN PUMP D/S BLEED CLOSED MANUALLY TEST: GOOD IGNITER OPERATION. 10 PSI PK/PK FP INLET OSC. WHEN D/S BLEED CLOSED. MFV DID NOT OPEN. SETUP ERROR. POSTTEST: COMBUSTOR CLEAN AND DRY.
017-003 (4/04/86)	LH ₂ BLOWDOWN (MFV MIN. POS. GATE)	GOOD IGNITER OPERATION. MFV DID NOT GET TO 25% WITHIN 300 ms. POSTTEST: GAS IN HYDRAULIC SYSTEM. BLEED SYSTEM. TEMPORARILY DISABLED MFV POS. C. O.
017-003 (4/09/86)	LH ₂ BLOWDOWN (DURATION TIMER)	PRETEST: CHILL TOOK LONGER THAN ON 4/4. IGN. GH ₂ REG. REQUIRED FREQUENT RESETTING. TEST: GOOD IGNITER FIRING FOR 3 SEC. MFV DID NOT OPEN ALTHOUGH MFV SERVO CURRENT INDICATED. TBV DID NOT OPEN @ C. O. POSTTEST: TBV AND MFV WORKED OK MANUALLY. NO ICE ON MFV CRANK (BAGGED) OR ON TBV. ADDED AMBIENT PURGE ON MFV ACTUATOR.

Table 25: Integrated Component Evaluator Test Log (Cont.)

TEST (DATE)	OBJECTIVES (CUTOFF)	COMMENTS
017-005 (4/09/86)	LH ₂ BLOWDOWN (FTP SPEED)	<p>PRETEST: MANUALLY CYCLED MFV & TBV A FEW DEGREES JUST BEFORE TEST. SAME IGN. GH₂ REGULATOR PROBLEM.</p> <p>TEST: GOOD IGNITER FIRING. FTP SPEED GOT TO 69KRPM (48K PRED). OTP REACHED 29KRPM. MFV & TBV WORKED OK. FUEL INJ. PRIMING TIME WAS 380 ms. FTP H/Q TRANSIENT WAS OK.</p> <p>POSTTEST: A SMALL EXPLOSION AND H₂ FIRE OCCURRED WHEN THE LH₂ TANK WAS PRESSURIZED FOR THE NEXT TEST. ONLY INSULATION WAS DAMAGED. LEAKS IN THE INLET PLUMBING WERE FOUND AND SEALED. A WARM GH₂ PURGE WAS ADDED TO THE EXTERIOR OF THE MFV AND MOV ACTUATORS.</p>
017-006 (4/14/86)	MAIN PROPELLANT IGN. (MAX. Pc = 250 PSIG)	<p>PRETEST: CYCLED MFV, MOV, TBV 10 DEGREES. IGN. GH₂ REG. SET AFTER MAIN TANK PRESSURIZATION. NO PROBLEM.</p> <p>TEST: OPERATED AS PLANNED UP TO CUTOFF. Pc & FTP SPEED REACHED 430 PSIA & 74KRPM. THUS SATISFYING OBJECTIVES OF NEXT PLANNED TEST.</p> <p>POSTTEST: INJECTOR/COMBUSTOR IN GOOD VISUAL CONDITION. SLIGHT DISCOLORATION ON INJECTOR FACE.</p>
017-007 (4/14/86)	TRANSITION TO FTP SPEED - 84KRPM (T/C ACCELEROMETER)	<p>PRETEST: L02 INJ SHUTDOWN PURGE PRESSURE REDUCED.</p> <p>TEST: GOOD IGNITION, TRANSITION TO 710 PSIA CHAMBER PRESSURE, 83KRPM FTP SPEED.</p>

the igniter and provided successful igniter ignitions in all six tests where ignition was attempted.

The successful oxidizer and fuel blowdown tests (001 and 005) defined the priming times for each propellant in the main injector. The main propellant valve sequencing they defined resulted in propellant ignitions on both attempts (tests 006 and 007). The main oxidizer and fuel valves were opened in the first part of the sequence with the turbine bypass valve (TBV) closed to accelerate the start and the oxidizer turbine bypass open as required by steady state target conditions for these tests. The TBV was later sequenced to a control position to limit chamber pressure. The TBV was commanded to ramp to 34 percent and begin to open on test 007 but cutoff was initiated before it became significantly effective.

Table 26 presents the remaining six engine systems test results. They provided a short transition into main combustion chamber ignition and finally into mainstage operation. Thermal equilibrium of the engine system was calculated to occur at about 10-seconds run time. Therefore, to conserve engine operation time and lower propellant and test costs, the mainstage tests were held to a maximum 10-second duration.

Tests 017-003, 017-005 and 017-006 demonstrated expander cycle operation: ignition, transition, steady state mainstage and shutdown. The highest fuel turbopump speed (87,400 RPM) was achieved on test 017-006 where the maximum test chamber pressure of 776 psia was also recorded. This chamber pressure was almost twice the current 400 psia operating point for expander cycle engines (RL10).

In test 017-006 the fuel turbopump #4 (turbine end) bearing failed, precluding any further testing. This fuel turbopump anomaly may be the result of a technology issue requiring resolution and culminating in internal design changes. Operation of all components excluding the fuel pump was satisfactory, however, during the tests. The oxidizer turbopump performed as predicted and the thrust chamber assembly resistances and heat loads appeared nominal. Since the engine system was an expander cycle, the failure consequences were rather benign and the shutdown was safe with no other secondary failure occurrences to the engine.

Both nominal and emergency shutdowns were achieved without causing any damage or distress to any system component. Unplanned fuel stoppage generally results in thrust chamber burnout or severe thermal distress. Neither of these resulted when the fuel pump

Table 26: I.C.E. Engine Systems Test Log

<u>Date</u>	<u>Test Objectives</u>	<u>Test Results*</u>	<u>Remarks</u>
1-15-87 017001	Fuel pump speed c/o at 75000 RPM	Test terminated before sequence start due to prep complete dropout. GH ₂ opening pressure loss on LH ₂ D/S bleed when Lox D/S bleed closed. GH ₂ D/S valve open micro switch dropped out. Fire started from LH ₂ leak at LH ₂ pump U/S bleed valve.	GN ₂ valve control pressure source replumbed. Valve stem packings tightened and purges increased. No engine or facility damage from fire.
1-23-87 017001	Fuel pump speed c/o at 75000 RPM	Test terminated at 1.08 sec. when igniter PC failed to reach 120 PSIG min R/L PR.	GH ₂ and GOX pressures were at correct values. Visual spark check o.k.
1-23-87 017002	Igniter only.	Igniter fired as planned.	
1-23-87 017002	Fuel pump speed c/o at 75000 RPM.	Test terminated at 2.01 sec due to combustor PC 250 PSI.	Redline value set too tight for PR rise rate. Reset R/L time to 2.5 sec.
1-28-87 017004	Fuel pump speed c/o at 75000 RPM	Test terminated at 1.08 sec when igniter PC failed to reach 120 PSIG min R/L PR.	Made GH ₂ and GOX blowdowns. Visual spark check o.k.
1-28-87 017005	Fuel pump speed c/o at 75000 RPM	Test terminated as planned at 2.9 sec.	NF = 77000 RPM PC = 675 PSIA
1-28-87 017006	7.5 sec duration	Test terminated at 5.75 sec when FP BAL PIST CAV PR dropped below R/L value of 1525 PSIG.	Pressure decay due to loss of FP speed. NF = 87000 RPM PC = 775 PSIA

* All times relative to MFV starting to open.

speed and pump pressure abruptly decayed. Visual inspection of the injector and thrust chamber show absolutely no evidence of heat distress due to the emergency shutdown.

BIBLIOGRAPHY

1. Baily, R., Enhanced Heat Transfer Combustor Technology - Interim Report, NAS3-23773 Tasks C.1 and C.2, RI/RD86-199, NASA CR-179541, December 16, 1986.
2. Brown, W., Enhanced Heat Transfer Combustor Technology - Final Report, NAS3-23773 Tasks C.3, C.4 and C.5, RI/RD91-235, NASA CR-189236, December 1991.
3. Cannon, I.; Balcor, S.; Cochran, M.; Klop, J.; Peterson, S., Definition, Technology Readiness Development Cost of the OTVE ICHM System Elements - Final Report, NAS3-23773 Task E.6, RI/RD91-150, NASA CR-187123, October 1991.
4. Coleman, P.; Darejeh, H.; Collins, J., ICHM Fiberoptic Shaft Monitor - Final Report, NAS3-23773 Task E.5, RI/RD90-177, NASA CR-185210, November 1989.
5. Erickson, C., Advanced Engine Study - Final Report, NAS3-23773 Task D.6, RI/RD90-180, NASA CR-187215, February 1992.
6. Erickson, C.; Hertzberg, D., Automated Preflight Methods Concept Definition - Final Report, NAS3-23773 Task E.7, RI/RD91-145, NASA CR-187190, December 1991.
7. Erickson, C.; Martinez, A.; Hines, B., Advanced Engine Study Phase II - Interim Report, NAS3-23773 Task D.4, RI/RD87-126, NASA CR-179602, February 1987.
8. Harmon, T.; Roschak, E., 7.5 Klb Thrust Rocket Engine Preliminary Design - Final Report, NAS3-23773 Tasks B.7 and D.5, RI/RD88-291, NASA CR-190754, December 1988.
9. Irvin, T., Soft Wear Ring Seals - Final Report, NAS3-23773 Task B.3, RI/RD 85-201, May 15, 1985.
10. Lariviere, B., High Velocity Ratio Diffusing Crossovers - Final Report, NAS3-23773 Task B.2, RI/RD89-111, NASA CR-194447, January 15, 1989.
11. Lariviere, B., Soft Wear Ring Seal Technology - Final Report, NAS3-23773 Task B.5, RI/RD90-214, NASA CR-189055, February 14, 1992.
12. Martinez, A., Orbit Transfer Rocket Engine Technology Program - Final Report. Vol. I: Executive Summary, NAS3-23172, RI/RD83-131-1, July 31, 1983.
13. Martinez, A., Orbit Transfer Rocket Engine Technology Program - Final Report. Vol. II: Study Results, NAS3-23172, RI/RD83-131-2, NASA CR-163158, July 31, 1983.
14. Martinez, A., Orbit Transfer Rocket Engine Technology Program - Final Report. Vol. III: Supplemental Data, NAS3-23172, RI/RD83-131-3, NASA CR-168316, July 31, 1983.
15. Martinez, A.; Erickson, C.; Hines, B., Advanced Engine Study Phase I - Interim Report, NAS3-23773 Tasks D.1, D.2 and D.3, RI/RD86-116, NASA CR-175084, January 1986.
16. Rockwell Intl., Rocketdyne Div., High Speed Turbopump Bearings - Final Report, NAS3-23773 Task B.6, RI/RD92-114, NASA CR-189230, January 1992.
17. Sutton, R., Two-Stage Partial Admission Turbine Tester - Final Report, NAS3-23773 Tasks B.1 and B.4, RI/RD86-214, NASA CR-179548, September 28, 1987.
18. Szemenyei, B., Combustor Wall Condition Monitoring - Final Report, NAS3-23773 Task E.5, RI/RD89-212, NASA CR-182275, August 1989.

